united nations
educational, scientific
and cultural
organization

international atomic
energy agency

the
abdus salam
international centre for theoretical physics

H4.SMR/1304-9

"COLLEGE ON SOIL PHYSICS"

12 March - 6 April 2001

Elementary Soil Hydrologic Processes: Infiltration, Redistribution, Evaporation and Evapotranspiration

M. Kutilek and D. R. Nielsen

Elsevier
Soil and Tillage Research (Journal)
Prague
Czech Republic

College on Soil Physics
ICTP, TRIESTE, 12-29 March, 2001

LECTURE NOTES

Elementary Soil Hydrologic Processes: Infiltration, Redistribution, Evaporation and Evapotranspiration

Extended text of the textbook
Soil Hydrology, 1994 by M. Kutílek and D.R. Nielsen

Miroslav Kutílek

Professor Emeritus
Nad Patankou 34, 160 00 Prague 6, Czech Republic
Fax/Tel. +420 2 311 6338
E-mail: kutilek@ecn.cz

6 ELEMENTARY SOIL HYDROLOGIC PROCESSES

In this chapter, for the sake of a lucid discussion of soil hydrology, we separate from the global hydrologic cycle those simple elementary processes which take place in the soil. The first group of elementary processes to be discussed are those to be described in the vertical direction and defined by simple boundary conditions. Here we discuss

-infiltration,
-redistribution of water within a soil following infiltration,
-drainage to a water table close to the soil surface,
-evaporation from a bare soil and
-evaporation and transpiration (evapotranspiration) from a vegetated soil surface.

Except for infiltration, all the above processes cause a water loss either from the entire soil profile or from at least a particular layer usually from the topsoil when 1-dimensional vertical flow is assumed. When two- and three-dimensional flow is considered owing to field circumstances, lateral subsurface and hypodermic flows may contribute to the water balance within the soil profile.

Meteorological situations actually control the extent of the elementary processes, and together with the water storage capacity of the soil profile, a particular stage of a hydrologic regime evolves over a long time period. If these stages are combined and averaged over still a longer span of time, we speak of a hydrologic regime of a soil. Analogously, as meteorological situations refer to weather during a period of weeks or months in a particular area, combined, long time averages are considered as the climate of the area.

6.1 PRINCIPLES OF SOLUTIONS

Our knowledge of elementary soil hydrologic processes stems partly from properly performed experiments and partly from mathematical solutions of equations describing physical processes. In each of the procedures we simulate the process either physically by an experiment or mathematically using either analytical or numerical methods. When we speak of properly performed experiments, we must experimentally impose exactly the initial and boundary conditions. Before imposing the boundary conditions, we first establish the initial conditions - the values of θ or h at all z of the 1-dimensional column at $t < 0$. When the initial condition demands a zero flux ($q = 0$), it is imperative that $dH/dz = 0$ along the entire column. When the initial value of the soil water content θ_i is assumed constant with depth ($d\theta_i/dz = 0$), a flux corresponding to a unit gradient of H exists, i.e. $q = -K(\theta_i)$ provided that a continuity of liquid water exists. If θ_i is very small, the downward flux may be negligibly small. Altering the value of the variable θ or h, respectively, at the boundary (i.e. at the topographical soil surface) induces a non-equilibrium condition that generates a soil water flux within the soil profile. Non-steady fluxes will then persist in the

system until an equilibrium is reached with $q = 0$, or until the flux is invariant with time ($dq/dt = 0$) and a steady state flux density is reached. Another possibility for causing water flow in soil is by imposing a defined flux density $q(t)$ on the boundary $q_o(t)$.

One boundary of a 1-dimensional soil column is its topographical surface. The other boundary is that of a column having either a finite or infinite length. A finite column is used to manifest a field condition, e.g. a ground water table ($h = 0$) or a defined water content or water flux at its bottom end. If the column extends to infinity, we speak of a semi-infinite column with its lower boundary $z \rightarrow \infty$.

If we establish a new value of the variable θ or h on a boundary for $t \geq 0$, we obtain Dirichlet's (or a concentration) boundary condition (DBC). When a flux density is imposed for $t \geq 0$ on a boundary, we have Neuman's (or a flux) boundary condition (NBC). If θ or h is specified on one boundary and a flux is specified on the other boundary, we have a mixed boundary condition (MBC).

When we solve a steady flow problem which is characterized by $dq/\mathrm{dt} = 0$ and $dq/dz = 0$, we do not define the initial condition because the flux and variables θ and h are independent of time. The solution is a particular value of the flux q for which a unique distribution of θ and h, respectively, along the z axis exists.

Formulations of non-steady flow problems yield distributions of θ or h, respectively in space and time. These distributions $\theta(z, t)$ and $h(z, t)$ for 1-dimensional problems are usually given as continuous functions $\theta(z)$ or $h(z)$ for specific times or time intervals. For DBC we are frequently searching additionally for the flux density at the boundary $q_o(t)$. In an experiment we must establish the initial θ_i or h_i at all depths for $t < 0$ and sustain θ_o or q_o at the boundary during the entire experiment. It is imperative that the experimental initial and boundary conditions are matched exactly with those described mathematically. Without such initial and boundary conditions, the experimental results cannot be properly evaluated and generalized.

In the mathematical treatment of problems, the initial and boundary conditions represent the limits of integration. Additionally, the properties of the soil need to be characterized. When we describe the process mathematically, we characterize the soil by its hydraulic characteristic functions K_S, θ_S, $h(\theta)$ and $K(\theta)$ or $K(h)$. $D(\theta)$ is obtained from $K(\theta)$ and $h(\theta)$ or is defined directly from primary measurements. Methods for obtaining the hydraulic functions will be discussed later in Chapter 7.

Mathematical solutions of the elementary hydrologic processes are either analytical or numerical. In *analytical procedures,* differential equations are usually integrated only after some kind of transformation. Many analytical procedures exist for somewhat trivial boundary conditions of unsteady flow in soils defined by simple hydraulic functions and for steady flow processes in homogeneous or distinctly layered soil columns. The analytical solutions typically involve infinite series or transcendental functions that are evaluated by numerical methods with the assistance of a computer. As a result, the calculated results are approximate in spite of having an exact analytical solution.

Close to analytical solutions are the *quasi-analytical solutions* for which a significant part of the procedure involves an analytical procedure. The overall

equation, often reduced to one or more ordinary differential equations, is integrated using a convergent iterative scheme. Alternatively, we split the higher order partial differential equation (e.g. Richards' equation) into lower order differential equations that are solved separately. In such cases an auxiliary function is frequently assumed with its value being determined by consecutive iterations. Analytical and quasi-analytical solutions developed for some elementary soil hydrological processes fit soils with simple, special forms of hydraulic functions. Such solutions, even if they are not directly applicable to field situations, have a great advantage. They lead to a full understanding of the physical process and provide estimates of deviations, e.g. owing to an alteration of a boundary condition. Moreover, these solutions allow errors of estimation of approximate and numerical procedures to be quantified. *Approximate solutions* are frequently exact analytical solutions developed for a soil characterized by a simple or even oversimplified hydraulic function. Or, they are exact solutions for a very simple flow process that only approximates reality in the field.

Numerical methods used in the solution of soil hydrologic processes are procedures which enable us to replace a differential equation with a set of approximate algebraic equations solved with a computer. These approximate numerical procedures are (i) the method of finite differences and (ii) the method of finite elements. Although their theoretical derivations are based upon different mathematical approaches, there are many similarities between both methods.

In the method of finite differences the spatial domain within which we search for a solution is sectioned by a system of normals into small segments. In 1-dimensional problems we obtain line segments, in 2-dimensional problems rectangle segments and in 3-dimensional problems parallelepiped segments. For each node of these geometric segments, we determine the value of the differential function describing the problem.

We replace the derivatives at a point by differences of the variable over a small finite interval. This method for the function $h(z)$ is therefore the inverse of the definition of its derivative

$$\frac{dh}{dz} = \lim_{\Delta z \to 0} \frac{h(z+\Delta z) - h(z)}{\Delta z}. \qquad (6.1)$$

Inasmuch as the approximation at one point depends to a certain degree upon approximations at neighboring points, local approximations are controlled by approximations applicable to the entire domain.

The continuous analytical equation is replaced by a set of algebraic equations with differences substituting for derivatives of functions obtained from Taylor's series expansions.

In finite element methods, the domain of the solution is subdivided into smaller sub domains, i.e. finite elements. The simplest scheme is composed of triangles with a triangular pyramid erected over each node. The value of the base functions represents the approximate solution with time taken as the finite difference. Local approximation is the characteristic feature of the finite difference method. In contrast, the finite element method manifests a global view. Assuming that the solution is expressible by a set of basic functions, the

6.2 INFILTRATION

The term infiltration denotes the entry of water into the soil through its surface. The soil surface could be plane, concave or convex, and could be formed by the walls of a cavity of a defined shape such as a sphere, cylinder etc. The source of water can completely or only partially cover the entire surface. Equations describing infiltration are usually for 1-dimensional water flow in either the vertical or horizontal direction. A limited number of solutions exist for 2- and 3-dimensional infiltration processes. Here, we restrict our discussion to 1-dimensional, vertical infiltration. Implicitly, our solutions are valid for infiltration through a plane horizontal surface.

Hydrologically, the infiltration process separates rain into two parts. One part stored within the soil supplies water to the roots of vegetation and recharges ground water. The other part which does not penetrate the soil surface is responsible for surface runoff. Infiltration is therefore a pivotal point within the hydrologic cycle.

Being consistent with present-day terminology, we shall call the flux density of water across a topographical soil surface the infiltration rate. However, this infiltration rate is often confusingly described by terms such as infiltration velocity, infiltration capacity, infiltrability etc. in relation to a specifically imposed boundary condition and in accordance with only some kind of subjective criteria. For non-steady flows it is clear that the flux density is time dependent and moreover, when boundary conditions are changed, the flux

density responds and is also time dependent. Thus, we could formulate a voluminous number of terms describing still the same phenomenon – the flux density across the top boundary of the soil.

We shall discuss separately steady and unsteady infiltration owing to the different hydraulic characteristics of both flows. Although steady infiltration is simpler to solve and to understand because only the Darcy-Buckingham equation is involved, unsteady infiltration is the dominant process in nature. We shall discuss unsteady infiltration in two sections according to the boundary conditions governing the type of infiltration. When the soil surface is instantaneously and excessively ponded as it is in an infiltration test performed with a ring infiltrometer, we have Dirichlet's boundary condition (DBC). When infiltration occurs under natural rainfall, we meet Neuman's boundary condition (NBC) for the full duration of the rain or for at least its initial occurrence. With these two types of flow being fundamentally different, we shall consider them separately.

6.2.1 Steady Infiltration

Steady infiltration is characterized by the condition that the flux density does not change with time nor with position in the unsaturated soil, i.e. $\partial q/\partial t = 0$ and $\partial q/\partial z = 0$. It follows from the equation of continuity (5.62) repeated here for 1-dimension

$$\frac{\partial \theta}{\partial t} = -\frac{\partial q}{\partial z} \tag{6.2}$$

that the soil water content does not change in time (i.e. $\partial\theta/\partial t = 0$ as well as $\partial h/\partial t = 0$). In order to satisfy the condition $\partial h/\partial t = 0$, we must define a non-variant hydraulic condition at the bottom of the soil column. The simplest practical provision is a constant ground water level at its bottom. Such conditions are simply demonstrated by the following process. A rain intensity q_R is constant in time ($\partial q_R/\partial t = 0$) and equals the infiltration rate as well as the flux density in the soil q provided that $q_R < K_S$. In this case, rainfall has been constant and infiltration has lasted long enough to allow the wetting front to reach the ground water level. We further assume that the ground water level is kept at a constant elevation by e.g. a drainage system. It is mathematically convenient to identify the origin of the z coordinate at the ground water level from which z increases positively upwards. As a result at $z = 0$, $h = 0$ and at the soil surface $z = Z$, $h = h_Z$ and $q = -q_R$. Some solutions derived for steady state conditions approximate non-steady infiltration after a long time has elapsed when $\partial q/\partial t \rightarrow 0$. For example, the development of a $h(z)$ or $\theta(z)$ profile in a crust-topped soil or in a soil with distinct horizons of different hydraulic functions and conductivities is practically identical for either steady state infiltration or the quasi-steady stage of non-steady infiltration after a long time.

6.2.1.1 Homogeneous Soil Profile

Here, inasmuch as the direction of flow is oriented downward while the positive direction of the z-axis is upward, the flux density $q < 0$. Equation (5.31) repeated here is

$$q = -K(h)\frac{dH}{dz} \tag{6.3}$$

where $H = (h + z)$. We obtain $q < 0$ when $dH/dz > 0$. If indeed, $dH/dz = 0$, we have a state of equilibrium with $q = 0$ and $h = -z$. The domain of $h(z)$ which satisfies (6.3) is therefore limited from the left side of the graph in Fig. 6.1 by $h = -z$ ($q = 0$) and from the right side of the domain by $q = -K_S$ with $dH/dz = 1$ and $dh/dz = 0$. For the determination of $h(z)$ we integrate (6.3) with an appropriate expression for $K(h)$. For an exponential expression of $K(h)$, see (5.39)

$$K = K_S \exp(ch)$$

we obtain for the limit $h = 0$ at $z = 0$

$$\int_0^z dz = -\int_0^h \frac{K_S\, dh}{q\exp(-ch) + K_S}. \tag{6.4}$$

After integration we have

$$z = \frac{1}{c}\ln\left[\frac{q + K_S}{q + K_S\exp(ch)}\right]. \tag{6.5}$$

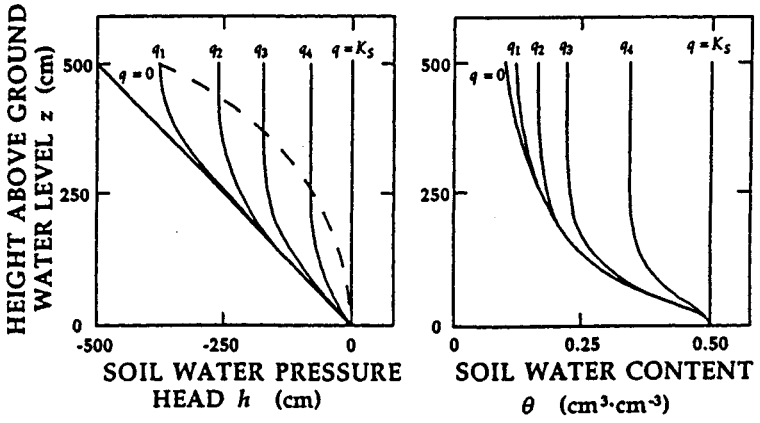

Figure 6.1. Steady flow infiltration. Pressure head profiles h(z) and soil water content profiles θ(z) are plotted for flux densities $q_0 = 0$, $q_1 = -10^{-3}$, $q_2 = -10^{-2}$, $q_3 = -6 \cdot 10^{-2}$, $q_4 = -10^{-1}$ cm·h^{-1} and $q = -K_S$ in a soil characterized by $K_S = 2$ cm·h^{-1} and $c = 0.02$ cm^{-1} in (6.5) and $\theta_S = 0.5$, $\theta_r = 0.015$, $n = 1.8$, $m = 0.44$ $\alpha = 0.015$ in (4.43). The dotted line separates the domain where $dh/dz = 0$.

Solution (6.5) is represented graphically in Fig. 6.2. For measured values of K_S and c, we obtain values of z for a series of selected values of h using the appropriate values of K_S/q. We obtain $\theta(z)$ shown in Fig. 6.1 using the soil water

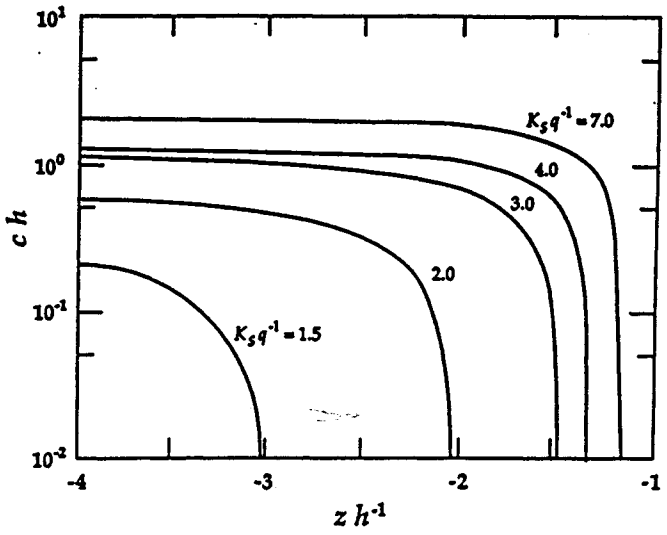

Figure 6.2. Steady flow infiltration. Graphical solution of (6.5) in dimensionless parameters (Bradáč and Kutílek, 1974).

retention curve SWRC. We see in the left graph that the depth of the zone having $dh/dz \approx 0$ increases with increasing absolute magnitudes of q. Also, within this zone $q \approx -K$ and $d\theta/dz \approx 0$. For example, for $q = -0.4$ cm·h^{-1}, (h, θ) at $z = 300$ and 500 cm are (-79.98, 0.3396) and (-80.46, 0.3387), respectively, see the right hand graph. Hence, if we measure h or θ for a series of steady-state infiltration fluxes q_n into a homogeneous soil with a water table at great depth, we obtain $K_n(h) = |q_n|$ or $K_n(\theta) = |q_n|$, respectively.

An equation similar to (6.5) is easily derived for a soil manifesting an air entry value h_A when a $K(h)$ function described by (5.40) is used in (6.3). Soil water pressure head profiles calculated for $h_A = -20$ cm are shown in Fig. 6.3 for some values of q_n given in Fig. 6.1. Note that the height of the water-saturated zone above the ground water level is not constant but rises with an increase of $|q|$. And, if $q = 0$, the height of the saturated zone above the ground water level reaches only its minimum value, $z = -h_A$, see Fig. 6.3. Such observations are a graphical illustration that hydrostatic conditions differ markedly from those involving systems where water is flowing.

Many additional solutions of infiltration for other expressions of $K(h)$ have been reported by Kutílek (1984b).

6.2.1.2 Layered Soil Profiles

The simplest case is the crust-topped profile. Rainfall frequently destroys soil aggregates within a soil surface. Or, if infiltration lasts for a long time and the source of water is from a river or waste discharge carrying suspensions of clay or

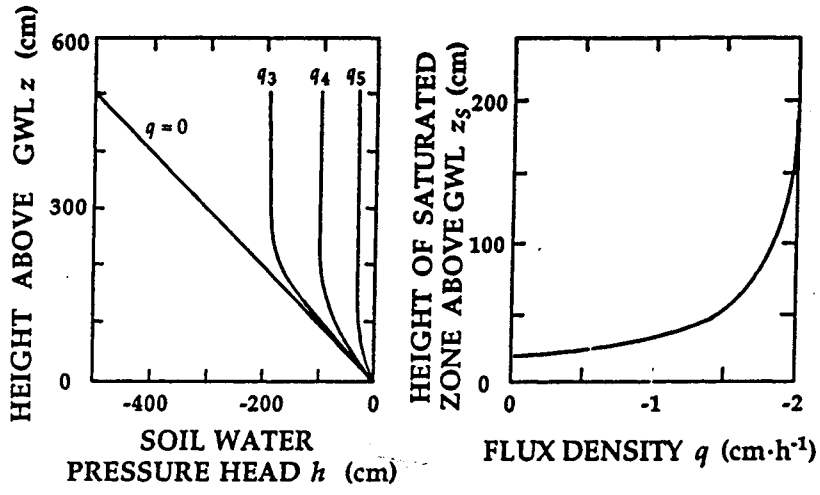

Figure 6.3. Steady flow infiltration. On the left, pressure head profiles h(z) if h_A = -20 cm, q_5 = -1.5 cm·h^{-1} and for other flux densities and soil characteristics identical to those in Fig. 6.1. On the right, the position of the saturated zone (elevation where h = -20 cm) depends upon the flux density.

fine particles, they are deposited on the soil surface or within the soil profile. Each of those processes denoted by sealing, crusting, collimation etc. results in the formation of a less permeable soil surface layer. Here for the sake of simplicity, we shall use the term crust for the result of all such processes. The characteristics of the crust will be denoted by the index 2, while those of the soil below the crust will be given the index 1, see Fig. 6.4. The origin of the z-axis is again identical with the position of the ground water level which is kept constant. The thickness of the soil between the ground water level and the crust is L_1, the thickness of the crust L_2 and the depth of water on the soil surface h_o. For steady-state flow, $q_1 = q_2$, and we have

$$-K_1\left(\frac{dH}{dz}\right)_1 = -K_2\left(\frac{dH}{dz}\right)_2. \tag{6.6}$$

If $K_{S1} \gg K_{S2}$, and $K_1(h_I) \gg K_2(h_I)$ where h_I is the value of h at the interface, we have

$$\left(\frac{dH}{dz}\right)_1 >> \left(\frac{dH}{dz}\right)_2 \tag{6.7}$$

and because $H = (h + z)$,

$$\left(\frac{dh}{dz}\right)_1 >> \left(\frac{dh}{dz}\right)_2. \tag{6.8}$$

This condition of a larger gradient of h occurring in the crust (layer 2) demands a sufficiently small value of h_I including $h_I < 0$. Because we assume that just below the interface in the subsoil (layer 1), $dH/dz \approx 1$, we can write

$$q = -K_1(h_I). \tag{6.9}$$

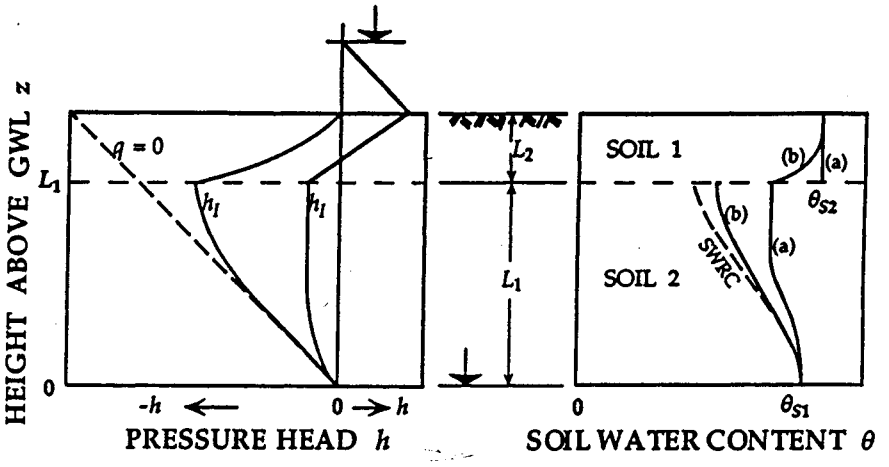

Figure 6.4. Steady flow infiltration into a crust-topped profile with h(z) on the left and θ(z) on the right for two cases. Case a., $h_I > h_{A2}$. Case b., $h_I < h_{A2}$. The pressure head at the boundary between crust and subsoil is h_I while h_{A2} is the air-entry value of the crust.

For the crust assuming it remains water-saturated,

$$q = -K_{S2}\left(\frac{h_o + h_I + L_2}{L_2}\right). \tag{6.10}$$

We also assume here that $h_{A2} = 0$ and $h_{A1} = 0$. The value of h_I is obtained by equating (6.9) and (6.10).

The criterion for $h_I < 0$ is derived from the total head loss between the free water level on the soil surface and that of the ground water - $(h_o + L_1 + L_2)$. Inserting this head loss into the modified Darcy equation (5.9) with the hydraulic resistance R_i for each of the two layers, we obtain

$$q = -\left(\frac{h_o + L_1 + L_2}{R_1 + R_2}\right). \tag{6.11}$$

The soil below the crust will be unsaturated if $|q| < K_{S1}$. From (6.11) it can be shown that the condition for unsaturation below the crust is

$$h_o < L_2\left(\frac{K_{S1}}{K_{S2}} - 1\right) \tag{6.12}$$

if $h_{A1} = 0$. For $h_{A2} > h_I$, the bottom part of the crust is also unsaturated, and $h(z)$ has a curved shape, see (b) in Fig. 6.4. For such cases, the above approach has to be modified, see e.g. Takagi (1960), Srinilta et al. (1966) and Bear et al. (1968). Kutílek (1984b) provides additional solutions when $dH/dz < 1$ below the interface.

Once $h(z)$ is known, we can determine $\theta(z)$ in the entire profile. Although h(z) has to be continuous, $\theta(z)$ is frequently discontinuous at the interface, see Fig. 6.4. When criterion (6.12) is fulfilled, the soil below the crust will be unsaturated if $h_{A1} > h_l$ provided the SWRC manifests h_A.

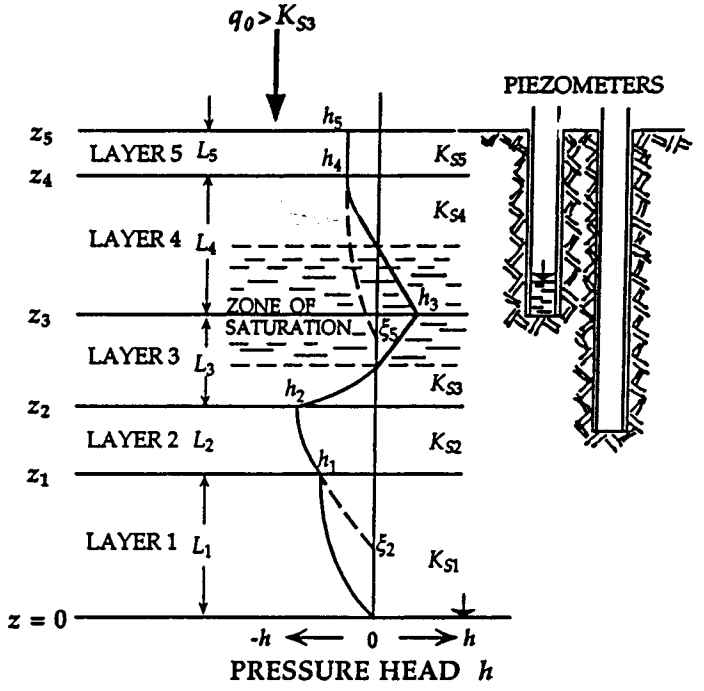

Figure 6.5. Steady flow infiltration into a layered soil profile. The pressure head profile h(z) indicates a water saturated zone. Note the position of the water level in the piezometers.

If a soil profile has n layers (or horizons) with each layer having its unique value of K_S and $K(h)$, we integrate in intervals identical with the height of the layers z_n. As a practical example, let us assume that the soil profile consists of 5 layers, see Fig. 6.5. The sequence of numbers again follows the positive direction of the z-axis with the layer in contact with the ground water level being 1, the next higher being 2 etc. Let us suppose that the soil has a strongly developed Bt horizon with a very small hydraulic conductivity, our layer 3. If $|q| > K_{S3}$ then for layer 3 we find that $(dH/dz)_3 > 1$, or $(dh/dz)_3 > 0$. For the other layers $|q| < K_{Si}, dH/dz \leq 1$ and $dh/dz \leq 0$, see Fig. 6.5. The distribution $h(z)$ can be found either analytically or with the graph in Fig. 6.2. We start with layer 1 as if it were a homogeneous profile to obtain h_1 on the boundary between layers 1 and 2. For layer 2 we find what would be the position of the

ground water level to obtain h_1 for the given value of q. Let us call this position ξ_2 a substitute ground water level for soil layer 2, see Fig. 6.5. With ξ_2 we determine $h(z)$ between z_1 ad z_2, and at z_2, $h = h_2$. In layer 3 which has the very small hydraulic conductivity, we assume $h_2 \geq h_{A3}$ and $h(z)$ is linear. If indeed $h_2 < h_{A3}$, we proceed analytically to obtain the distribution $h(z)$, see Kutflek (1984b). Or, alternatively, we approximate reality by a linear relation as we did for $h_2 > h_{A3}$. Note that a linear increase of h for the sub layer with $h > h_A$ or for $h > 0$ is exact. Having obtained the value of h_3, we use in layer 4 Darcy's equation for the saturated flow which occurs in the domain $h \geq 0$. From the elevation z where $h = 0$, we follow the same procedure as that already described for a simple 2-layer soil profile.

It follows from the above analysis that the less permeable layer in a profile acts as a hydraulic resistance which causes the development of a saturated zone in and above this layer provided that the flux density is greater than K_S of this less permeable layer. The thickness of the saturated zone increases with q, or for a given q, it increases with a decrease of K_S in the less permeable layer.

In Fig. 6.5, the zone of saturation starts above the top boundary of the less permeable layer 3 and ends above the bottom boundary of layer 3 provided that $h_{A3} = 0$. For $h_{A3} \neq 0$ the thickness of the saturated zone is greater.

The example described above also explains the conditions for a pseudo-gley formation in layers 3 and 4 during long term steady rainfall, even without the presence of a permanent ground water table.

6.2.2 Unsteady Infiltration, Dirichlet's Boundary Condition (DBC)

Assuming that a soil surface is continuously flooded with a negligibly small depth of water at time $t \geq 0$, the surface soil will be water-saturated. Before the soil surface is flooded ($t \leq 0$), we assume that the initial soil water content $\theta = \theta_i$. Water supplied to the surface keeps the surface soil at saturation ($\theta = \theta_S$) but is never allowed to rise significantly above the soil surface.

Such a situation defines Dirichlet's boundary condition (DBC) for infiltration into a semi-infinite homogeneous soil. With z increasing positively downward and $z = 0$ identified at the soil surface, the DBC is

$$t \geq 0 \qquad z = 0 \qquad \theta = \theta_S, \tag{6.13}$$

or

$$t \geq 0 \qquad z = 0 \qquad h = h_o, \tag{6.14a}$$

$$t \geq 0 \qquad z = 0 \qquad h = 0. \tag{6.14b}$$

We use (6.13) when the diffusivity form of the Richards' equation (5.68) is solved and (6.14) for the capacitance form (5.66). Less frequently, the time dependent behavior of $\theta(t)$ or $h(t)$ are defined at the soil surface.

The initial condition for the simplest case is

$$t = 0 \qquad z > 0 \qquad \theta = \theta_i \tag{6.15}$$

Initial conditions were discussed in detail at the beginning of section 6.1. The initial condition is sometimes considered as a boundary condition with $t = 0$ taken as a boundary similarly to $z = 0$.

Boundary condition (6.14a) has the advantage that it specifies the depth of water flooding the surface, i.e. the pressure head on the surface. Flooded alluvium along a river, flooded infiltration in an irrigation basin or in a basin for tertiary sewage treatment are practical examples of that boundary condition. Or, late periods of some rainfall events are other examples of (6.13). If a basin is flooded at $t = 0$ without additional water being provided, the decreasing level of water in the basin equals the cumulative infiltration I. Inasmuch as I is a function of t, we have for the DBC at $z = 0$, $h(t) = [h_o - I(t)]$ where $h = h_o$ at $t = 0$.

Infiltration caused by a DBC is frequently demonstrated with data from infiltration tests using double ring infiltrometers. The infiltration rate is measured by observing the decreasing water level within the inner ring, or even better, by measuring the inflow provided from a mariotte flask to the ring in order to keep a constant water level. The outer ring serves as a hydraulic buffer zone to minimize lateral flow below the inner ring. As a result, flow paths below the inner ring are nearly vertical, see Fig. 6.6. However, because a slight divergence of flow paths in the inner ring cannot be avoided, the measured data do not represent exactly 1-dimensional infiltration. Generally, the error is negligible compared with the inaccuracy of field experimentation and the spatial and temporal variability of the soil hydraulic functions provided that the soil is vertically homogeneous.

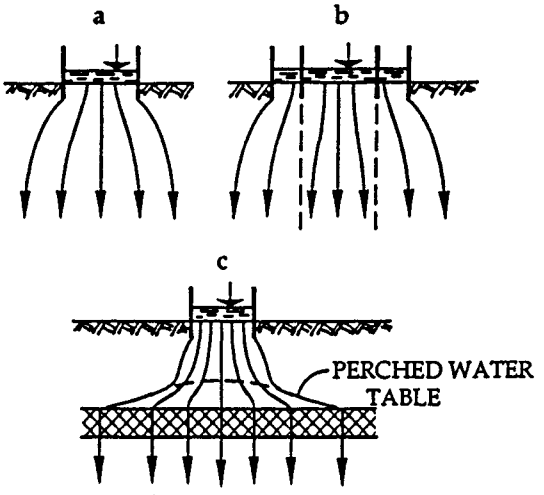

Figure 6.6. Flow paths when infiltration is measured a. by a single ring and b. by a double ring infiltrometer and c. is the influence of a less permeable layer (Bouwer, 1986).

When distinct soil layers exist in a profile, a strong divergence of flow paths occurs and the assumption regarding 1-dimensionality of the experiment is violated, see Fig. 6.6c. Hence, the measured data can be evaluated only for the period up to the time when the wetting front reaches the top boundary of the lesser permeable layer.

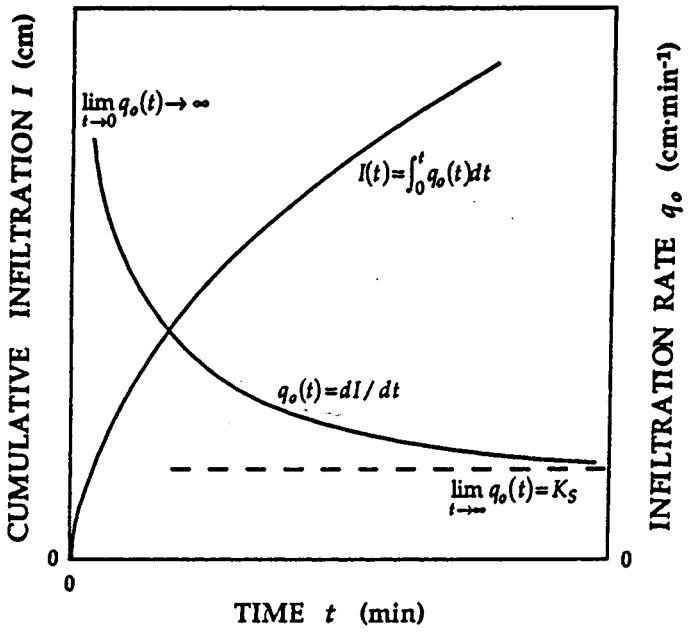

Figure 6.7. Time dependence of the cumulative infiltration I [L] and of the infiltration rate q_o [LT^{-1}] for DBC.

6.2.2.1 Characteristics of Infiltration

The primary data are measured values of cumulative infiltration I expressed as [L], usually in cm as a function of time. The values represent the total amount of water infiltrated into the soil surface from the beginning of the infiltration test at $t = 0$. A typical $I(t)$ relationship is a smooth, monotonically rising curve, see Fig. 6.7. The infiltration rate $q_o = dI/dt$ where the subscript o refers to the soil surface at $z = 0$. The value of q_o initially decreases rapidly with time and eventually approaches a constant value. For $t = 0$, $q_o \to \infty$, and for $t \to \infty$, q_o = constant. Theoretically, $q_o \to K_S$ as $t \to \infty$, see Fig. 6.7. Practically, the infiltration rate starts to be constant for coarse textured soils only after decades of minutes while that for fine textured loams is in the order of hours, depending upon the hydraulic functions of the soil and θ_i. Infiltration sometimes denoted as quasi-steady after this time limit will be discussed more fully in section 6.2.2.2. Steady infiltration into a crust-topped profile or into a layered profile can be successfully analyzed when 1-dimensional flow is guaranteed, e.g. by ponding water on a large area at $t = 0$ when the ground water level is at great depth or absent. The shape of $q_o(t)$ is empirically approximated by either a hyperbolic or exponential curve.

For a solution of the infiltration problem we first search for $h(z, t)$ and from it we obtain $\theta(z, t)$ from the SWRC. Some solutions provide $\theta(z, t)$ directly. Two examples of $\theta(z, t)$, one for sand and one for light clay are given in Fig. 6.8.

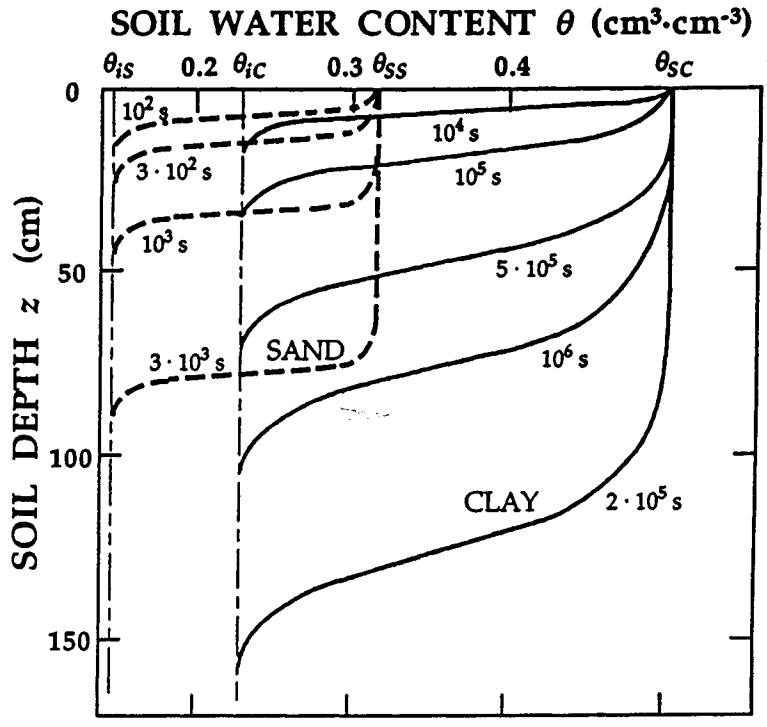

Figure 6.8. Soil water content profiles θ(z, t) in a sand and in a light clay for infiltration with DBC. θ_{is} is the initial water content of the sand, θ_{ic} the initial water content of the clay, θ_{Ss} the saturated water content of the sand and θ_{Sc} the saturated water content of the clay after Haverkamp et al. (1977).

The profiles are "piston-like", particularly for the sand. Where θ decreases steeply with z is called the wetting front. The rate of progress of the wetting front into the sand profile is more than two orders of magnitude greater than that into the clay profile. As the depth of wetting increases the shape of the wetting front becomes more gradual, especially for the clay. As infiltration proceeds, the shapes of $\theta(z)$ profiles for a given soil become nearly identical. Theoretically, the shapes are identical as $t \to \infty$.

Integration of the soil moisture profile at time t defines the cumulative infiltration at time

$$I = \int_{\theta_i}^{\theta_s} z \, d\theta \tag{6.16}$$

which according to (6.15) will decrease as θ_i increases. The influence of the initial value of water content θ_i is demonstrated in Fig. 6.9 for the light clay. If $\theta_i / \theta_S \geq 0.95$, the infiltration rate q_o can be approximated by $q_o \approx K_S$. The influence of the depth of ponding on the soil surface upon $q_o(t)$ is illustrated in Fig. 6.9. For $0 \leq h_o \leq 2$ cm, the influence is negligibly small. For $h_o = 10$ cm, the value of

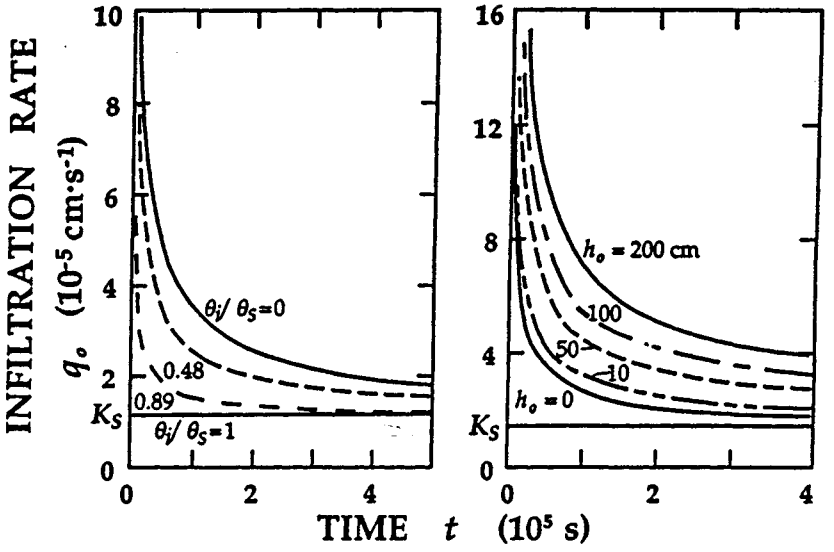

Figure 6.9. The influence of initial soil water content θ_i upon the DBC-infiltration rate q_o (left, Philip, 1957c) and the influence of the depth of ponding water h_o on the soil surface upon q_o (right, Philip, 1958) for Yolo light clay.

1958 b)

q_o is increased by 20% for large times and by more than 50% for short times in light clay. These relationships demonstrate how important it is to keep the value of h_o constant and as small as possible in experiments when the DBC (6.13) is applied.

Solutions to this type of infiltration can be divided into the three classes – (i) analytical and semi-analytical procedures, (ii) approximate solutions and (iii) empirical equations.

6.2.2.2 Analytical and Semi-Analytical Procedures

Richards' equation in its diffusivity form (5.68) is repeated here for the vertical coordinate oriented positively downward from the soil surface located at $z = 0$

$$\frac{\partial\theta}{\partial t} = \frac{\partial}{\partial z}\left[D(\theta)\frac{\partial\theta}{\partial z}\right] - \frac{dK}{d\theta}\frac{\partial\theta}{\partial z}. \qquad (6.17)$$

This equation, sometimes denoted as the non-linear Fokker-Planck equation (Philip, 1969a), is non-linear owing to the strong dependence of D and K upon θ. The first term on the right-hand-side of (6.17) describes the transport of water owing to the initial degree of unsaturation of the soil profile. Therefore, as θ_i increases, the importance of this term decreases. The second term on the right-hand-side of (6.17) originates because the gravitational potential. Hence, it is called the gravitational term and describes the flow of water owing to the force of gravity.

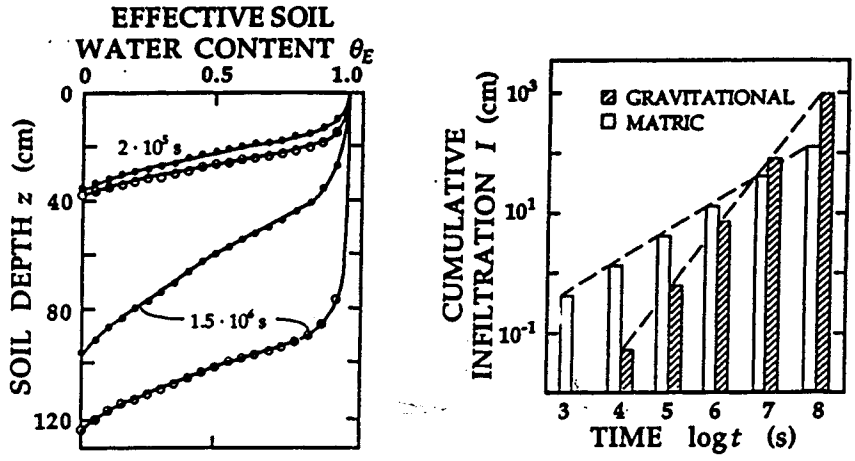

Figure 6.10. The influence of gravity upon the vertical DBC-infiltration into Yolo light clay. On the left, soil water content profiles for either vertical or horizontal infiltration. On the right, the partitioning of cumulative infiltration into matric and gravitational quantities (Kunze and Nielsen, 1982).

Philip's (1957b) solution of (6.17) is based upon the idea of separating the infiltration into its two components – those caused by the matric potential force and by the gravitational potential force. The idea is illustrated in Fig. 6.10. In the first step, he neglected the gravitational force and obtained a solution for horizontal infiltration in the form $x(\theta, t)$. Here, the dependent variable was changed to that of the horizontal axis x. Next, he assumed that the real $z(\theta, t)$ for vertical infiltration was the horizontal component $x(\theta, t)$ plus a correction , see Fig. 6.10. The correction owing to the gravitational force is time dependent. The influence of gravity upon infiltration is shown in Fig. 6.10 when θ_i is small. For short infiltration times its influence is very small, but with time it increases and for very large times, the force of gravity dominates the process. Hence, we first study horizontal infiltration.

Our horizontal soil column, initially at an unsaturated water content θ_i, has its end at $x = 0$ maintained at water saturation θ_S. Hence, for

$$t \geq 0 \qquad x = 0 \qquad \theta = \theta_S \tag{6.18}$$

$$t = 0 \qquad x > 0 \qquad \theta = \theta_i \tag{6.19}$$

we solve (6.17) without the gravitational term

$$\frac{\partial \theta}{\partial t} = \frac{\partial}{\partial x}\left[D(\theta) \frac{\partial \theta}{\partial x} \right]. \tag{6.20}$$

It is only here for a homogeneous soil (i.e. not layered) that the gradient of θ represents the driving force of the process. When D is a constant in (6.20), the solution is according to Carslaw and Jaeger (1959)

$$\frac{\theta - \theta_i}{\theta_S - \theta_i} = erfc\left(\frac{x}{2\sqrt{Dt}} \right). \tag{6.21}$$

When D is a function of θ, we transform (6.20) into an ordinary differential equation using the Boltzmann transformation. The transformed equation has a new variable η instead of the two original variables x and t. The new variable η defined by the Boltzmann transformation

$$\eta(\theta) = xt^{-1/2} \tag{6.22}$$

leads to

$$\frac{\partial \eta}{\partial t} = -\frac{1}{2} xt^{-3/2} = -\frac{\eta}{2t} \tag{6.23}$$

$$\frac{\partial \theta}{\partial t} = \frac{d\theta}{d\eta}\frac{\partial \eta}{\partial t} = -\frac{\eta}{2t}\frac{d\theta}{d\eta} \tag{6.24}$$

$$\frac{\partial \eta}{\partial x} = t^{-1/2} \tag{6.25}$$

and

$$\begin{aligned}\frac{\partial}{\partial x}\left[D(\theta)\frac{\partial \theta}{\partial x}\right] &= \frac{\partial}{\partial \eta}\left[D(\theta)\frac{d\theta}{d\eta}\frac{\partial \eta}{\partial x}\right]\frac{\partial \eta}{\partial x} \\ &= \frac{\partial}{\partial \eta}\left[D(\theta)\frac{d\theta}{d\eta}t^{-1/2}\right]t^{-1/2}.\end{aligned} \tag{6.26}$$

From the above (6.20) transforms to

$$-\frac{\eta}{2}\frac{d\theta}{d\eta} = \frac{\partial}{\partial \eta}\left[D(\theta)\frac{d\theta}{d\eta}\right]. \tag{6.27}$$

The transformed boundary conditions are

$$\eta = 0 \qquad \theta = \theta_S \tag{6.28}$$

and

$$\eta = \infty \qquad \theta = \theta_i. \tag{6.29}$$

The solution for which we search is simply $\theta(\eta)$, see Fig. 6.11. Measured soil water profiles $\theta[x(t_1)]$, $\theta[x(t_2)]$, $\theta[x(t_3)]$ etc. are thus transformed into the unique $\theta(\eta)$ relationship by merely dividing x by $t_1^{1/2}$ for the first profile, $t_2^{1/2}$, for the second profile etc. Note that for $t = 1$, $x \equiv \eta$. Hence, the physical reality of $\theta(\eta)$ is the soil water profile $\theta(x)$ when the infiltration time is unity.

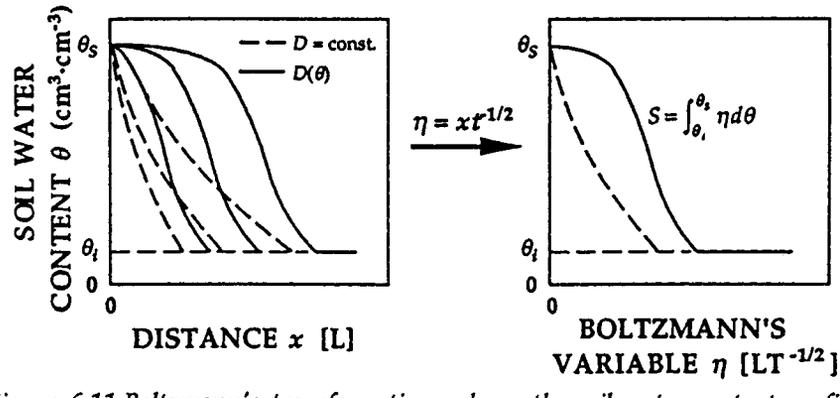

Figure 6.11. Boltzmann's transformation reduces the soil water content profiles $\theta(x)$ for a series of times t to a unique profile $\theta(\eta)$ with $\eta = xt^{-1/2}$ for horizontal infiltration (absorption). Broken curves are for a "linear soil" with D = constant while the full curves are for a soil with $D(\theta)$.

Philip (1960) and Kutílek (1984) have shown for which analytical expressions of $D(\theta)$ analytical solutions of (6.27) subject to (6.28) and (6.29) exist. Because it is exceptional that any of those analytical expressions accurately describe $D(\theta)$ of a real soil, an iterative procedure proposed by Philip (1955) is commonly used to calculate $\theta(\eta)$ from measured distributions of D versus θ.

With the content of infiltrated water being denoted as cumulative infiltration I,

$$I = \int_{\theta_i}^{\theta_s} x \, d\theta \tag{6.30}$$

or with (6.28),

$$I = \int_{\theta_i}^{\theta_s} \eta(\theta) \, t^{1/2} \, d\theta . \tag{6.31}$$

Inasmuch as $\eta(\theta)$ is unique for each soil, Philip (1957b) introduced the term sorptivity S [$LT^{-1/2}$]

$$S = \int_{\theta_i}^{\theta_s} \eta(\theta) \, d\theta \tag{6.32}$$

and

$$I = S \, t^{1/2}. \tag{6.33}$$

Because the infiltration rate

$$q_o = dI / dt, \tag{6.34}$$

we have

$$q_o = \frac{1}{2} S \, t^{-1/2}. \tag{6.35}$$

Here, we note that the sorptivity is physically the cumulative amount of water infiltrated at $t = 1$, and at that time, the infiltration rate has diminished to one-half the value of S. Sorptivity depends not only upon the $D(\theta)$ function but upon θ_i. The value of S decreases with increasing θ_i and as $\theta_i \rightarrow \theta_S$, $S \rightarrow 0$, see Fig. 6.12. When S is measured for a particular θ_{i1}, we can linearly interpolate between θ_{i1} and θ_S in order to obtain a first approximation of S for $\theta_{i2} > \theta_{i1}$. A more laborious, exact procedure is described by White and Broadbridge (1989). If $\theta_o < \theta_S$ is used in (6.18) instead of θ_S, we proceed in the same manner to derive S. However, the resulting value of $S(\theta_i, \theta_o)$ may indeed drop substantially from that of $S(\theta_i, \theta_S)$.

Sorptivity is an integral part of most investigations describing vertical infiltration. As a first approximation of the solution of (6.17) subject to (6.18) and (6.19), Philip used (6.22), the solution of (6.20) for horizontal infiltration, i.e. $z_1(\theta, t) = x(\theta, t)$. He corrected this approximation with the term y, i.e. $z = z_1 + y$. However, because an exact value of y cannot be obtained, its approximation y_1 defines another correction u, i.e. $y = y_1 + u$. Again, instead of an exact u we can only find still another estimate u_1 etc. Hence, Philip obtained the infinite series solution

$$z(\theta,t) = \eta_1(\theta) t^{1/2} + \eta_2(\theta) t + \eta_3(\theta) t^{3/2} + \cdots + \eta_n(\theta) t^{n/2} \tag{6.36}$$

where the functions $\eta_1, \eta_2, \eta_3, \cdots \eta_n$ are defined with $D(\theta)$, $K(\theta)$ and η_{n-1}. The procedure for computing terms η_n is described in detail by Kirkham and Powers (1972).

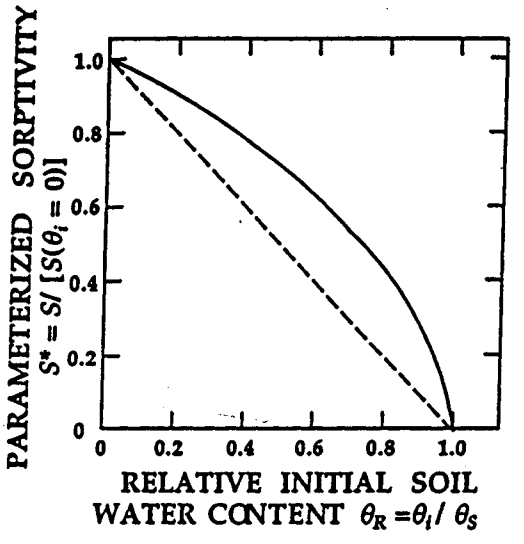

Figure 6.12. The dependence of the parameter S^* [$LT^{-1/2}$] upon the relative soil water content θ_i/θ_S. Broken curve is for a "linear soil" with D = constant while the full curve is for a soil with $D(\theta)$.

Inasmuch as the cumulative infiltration I according to (6.16) is

$$I = \int_{\theta_i}^{\theta_s} z\,d\theta, \tag{6.37}$$

Philip formulated analogously to the sorptivity equation (6.32) for horizontal infiltration, the following equation from (6.36)

$$I = S\,t^{1/2} + (A_2 + K_i)t + A_3 t^{3/2} + \cdots + A_n t^{n/2} \tag{6.38}$$

where

$$A_n = \int_{\theta_i}^{\theta_s} \eta_n(\theta)\,d\theta \qquad\qquad n = 2, 3, \cdots$$

and K_i is $K(\theta_i)$. Note that $K_i t$ expresses the cumulative water flow with $dH/dz = -1$ at $\theta = \theta_i$. Thus, we understand physically that boundary condition (6.19) can be kept only if we impose a steady flux density $q_o = K(\theta_i)$ for $z \geq 0$ within the semi-infinite column.

The series (6.38) converges for short and intermediate times of infiltration and the infiltration rate $q_o(t)$ obtained by differentiation is

$$q_o = \frac{1}{2} S\,t^{-1/2} + (A_2 + K_i) + \frac{3}{2} A_3 t^{1/2} + \cdots + \frac{n}{2} A_n t^{n/2-1}. \tag{6.39}$$

For large times, (6.38) does not converge. Inasmuch as the shape of the wetting front remains invariant at large times, the wetting front moves downward at a rate

$$v = \left(\frac{K_S - K_i}{\theta_S - \theta_i} \right) \tag{6.40}$$

while the infiltration rate for $t \to \infty$ is

$$q_o = K_S\,. \tag{6.41}$$

Equations (6.40) and (6.41), commonly called the infinite time solutions, are theoretically traveling wave solutions (Philip, 1969a).

The times for which (6.38) or (6.39) continue to converge was found to range broadly from 0.67 h for sand to 250 h for light clay (Haverkamp et al., 1988). Similarly, the times for which the infinite time solution is applicable varies widely from approximately 100 min for a silt loam (Nielsen et al., 1961) to about 10^5 min for light clay (Kunze and Nielsen, 1982). Piece wise solutions for 1-dimensional infiltration have been discussed by Philip (1987).

In order to obtain an intermediate time solution, Swartzendruber (1987) adjusted Philip's time series solution of q to apply between the limits $t \to 0$ and $t \to \infty$. Inasmuch as the solution for infiltration into linear soils as well as some approximate solutions lead to exponential forms of $I(t)$, Swartzendruber proposed intuitively the form

$$I = \frac{S}{A_o}\left[1 - \exp\left(-A_o t^{1/2} - B_o t - C_o t^{3/2} - \cdots\right)\right] + K_S t \tag{6.42}$$

where A_o, B_o, C_o, $\cdots$ are constants depending upon the soil hydraulic functions as well as θ_i and θ_S. The time derivative of (6.42) gives the infiltration rate

$$q_o = \frac{S}{A_o}\left[1 - \exp\left(-A_o t^{1/2} - B_o t - C_o t^{3/2} - \cdots\right)\right] \cdot \left[\frac{A_o}{2} t^{-1/2} + B_o + \frac{3}{2} C_o t^{1/2} + \cdots\right] + K_S. \tag{6.43}$$

Parlange (1971), realizing that Richards' equation originated from a combination of the Darcy-Buckingham equation and the equation of continuity, also obtained a solution. His original procedure consisting of iterative processes was gradually corrected by Císler (1974) and further modified (Parlange et al., 1982, and Parlange et al., 1985) to its present form (Haverkamp et al., 1990). The procedure, based upon an integral moment balance (Raats, 1988), uses a double integration of the equation of continuity (6.2). The starting point is

$$\int_0^{\infty} (q - q_-)\, dz = \frac{\partial}{\partial t} \int_0^{\infty} (\theta - \theta_-)\, dz. \tag{6.44}$$

When the diffusivity form of the Darcy-Buckingham equation was combined with (6.44), Haverkamp et al. (1990) using two approximation steps obtained two well behaved equations. Owing to this contribution of Parlange and Haverkamp, we call them the P-H equations. In their dimensionless form they are

$$I^* = \frac{\gamma}{q_o^* - 1} + (1 - \gamma) \ln\left[1 + \frac{1}{q_o^* - 1}\right] \tag{6.45}$$

and

$$t^* = (1 - 2\gamma) \ln\left[1 + \frac{1}{q_o^* - 1}\right] + \frac{\gamma}{q_o^* - 1} - \frac{1 - \gamma}{q_o^*} \tag{6.46}$$

where

$$q_o^* = \frac{dI^*}{dt^*},$$

$$I^* = [I - K_i t]\frac{2(K_s - K_i)}{S^2 + 2K_i h_o (\theta_s - \theta_i)},$$

$$t^* = \frac{2(K_s - K_i)^2 t}{S^2 + 2K_i h_o (\theta_s - \theta_i)}$$

and

$$\gamma = \frac{2K_s(h_o - h_w)(\theta_s - \theta_i)}{S^2 + 2K_i h_o (\theta_s - \theta_i)}.$$

The value of h_w is the water entry value on the wetting branch of the SWRC. After I^* and t^* are computed for chosen values of q_o^*, all three terms are transformed back to the dimensional forms I, q_o and t.

The integral method can also involve a mass balance formulation where (Raats, 1988)

$$\int_0^t [q_o(t) - q_-]\,dt = \int_{\theta_i}^{\theta_s} z\,(\theta, t)\,d\theta \qquad (6.47)$$

which is also obtained by integrating the equation of continuity. Philip (1973) and Philip and Knight (1974) managed to reduce the number of independent variables of the infiltration problem by using a guessed shape for the ratio of flux densities q/q_o. With the main idea of this "flux-concentration relation" method being explained in more detail in section 6.2.3.2., only the principle is given here.

The parameterized flux density F related to the parameterized water content θ_R for *horizontal infiltration* is

$$F(\theta_R, t) = \frac{q}{q_o} \qquad (6.48)$$

or with (6.32)

$$F(\theta_R) = \frac{\int_{\theta_i}^{\theta} \eta(\theta)\,d\theta}{\int_{\theta_i}^{\theta_s} \eta(\theta)\,d\theta} \qquad (6.49)$$

where

$$\theta_R = \frac{\theta - \theta_i}{\theta_s - \theta_i}.$$

Relation (6.49) is the ratio of the partial and total sorptivities calculated from (6.32) and illustrated in Fig. 6.13. $F(\theta_R, t)$ is the guessed shape which is inserted into the diffusivity form of the Darcy-Buckingham equation to obtain

$$F(\theta_R, t) = -\frac{D(\theta)}{q_o}\frac{\partial \theta}{\partial x}. \qquad (6.50)$$

With

$$q_o = \frac{1}{2} S t^{-1/2}$$

the sorptivity is (Philip and Knight, 1974)

$$S = \left[2\int_{\theta_i}^{\theta_s} \frac{(\theta - \theta_i) D(\theta)}{F(\theta_R)}\,d\theta\right]^{1/2}. \qquad (6.51)$$

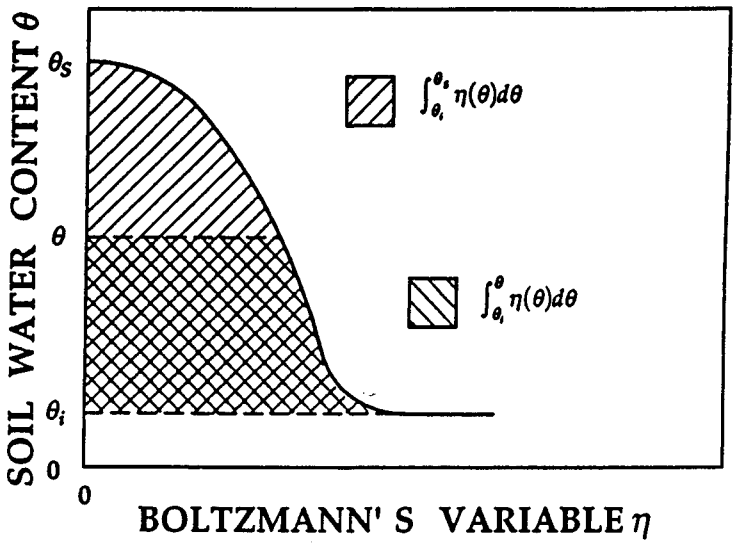

Figure 6.13. Flux concentration relation $F(\theta)$ is expressed as the ratio of these two integrals.

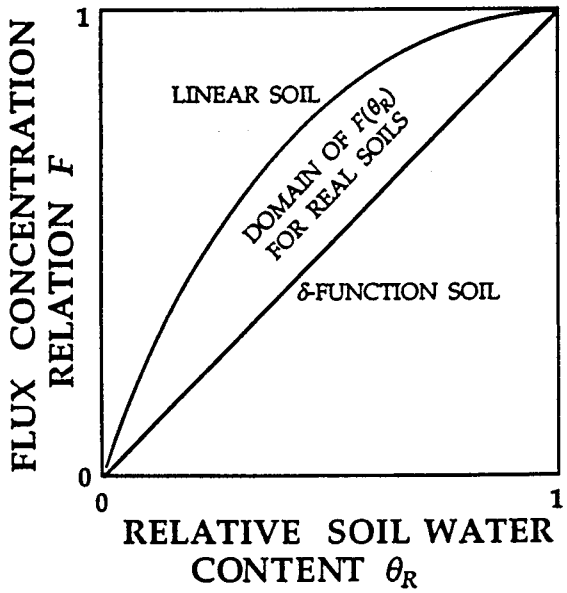

Figure 6.14. Dependence of the flux concentration relation F upon relative soil water content θ_R for DBC-horizontal infiltration according to Philip (1973).

If $F(\theta_R)$ is known, the above solution is available. Inasmuch as the time dependence of $F(\theta_R)$ is neglected, the solution is approximate. Philip (1973) has demonstrated that $F(\theta_R)$ can only exist within a relatively narrow domain. In Fig. 6.14 it can be seen that the domain is limited on one side by the curve which represents a linear soil having a constant D and from the other side by the straight line ($F = \theta_R$) which is descriptive of a soil having a $D(\theta)$ equal to a Dirac δ-function. For $\theta_R = 0$, $F = 0$, and for $\theta_R = 1$, $F = 1$. These two soils should represent the extremes of existence of $D(\theta)$ for real soils. Although the difference between the $F(\theta_R)$ relationships for these two soils appears slight in Fig. 6.14, their soil water content distributions for horizontal infiltration are strikingly different, see Fig. 6.16.

For vertical infiltration (6.48) is modified to

$$F(\theta_R, t) = \frac{q - K_i}{q_o - K_i} \tag{6.52}$$

and the $F(\theta_R)$ relationships for the two extreme soils are given in Fig. 6.15.

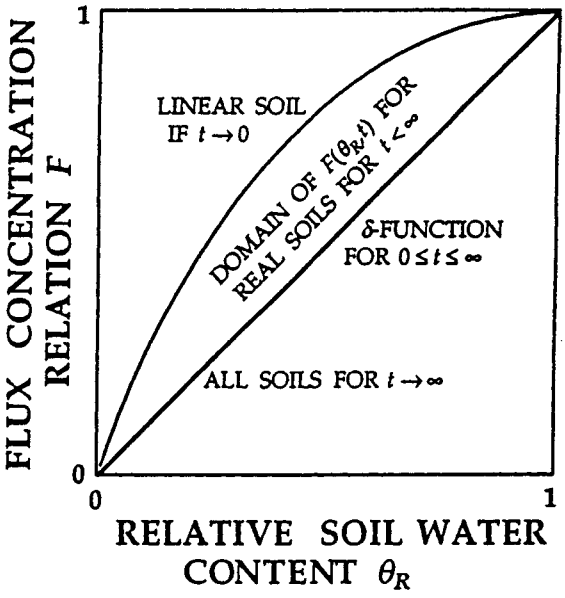

Figure 6.15. Dependence of the flux concentration relation F upon relative soil water content θ_R for DBC-vertical infiltration according to Philip (1973).

The solutions for the two extreme soils have the typical features of a theoretical treatment with no direct applicability to reality. Linear soil, characterized by a constant D and a K proportional to θ_R leads to h being proportional to $\ln\theta_R$ – a relationship for a SWRC which is not realistic for soils or other porous media. It would appear that for δ-function soils, infiltration

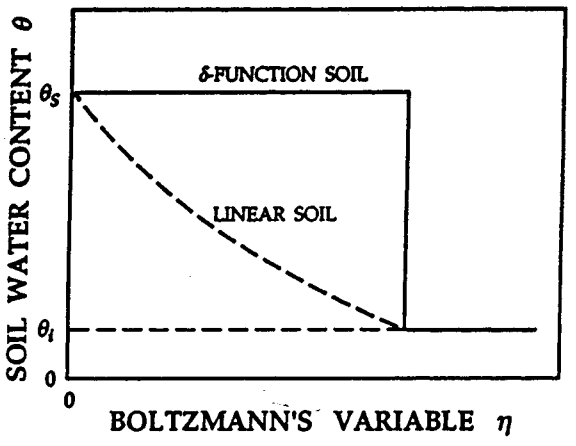

Figure 6.16. Soil water content profile θ(η) for DBC-horizontal infiltration for the "linear soil" (broken curve) and for a δ-function soil (full curve).

should be easily approximated owing to the steep rise of D with θ_R and that $F(\theta_R) = \theta_R$ looks like a good approximation for the ratio of flux densities. However, when the sorptivities computed for δ-function soils were compared to those obtained analytically for soils having a very steep $D(\theta)$, relative errors exceeded 20% (Kutílek and Valentová, 1986). Therefore, for most soils the iterative procedures proposed by Philip and Knight (1974) should be adopted.

In order to obtain solutions for models characteristic of real soils, proper functional relationships $D(\theta)$, $K(\theta)$ and $h(\theta)$ are required. To obtain them Richards' equation is linearized with transformations, e.g. those of Storm or Hopf and Cole. A review of such solutions identifying the authors of each transformation is provided by Raats (1990).

6.2.2.3 Approximate Solutions

The solution of the infiltration process, approximated physically or mathematically, is usually not kept wholly within either category but relies more heavily upon one or the other. A physical approximation is dominant in the procedure of Green and Ampt (1911) while mathematical approximations prevail in remaining, more recent procedures.

Green and Ampt (1911) simplified a real soil water profile of infiltration to a step-like profile, see Fig. 6.17. In this model, water penetrates into the soil like a piston which proceeds with time to greater depths. Below the abrupt, horizontal wetting front, the soil remains dry at its initial value of $\theta = \theta_i$. In the saturated upper part of the soil, flow is now simply described by Darcy's equation. If at time t the position of the wetting front is $z = L_f$ (the thickness of the soil saturated with water is also L_f), the infiltration rate is

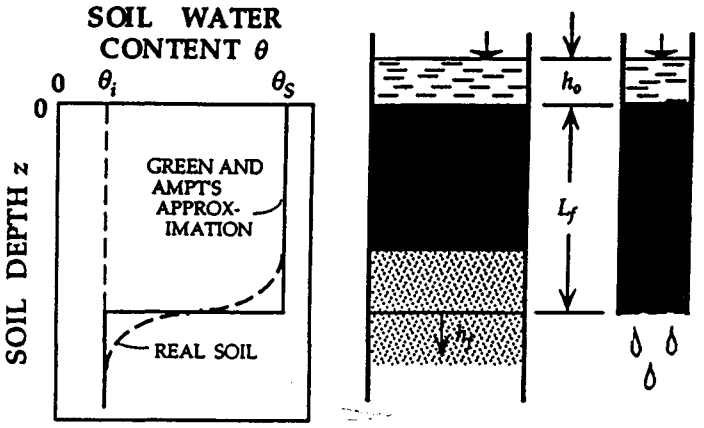

Figure 6.17. Solution of DBC-vertical infiltration according to Green and Ampt's approximation where the real soil water content profile θ(z, t) given by the broken curve is replaced by the step-like profile given by the full line.

$$q_o(t) = -K_s\left\{\frac{h_f - [h_o - L_f(t)]}{L_f(t) - 0}\right\} = K_s\left\{\frac{h_o + L_f(t) - h_f}{L_f(t)}\right\} \qquad (6.53)$$

where h_o is the pressure head at the soil surface (i.e. the depth of water on the surface). Note that L_f is time dependent. The term h_f is the soil water pressure head at the wetting front owing to the unsaturated condition of the soil below z with $h_f < 0$. If there were no soil below $z = L_f$ and water was freely falling out of the saturated soil column ($h = 0$ at $z = L_f$), the water flux throughout the column of thickness L_f would be

$$q_o = q = K_s\frac{h_o + L_f(t)}{L_f},$$

see Fig. 6.17. Because there is dry soil below $z = L_f$, its unsaturated condition causes the flux to increase. Green and Ampt added the term h_f to the driving force to account for the extra force acting at the wetting front. Neuman (1976) has shown that

$$h_f = \frac{1}{K_s}\int_0^{h_i} K(h)\,dh \qquad (6.54)$$

and

$$h_f = \frac{1}{K_s}\int_{\theta_s}^{\theta_i} D(\theta)\,d\theta. \qquad (6.55)$$

Or, using the Parlange (1975) solution

$$h_f = \frac{1}{2}\int_0^{h_i}\left(\frac{\theta_s - \theta(h) - 2\theta_i}{\theta_s - \theta_i}\right)\left[\frac{K(h)}{K_s}\right]dh. \qquad (6.56)$$

Obviously, without knowing the original publication of Green and Ampt, Budagovskij (1955) based his monographic study upon the same principle.

Theoretically, the procedure is based upon the expected shape and similarity of the $\theta(z, t)$ profiles. Philip (1957b, 1973b) showed that the following Green and Ampt approximation is an exact solution only if $D(\theta)$ is expressed as a Dirac δ-function. Considering (6.53), we know $q_o = dI/dt$ and $I = L_f \Delta\theta$ where $\Delta\theta = \theta_S - \theta_i$, and hence,

$$q_o = \frac{dL_f}{dt}\,\Delta\theta. \tag{6.57}$$

The rate of progress of the wetting front is linearly dependent upon the infiltration rate for all t > 0. When the force of gravity is neglected, i.e. for horizontal infiltration, substituting (6.57) into (6.53), we have

$$\frac{dL_f}{dt}\,\Delta\theta = K_S\left(\frac{h_o - h_f}{L_f(t)}\right), \tag{6.58}$$

and after separating variables

$$\int_0^{L_f} L_f\,dL_f = \int_0^t K_S\left(\frac{h_0 - h_f}{\Delta\theta}\right)dt. \tag{6.59}$$

After integrating,

$$L_f = \left[2K_S\left(\frac{h_0 - h_f}{\Delta\theta}\right)\right]^{1/2} t^{1/2} \tag{6.60}$$

or with $L_f = I/\Delta\theta$,

$$I = \left[2K_S\left(h_0 - h_f\right)\Delta\theta\right]^{1/2} t^{1/2}. \tag{6.61}$$

Comparing (6.61) with (6.33), we obtain the sorptivity S

$$S = \left[2K_S\left(h_o - h_f\right)\Delta\theta\right]^{1/2}. \tag{6.62}$$

Equation (6.61) can also be used to estimate I during a brief initial period of vertical infiltration. Equation (6.62) defines approximately how S depends upon θ_i.

When gravity is not neglected, (6.53) becomes

$$\Delta\theta\,\frac{dL_f}{dt} = K_S\left\{\frac{L_f(t) + \left(h_o - h_f\right)}{L_f(t)}\right\}. \tag{6.63}$$

After separating variables and integrating between the limits (0, t) and (0, L_f), we obtain

$$t = \frac{\Delta\theta}{K_S}\left\{L_f - \left(h_o - h_f\right)\ln\left[1 + \frac{L_f}{\left(h_o - h_f\right)}\right]\right\}. \tag{6.64}$$

Notice that this solution does not allow $I(t)$ to be described explicitly. Such an implicit transcendental function is typical for all solutions embracing the Green and Ampt approach even when it is not apparent in some more sophisticated developments. When (6.64) is transformed with dimensionless terms

$$t^* = \frac{K_S t}{\Delta\theta\left(h_o - h_f\right)} \tag{6.65a}$$

and

$$I^* = \frac{I}{\Delta\theta\left(h_o - h_f\right)} \tag{6.65b}$$

we have

$$t^* = I^* - \ln\left(1 + I^*\right) \tag{6.66}$$

which can be evaluated graphically (see Fig. 6.24) or by computing t for a series of values of L_f with $I = L_f\Delta\theta$.

Because the procedure is simple, the Green and Ampt approximation has been widely used in research as well as in the solution of many practical engineering problems. It has also been applied to the description of infiltration into layered profiles and those having a crust surface. However, we have to keep in mind that real soils do not manifest a δ-function $D(\theta)$, and hence, the method offers results of disappointingly poor accuracy. For example, the error involved in predicting $I(t)$ or $q_o(t)$ can approach 30% in homogeneous soil profiles. Its use should be limited to those wanting only a convenient, rough estimate of infiltration.

Within the second category of approaches, Philip's (1957b) algebraic infiltration equation is the most common. This approximate equation is merely the first two terms of the series solution (6.38) with the cumulative infiltration $I(t)$ being

$$I = St^{1/2} + At \tag{6.67}$$

and the infiltration rate q_o (= dI/dt) being

$$q_o = \frac{1}{2}St^{-1/2} + A. \tag{6.68}$$

These equations like their parent time series solution (6.38), are applicable to relatively short times. The magnitude of A is $(A_2 + K_i + \varepsilon)$ where ε is the truncation error for having used only the first two terms of (6.38). It was expected that A be related to K_S by a simple, sufficiently accurate relation $A = mK_S$. Although the most frequently used value of m is 2/3, its value ranges between 0.2 and 0.67 (Philip, 1987). However, detailed studies show that m depends upon both θ_i and time and sometimes exceeds a theoretical upper limit of 2/3. The error of estimate of K_S derived from A could theoretically reach about 30% in a relatively dry homogeneous soil (Kutílek et al., 1988). Therefore, (6.67) cannot be reliably used for estimating the value of K_S from infiltration tests.

Sorptivity S in (6.67) and (6.68) is an estimate of the theoretical value of sorptivity for a soil having initial water content θ_i. The truncation error influences the estimated value of the sorptivity to a lesser degree than that of A. Thus, S evaluated from the early stage of infiltration is considered a reliable value (Kutílek et al., 1988).

In order to reduce the truncation error, Kutílek and Krejča (1987) proposed to use three terms of the time series solution (6.38)

$$I = C_1 t^{1/2} + C_2 t + C_3 t^{3/2} \tag{6.69}$$

where C_1 is the estimate of sorptivity S, C_2 the estimate of $(A_2 + K_i)$ and C_3 the value of $(A_3 + \varepsilon_1)$ where ε_1 is the truncation error for having used three terms of (6.38). If we approximate the limiting time for which the truncated series (6.69) converges as the value of t when $dq_o/dt \rightarrow 0$, we have

$$t_{lim} = \frac{C_1}{3C_3}. \tag{6.70}$$

And, if we make an additional approximation that $q_o(t_{lim}) \approx K_S$, we obtain the estimate

$$K_S \approx (3C_1C_3)^{1/2} + C_2. \tag{6.71}$$

Simplifying (6.42) in a manner similar to (6.67), Swartzendruber (1987) suggested using

$$I = \frac{S}{A_o}\left[1 - \exp\left(-A_o t^{1/2}\right)\right] + K_S t. \tag{6.72}$$

Substituting $4K_S/3S$ for A_o into the above equation, we obtain the two-parameter infiltration equation proposed by Stroosnijder (1976). On the other hand, if we consider only the first four terms of a series expressing the exponential term $\exp(-A_o t^{1/2})$, we obtain an equation identical to (6.69).

Equations (6.69) and (6.72) have similar disadvantages. Parameters C_2, C_3 and A_o are not simply calculated or predicted from known hydraulic functions K_S, $K(h)$ and $\theta(h)$. When those equations are used for estimating S and K_S from measured values of $I(t)$, the estimates are reliable only for a strictly homogeneous soil column with an initial condition $d\theta_i/dz = 0$. When the equations are applied to field data, significant, intolerable errors are sometimes apparent. For example, when K_S is being evaluated, physically unreal values of $K_S<0$ are sometimes obtained (Kutílek and Krejča, 1987, and personal communication from Krejča, 1989).

Brutsaert (1977) also began with the horizontal solution of Philip (1957a) and subsequently sought a correction for the gravitational force. He obtained

$$I = K_S t + \frac{S^2}{BK_S}\left\{1 - \frac{1}{\left[1 + \left(BK_S t^{1/2}\right)/S\right]^2}\right\} \tag{6.73}$$

and

$$q_o = K_S + \frac{1}{2} S t^{1/2}\left\{\frac{1}{\left[1 + \left(BK_S t^{1/2}\right)/S\right]^2}\right\}. \tag{6.74}$$

He considered values of $B = 1/3$, $2/3$ or 1 each descriptive of physical reality, but for most practical purposes, recommended $B = 1$. Values of $I(t)$ computed with (6.73) are nearly identical to those from (6.38) when the hydraulic functions of the soil are known. And, inversely, estimates of S and K_S from the experimental data using (6.73) appear more reliable than those using other approximate equations based on comparative theoretical errors.

From this and the previous section, we conclude that both $I(t)$ and $q_o(t)$ can be quickly and reliably computed for trivial initial and boundary conditions with (6.45) and (6.46) or (6.73) and (6.74), respectively. The value of S is advantageously obtained using the approximate expression of Parlange (1975)

$$S^2 \approx \int_{\theta_i}^{\theta_s} (\theta_S + \theta - 2\theta_i) D(\theta) d\theta \tag{6.75}$$

or the iterative procedure described by Philip and Knight (1974) or by White (1989) for the solution of (6.51).

From the authors' experience, increasing the number of parameters brings a theoretical improvement especially when soil hydraulic characteristics are evaluated from infiltration tests. For example, if we deal with approximate equations based upon the infinite series solution, the truncation error is reduced with an increased number of terms. However, equations with three or more parameters are more vulnerable to the field soil not being homogeneous and the boundary conditions deviating from the trivial ones assumed in the theoretical development. This vulnerability is realized when a number of physically non-realistic parameters are obtained (e.g. a negative value of K_S in the inverse solution).

6.2.2.4 Empirical Equations

Historically, empirical equations have been used to describe a decreasing infiltration rate q_o as a function of time t. The shape of a smooth curve drawn through measured values of $q_o(t)$ was simply compared with that of an analytic function. Inasmuch as both equations and experiments were empirical, it is useless to try to physically interpret the coefficients of the equations. The coefficients have the character of fitting parameters only with no scientific merit (Haverkamp et al., 1988, and Kutflek et al., 1988). On the other hand, because of their popularity in the literature and their usage persists, we briefly present them here.

Kostiakov's (1932) equation of $q_o(t)$ is the hyperbola

$$q_o = c_1 t^{-\alpha} \tag{6.76}$$

with

$$I = \frac{c_1}{1-\alpha} t^{(1-\alpha)} \tag{6.77}$$

where c_1 and α are empirical coefficients. The value of c_1 should equal q_{o1}, the infiltration rate at one unit of time (usually 1 min), and $0 < \alpha < 1$. The equation does not describe infiltration at large times inasmuch as $q_o \to 0$ when $t \to \infty$. Mezencev (1948) overcame this inconvenience by shifting the q_o-axis

$$q_o = c_2 + c_3 t^{-\beta} \tag{6.78}$$

with

$$I = c_2 t + \frac{1}{1-\beta} c_3 t^{(1-\beta)} \tag{6.79}$$

where c_2, c_3 and β are empirical coefficients. With the shift, as $t \to \infty$, $c_2 \to q_{oc}$, the constant infiltration rate when quasi-steady infiltration is reached, and hence, $q_{oc} \approx K_S$. The infiltration rate after the first time unit $q_{o1} = (c_2 + c_3)$.

Horton's equation (1940) represents an exponential decay of $q_o(t)$

$$q_o = c_4 + c_5 \exp(-\gamma t) \tag{6.80}$$

with

$$I = c_4 t + \frac{c_5}{\gamma}\left[1 - \exp(-\gamma t)\right] \tag{6.81}$$

where c_4, c_5 and γ are empirical coefficients. In contradiction to the theory of

infiltration for a DBC, q_o has a finite value at $t = 0$. As $t \to \infty$, $c_4 \to q_{oc}$ which yields a value of $c_4 \approx K_S$. With this approximation for K_S, the value of $c_5 = [q_o(0) - K_S]$ where $q_o(0)$ is q_o at $t = 0$. Inasmuch as Horton derived his equation for infiltration of a high intensity rainfall, the physical objection against a finite value of $q_o(0)$ is largely eliminated as we shall see in the next section.

Holtan's equation (1961) for a decay of q_o with I is

$$q_o = c_6 (W - I)^{\varepsilon} + c_7 \tag{6.82}$$

where c_6, c_7 and ε are empirical coefficients, $c_7 = q_{oc}$, W is soil water storage above an impeding layer and ε, not an integer, is most frequently greater than unity. Equation (6.82), incorporated into the USDA Hydrograph Laboratory model USDAHL, has empirical coefficients related to the soil mapping units in USA (Holtan and Lopez, 1971).

6.2.3 Unsteady Infiltration, Neuman's Boundary Condition (NBC)

When we describe rainfall infiltration, we consider that the REV is defined at the Darcian scale. Therefore, we do not describe individual raindrop events, but consider the rain as a continuous flux with the intensity of the rain q_r being the flux density passing either totally or at least partially through the surface of the soil. The boundary condition at $z = 0$ and $t \geq 0$ is formulated by the Darcy-Buckingham equation (5.31)

$$q_o = -K \frac{\partial H}{\partial z} \tag{6.83a}$$

or in diffusivity form (5.69)

$$q_o = K(\theta) - D(\theta) \frac{\partial \theta}{\partial z}. \tag{6.83b}$$

Condition (6.83), called Neuman's boundary condition, describes not only rainfall infiltration, but infiltration caused by sprinkler irrigation or by a special flux controlled technique, e.g. by a peristaltic pump providing a constant flux through a membrane placed upon the soil surface. For drip irrigation, we have a 2-dimensional problem with boundary conditions appropriately modified. Field measurements of infiltration with boundary conditions (6.83) are usually performed with rain simulators, see a review of Amerman (1983). Nozzles or hypodermic needles are used to produce drops similar to raindrops at a certain height above the soil surface. Regardless of how boundary condition (6.83) is achieved, the initial condition is kept the same as that for the DBC.

6.2.3.1 Description of the Process

We denote this description into the three categories (i) constant rain intensity $q_r > K_S$, (ii) constant rain intensity $q_r < K_S$ and (iii) rain intensity $q_r(t)$. In all three categories soil water profiles $\theta(z)$ at intermediate times do not resemble $\theta(z)$ during early stages of infiltration. The distinguishing feature is that the soil water content $\theta_o(t)$ increases at the surface with time.

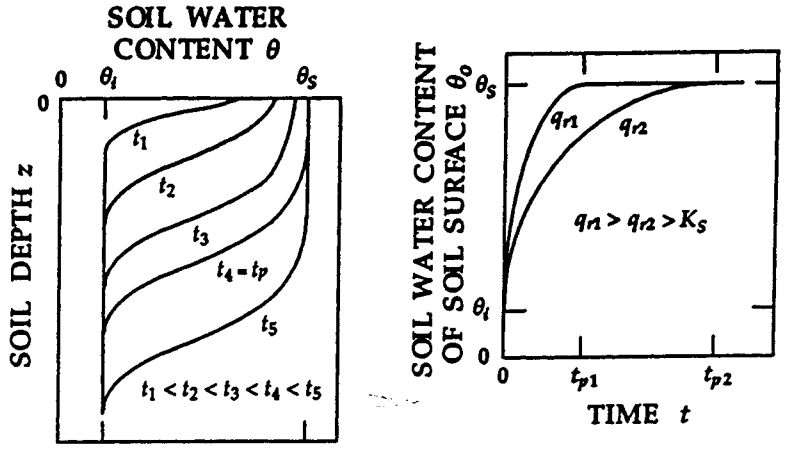

Figure 6.18. Constant rainfall infiltration with rain intensity $q_r > K_S$. Soil water content profiles $\theta(z, t)$ on the left, and the soil water content of the soil surface $\theta_o(t)$ increasing with time on the right. Note that ponding time t_p depends upon q_r.

Constant rain intensity $q_r > K_S$. The value of the soil water content of the surface θ_o increases steeply with time until it reaches θ_S, see Fig. 6.18. The greater is q_r, the steeper is $\theta_o(t)$. If rain continues, water ponds on the surface and the start of ponding is called ponding time t_p. If surface runoff is prevented, the depth of water on the surface $h_o(t)$ increases with time and $h_o > 0$ for $t > t_p$. With the increase of h_o being time dependent, $dh_o/dt < q_r$. The shape of the soil water profile at $t < t_p$ depends upon both q_r and the hydraulic functions of the soil, see Fig. 6.22. For $t = t_p$ the thickness of the saturated zone L_f extending below the soil surface is (Rubin and Steinhardt, 1964)

$$L_f = a\left(\frac{h_A K_S}{q_r - K_S}\right) \tag{6.84}$$

where a is an empirical parameter. For $t \geq t_p$ the soil water profile $\theta(z, t)$ resembles the profile with a DBC, i.e. with water ponded on the soil surface. Hence, we specify the boundary conditions as follows

$$q_r = K(\theta) - D(\theta)\frac{\partial\theta}{\partial z} \qquad z = 0 \qquad 0 < t < t_p \tag{6.85}$$

$$\theta = \theta_S \qquad z = 0 \qquad t \geq t_p \tag{6.86}$$

or, more exactly

$$h = 0 \qquad z = 0 \qquad t = t_p \tag{6.87}$$

and either

$$h = 0 \qquad z = 0 \qquad t > t_p \tag{6.88}$$

or

$$h = h_o(t) \qquad z = 0 \qquad t > t_p \tag{6.89}$$

Ponding time t_p separates the infiltration event into two different periods. The first is governed by the NBC (6.85) while the second is governed by the DBC (6.86) or (6.87) to (6.89).

Constant rain intensity $q_r < K_S$. For the entire duration of infiltration, the flow is governed by NBC (6.85) where the term t_p does not exist. On the soil surface the value of q_o is alwys less than that of q_S and hence, t_p cannot appear.

For *non-constant rain intensity* $\theta_r(t)$, we formulate the functional dependence $\theta_r(t)$ in the NBC (6.85).

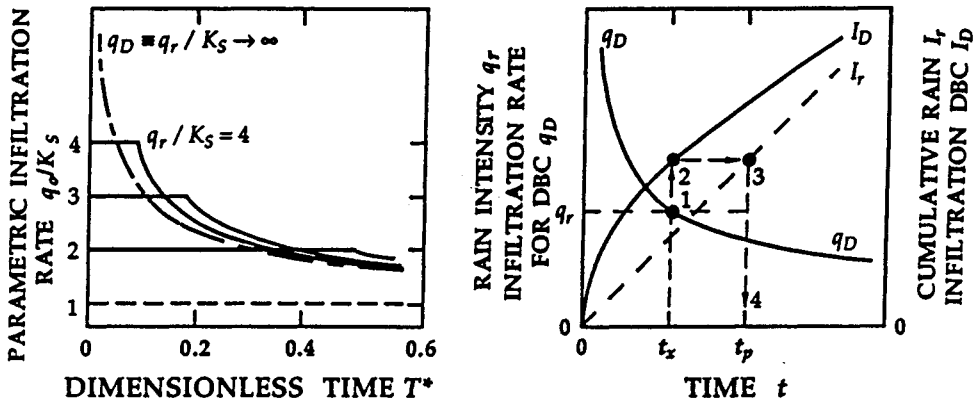

Figure 6.19. Infiltration rate versus time for several constant rainfall intensities $q_r > K_S$ *(left). The estimation of ponding time* t_p *for a given* q_r *when infiltration rate* q_D *and cumulative infiltration* I_D *for DBC are known (right).*

6.2.3.2 Approximate Solutions

Constant rain intensity $q_r > K_S$. For an approximate intuitive derivation of t_p we compare infiltration for a DBC with that for a NBC. The parameters will be indexed by D for DBC and by N for NBC. Rubin (1966) has shown that the ponding time t_p decreases with an increase of q_r and that $t_p > t_x$ where t_x is the intersection of q_r and q_D, see Fig. 6.19. In order to satisfy boundary conditions (6.85) and (6.86) as the NBC transforms to DBC, we assume the soil water profiles $\theta(z, t_p)_N$ and $\theta(z, t_x)_D$ are identical. Hence, we are searching t_x and t_p which satisfy two conditions. The first one is $I_N(t_p) = I_D(t_x)$, or

$$\int_0^{t_p} q_r(t)\,dt = \int_0^{t_x} q_D(t)\,dt. \tag{6.90}$$

The second condition is

$$q_r(t_p) = q_D(t_x) \tag{6.91}$$

and for a constant value of q_r we obtain

$$t_p = \frac{1}{q_r}\int_0^{t_x} q_D(t)\,dt \tag{6.92}$$

where t_x is the time at which q_r and q_D intersect. Graphical interpretation of (6.90) and (6.91) is given in Fig. 6.19. With $q_D(t)$ expressed by Philip's approximate algebraic equation (6.68), we obtain

$$t_p = \left(\frac{S}{A}\right)^2 \frac{2Q_r^* - 1}{4Q_r^*\left(Q_r^* - 1\right)^2}. \tag{6.93}$$

where $Q_r^* = q_r/A$. By approximating $F(\theta_R) = \theta_R$, Kutflek (1980) also analytically derived this equation, see section 6.2.3.3. Similarly, $q_D(t)$ from other approximate solutions can be used to calculate t_p.

At $t \leq t_p$ the infiltration rate $q_o = q_r$. At $t > t_p$ the infiltration rate can be approximated by shifting $q_D(t)$ by $(t_p - t_x)$. With (6.92) and with

$$t_x = \left(\frac{S}{A}\right)^2 \frac{1}{4\left(Q_r^* - 1\right)^2} \tag{6.94}$$

we obtain the infiltration rate $q_o(t)$ for $t > t_p$

$$q_o = \frac{1}{2} S \left[t - \frac{S^2}{4A^2 Q_r^*\left(Q_r^* - 1\right)}\right]^{-1/2} + A. \tag{6.95}$$

All of the above approximations as well as many others in the literature have two disadvantages. First, the equality $I_N(t_p) = I_D(t_x)$ is just an assumption teoretically derived by Mls (1980) and the same is for post-ponding infiltration rates when they are computed as simple translations of the rate q_D. Second, the simple explicit formulation of $q_D(t)$ is, in reality, only an approximation. Therefore, the purpose of our above discussions was to illustrate as simply as possible the nature of infiltration under two different boundary conditions. The equations can be used for rough engineering estimations provided that the soil surface quality is not altered during the process, see section 6.2.4.1.

Constant rain intensity $q_r < K_S$. Here, the value of the soil water content on the surface $\theta_o(t)$ increases similarly to the first case but its limiting value is $\theta_f < \theta_S$. Inasmuch as $dH/dz \rightarrow -1$ at the soil surface as $t \rightarrow \infty$, we obtain a quasi-steady infiltration rate $q_o \equiv q_r = K(\theta_f)$. And, the value of $\theta_o(t)$ approaches θ_f asymptotically in time, see Fig. 6.20. The shapes of the soil water profile vary with both time and infiltration rate. In Fig. 6.22 we see the importance of the hydraulic characteristics of the soil for a constant infiltration rate at different times. This example from Broadbridge and White (1988) is for two different forms of the SWRC which are derived from the solution having an empirical coefficient C. The influence of the value of C upon the shape of the SWRC is shown in Fig. 6.22. The details of the solution are described by the authors.

Non-constant rain intensity $q_r(t)$. When $q_r(t)$ is strongly time dependent as it is in a great majority of heavy rainfalls, we obtain an estimate of t_p using the procedure described for a constant value of $q_r > K_S$. Note that t_x is no longer the intersection of $q_r(t)$ with $q_D(t)$ as it was derived for constant rain intensity infiltration. Equations (6.90) and (6.91) can be solved iteratively. Or, if $q_r(t)$ is capable of being expressed as a probability distribution function, we can solve them analytically. Regardless of the procedure, we recall that the solution remains only an approximation owing to the use of $q_D(t)$. Figure 6.21 shows the example of the graphical solution of (6.90) and (6.91) for ponding time t_p. By simply shifting q_D by $(t_p - t_x)$ we obtain estimates of the infiltration rate for $t > t_p$ and the hydrologically effective rainfall. The same priciple was applied for a

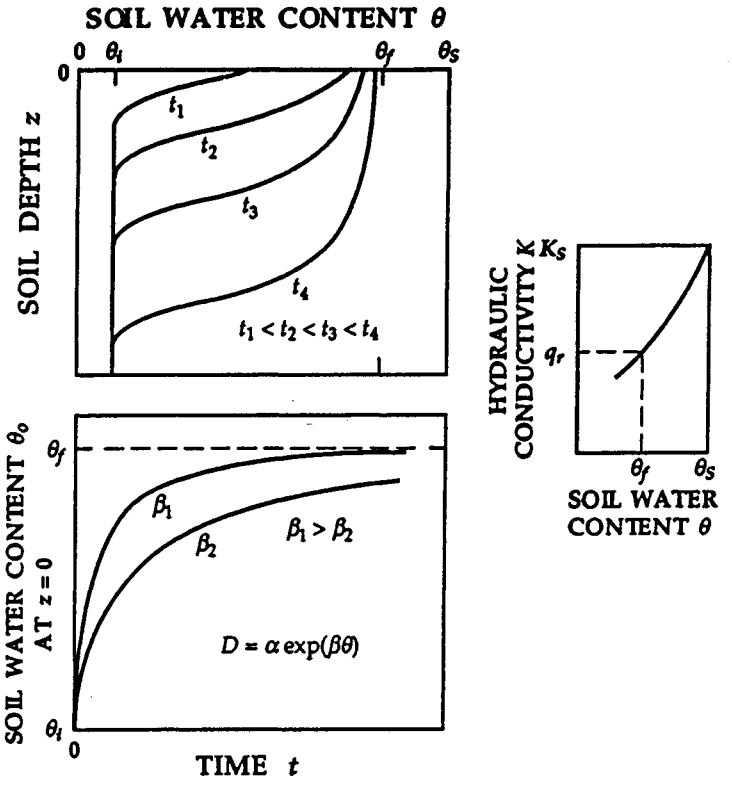

Figure 6.20. Constant rainfall infiltration with rain intensity $q_r < K_S$. Soil water content profiles $\theta(z, t)$ on the top. Soil water content of the soil surface $\theta_o(t)$ increasing with time on the bottom. The asymptotic value of θ_f at $t \to \infty$ follows from the condition $K(\theta_f) = q_r$.

histogram of rainfall intensity. Details regarding the construction or computation are described by Peschke and Kutflek (1982).

White et al. (1989) proposed the approximate analytic solution

$$t_p = \frac{1}{\bar{q}_r} M \frac{S^2}{K_S} \ln\left[\frac{q_r(t_p)}{q_r(t_p) - K_S}\right] \tag{6.96}$$

where $\bar{q}_r$ is the mean q_r during the time interval $(0, t_p)$ and $0.5 \le M \le 0.66$. More than a decade earlier Parlange and Smith (1976) had derived a very similar expression. Both expressions have features like those of the Green and Ampt solution. In order to avoid redistribution, these expressions require $q_r(t)$ not to decrease, see section 6.3.

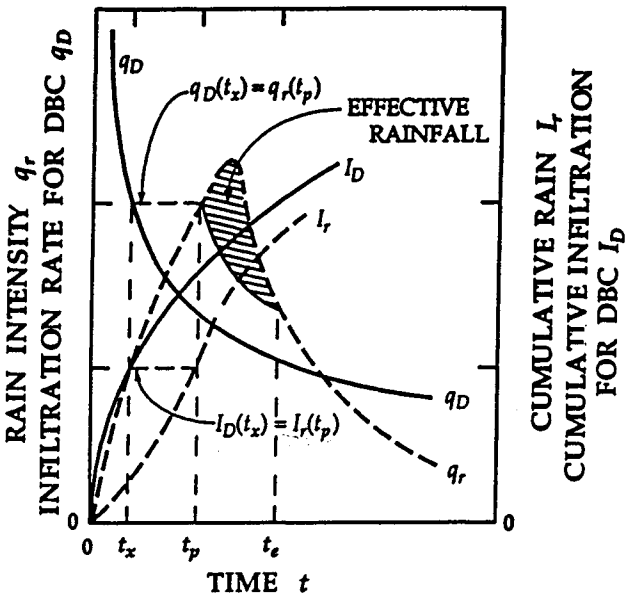

Figure 6.21. Time-dependent rainfall infiltration. Equations (6.90) and (6.91) were applied for estimating the ponding time t_p. With the exception of the time interval $(t_p - t_e)$, the actual infiltration rate equals the rain intensity $q_r(t)$ if the excessive rain runs off. For $t_p < t < t_e$ the infiltration rate is obtained by shifting $q_D(t)$, i.e. the DBC infiltration rate.

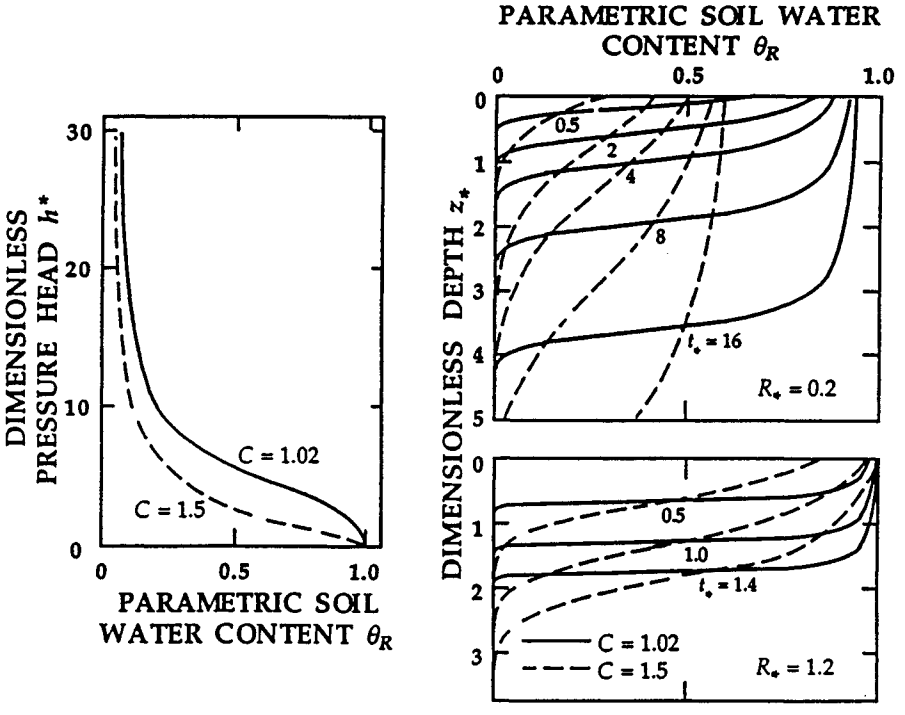

Figure 6.22. Dimensionless soil water content profiles for two rain intensities q_r expressed as $R_* = (q_r - K_i)/(K_S - K_i)$ and for two different soils characterized by the parameter C in the SWRC of Broadbridge and White (1988).

6.2.3.3 Analytical Solutions

If we neglect early approximate solutions based upon the Green and Ampt approach (e.g. Mein and Larson, 1973), four scientists eventually achieved an analytical solution for t_p. Parlange (1972) provided the initial effort which was subsequently modified by Philip (1973) and by Philip and Knight (1974). Philip and Knight utilized the concept of "flux concentration relation" [for convenience, (6.52) is repeated here]

$$F(\theta_R, t) = \frac{q - K_i}{q_o - K_i}$$

and neglected its time dependence which is even weaker than that for the DBC. When the above expression for $F(\theta_R, t)$ is inserted into the diffusivity form of the Darcy-Buckingham equation (5.69)

$$q = -D(\theta)\frac{\partial \theta}{\partial z} + K(\theta) \tag{6.97}$$

we obtain with $q_o = q_r$

$$F(\theta_R)(q_r - K_i) - [K(\theta) - K_i] = -D(\theta)\frac{\partial \theta}{\partial z}. \tag{6.98}$$

Integrating from $z = 0$ yields

$$z = \int_{\theta_i}^{\theta_o(t)} \frac{D(\theta)\, d\theta}{F(\theta_R)(q_r - K_i) - [K(\theta) - K_i]} \tag{6.99}$$

where $\theta_o(t)$ remains unknown. Integrating the equation of continuity (5.62) with q_r constant between the limits $(0, t)$ and $(0, z)$ gives

$$-(q_r - K_i)t = \int_{\theta_o(t)}^{\theta_i} z\, d\theta. \tag{6.100}$$

Combining (6.99) and (6.100) and integrating leads to

$$(q_r - K_i)\, t = \int_{\theta_i}^{\theta_o(t)} \frac{(\theta - \theta_i)\, D(\theta)\, d\theta}{F(\theta_R)(q_r - K_i) - [K(\theta) - K_i]}. \tag{6.101}$$

From (6.101) the evolution of the water content of the soil surface $\theta_o(t)$ is ascertained. When we know θ_o for a particular time t, we compute the soil water profile $\theta(z)$ from (6.99). If $q_r > K_S$ we compute the ponding time t_p from (6.101)

$$t_p = \frac{1}{q_r - K_i} \int_{\theta_i}^{\theta_s} \frac{(\theta - \theta_i)\, D(\theta)\, d\theta}{F(\theta_R)(q_r - K_i) - [K(\theta) - K_i]}. \tag{6.102}$$

A detailed step-by-step development of the procedure shows that the authors treat component equations of the Richards' equation and integrated the Darcy-Buckingham equation by using a guessed shape of the flux concentration relation $F(\theta_R)$.

Proper judgment for an appropriate value of $F(\theta_R)$ is critical. Philip's (1973) calculations of $F(\theta_R)$ for horizontal infiltration into linear and δ-function soils lead to approximations for early stages of infiltration limited to values of $q_r \gg K_S$. Another approximation for a constant flux infiltration was found assuming $F(\theta_R) = \theta_R^n$ with $0.8 \leq n \leq 1$ (Kutflek, 1980, Perroux et al., 1981, and Boulier et al., 1984). In general, errors associated with the uncertainty in $F(\theta_R)$ are less than those owing to our uncertainty in estimating $D(\theta)$. Considering the

joint development of (6.102), the procedure should be called the Parlange-Císler-Philip-Knight (PCPK) method' see our introductory remarks and comments to (6.44) and (6.47).

Morel-Seytoux (1982) also provided an acceptable approximation for a constant intensity rainfall. For a variable rainfall his solution is restricted to soils having $K/K_S = \theta_R^n$ and to that initial part of a rainfall when its intensity is increasing with time. His method cannot be applied to the receding part of rainfall inasmuch as the procedure does not consider θ_0 decreasing as water redistributes within the profile. Generally, infiltration stemming from a variable rainfall can only be accommodated by numerical procedures.

The most versatile analytical solution of constant rate infiltration was published by Broadbridge and White (1988). They allowed the soil hydraulic functions to exist in broad limits between those of linear and δ-function soils. The hydraulic functions typical of real soils are expressed by a simple, free parameter C which is easily measured in the field. A detailed description of the procedure involving Kirchoff, Storm, Hopf and Cole and Laplace transformations is beyond the scope of this book. Their strictly analytical solution in parametric form given in Fig. 6.22 is most useful for testing numerical schemes. Moreover, the application of their solution to practical examples contributed to our knowledge of infiltration discussed in the previous section.

Numerical solutions have been reviewed by Vauclin et al. (1979) and van Genuchten (1981). Among improvements provided in the last decade are those of Mls (1982).

6.2.4 Field Infiltration

When field infiltration tests are performed and evaluated, we meet a complex set of effects not fully accounted for by exactly defined infiltration equations. These effects more or less influence the observed data and the applicability of infiltration theory to runoff hydrology, irrigation and other practical domains involving infiltration. Some of these effects will be discussed.

6.2.4.1 Soil Sealing and Crusting

During *ponded infiltration* tests (DBC), the abrupt contact of the soil surface with excess water causes weak aggregates to disintegrate and slake. The migrating smaller particles quickly form a seal on the soil surface within a short period of only a few minutes. The slaked clay particles are gel-like and exhibit a thixotropic behavior not yet fully studied in detail. We expect in the presence of mono-valent cations that this peptization of clays leads to the separation of individual sheets of clay minerals that subsequently reorient into horizontal, parallel configurations that tend to seal the soil surface causing an extremely small value of K_S. Bi-valent cations allow the clay sheets to remain coagulated and in a face-to-edge configuration. Hence, the value of K_S of the seal for bi-

Extension of 6.2.4.

For field infiltration we have assumed a continuous and distinct wetting front in accordance with the assumed homogeneous porous system. If the bi-modal porous system is typical for a given soil, we have to apply a model corresponding to Fig. 2.20 and the resulting invasion percolation is different from the assumed developments of soil water profiles and wetting front in homogeneous porous system, see Fig. 6.22a

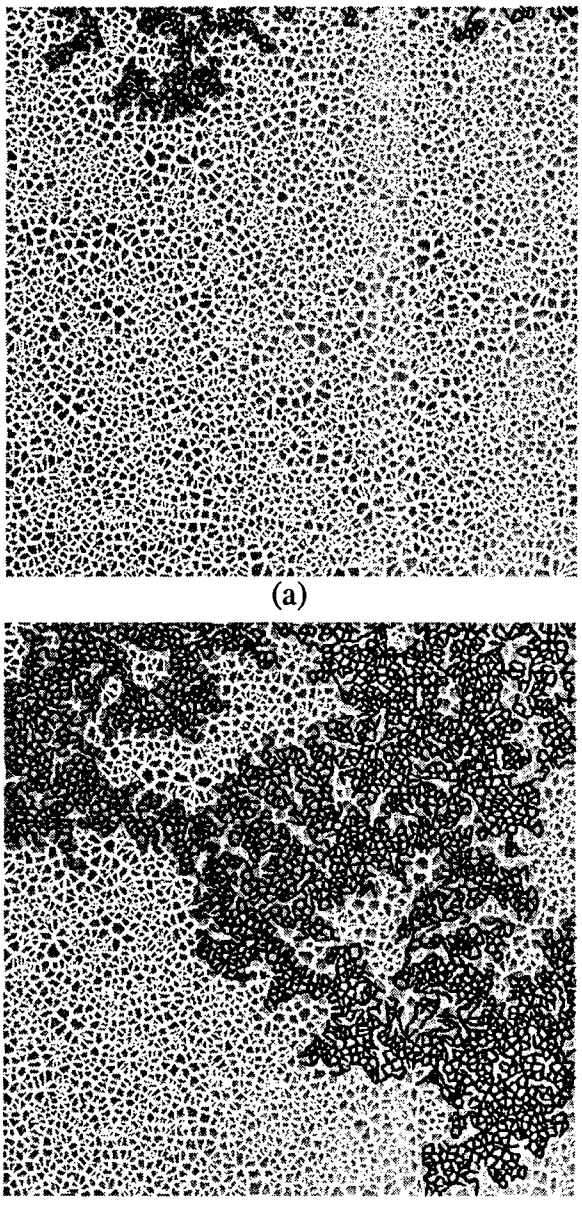

(a)

Figure 6.22a: Infiltration demonstrated as invasion percolation of water into porous systm modeled by Fig. 2.20.

Generally, we meet often **preferential flow**

Three types of preferential flow are detected in some field situations:

1. In soil porous system due to soil micro- and macro-morphology.
2. Fingering mainly due to instability on the wetting front.
3. Irregularities in hydrophility.

1.1. Preferential flow in interaggregate (interpedal) pores, i.e. category of soil pores 2.2.: If saturated hydraulic conductivity of matrix is K_S = 1, then matrix plus interaggregate K_S = approx. 10^2. Unsaturated flow in matrix is negligible in the first approximation. This type of preferential flow is sometimes misinterpreted as flow in macropores.

1.2. Preferential flow in macropores, i.e. Category 3. K_S is by one order or more greater than in saturated micropores. Unsaturated flow does not exist. Flow in cracks reaches to the depth 100 cm maximum. In biopores it reaches usually below the pedogenetic depth.

Partial review of the problem is in a serie of papers of Ju et al. (1997). However, there is a mess in terminology and definitions. It is frequent that the flow in category 2.2 of pores is denoted as flow of mobile water, while the water in the category 2.1. is named immobile water. Flow in 2.2 is named funnel flow, too.

2. Preferential flow due to fingering

A wide variety of instabilities may occur when flow of water is realized in porous media. Most frequently, they are driven either by viscous and gravity forces. Gravity driven instabilities are related to infiltration and redistribution of water in soil. The linear stability analysis suggests that the water-air interface will be unstable if its velocity is less than the saturated conductivity of the medium. This wetting front instability results in formation of fingers where the transport of water (and solutions) is realized.

The hydrodynamic instability of flow in unsaturated soil may take place due to the soil stratification and the imposed initial and boundary conditions. It is observed when hydraulic conductivity increases with depth and the fluid meets an interface of great variation of K i.e. from a smaller value (fine texture soil, or compacted upper layer) to a greater value of K (coarse texture soil, or loose sublayer). The Richards´eq. which usually describes the transport of water, assumes the validity of the hypothesis on wetting front stability. As this condition is not met, the mentioned equations are not applicable. Due to the instability of the front, narrow zones, „fingers" of nearly saturation, or of increased water content are formed ahead of remaining wetting front and these fingers are protruded in time. They occur not only during infiltration, but they have been observed in redistribution, too. Fingers are domains of preferential flow. Studies on fingering have been carried out through visual observations, light transmission, immage processing and magnetic resonance imaging, see Onody et al. (1995), Fig. 6.22b.

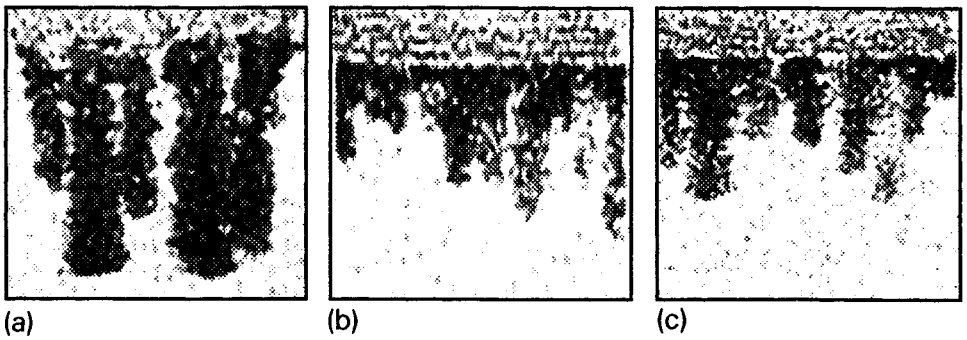

Fig. 2. Images obtained with the MRI system, showing three transverse sections of the fingering phenomenon in steady-state conditions. Each section represents a slice, 2.0 cm thick, 15.0 cm wide and 14.5 cm high, of the cubic soil column, $15 \times 15 \times 15$ cm^3. We can clearly notice the spatial variability of the phenomenon in these three images. In (a) the fingers are close to the bottom of the box. In (b) and (c) they are close to the central part of the cubic column; still halfway to the bottom (Posadas, 1994).

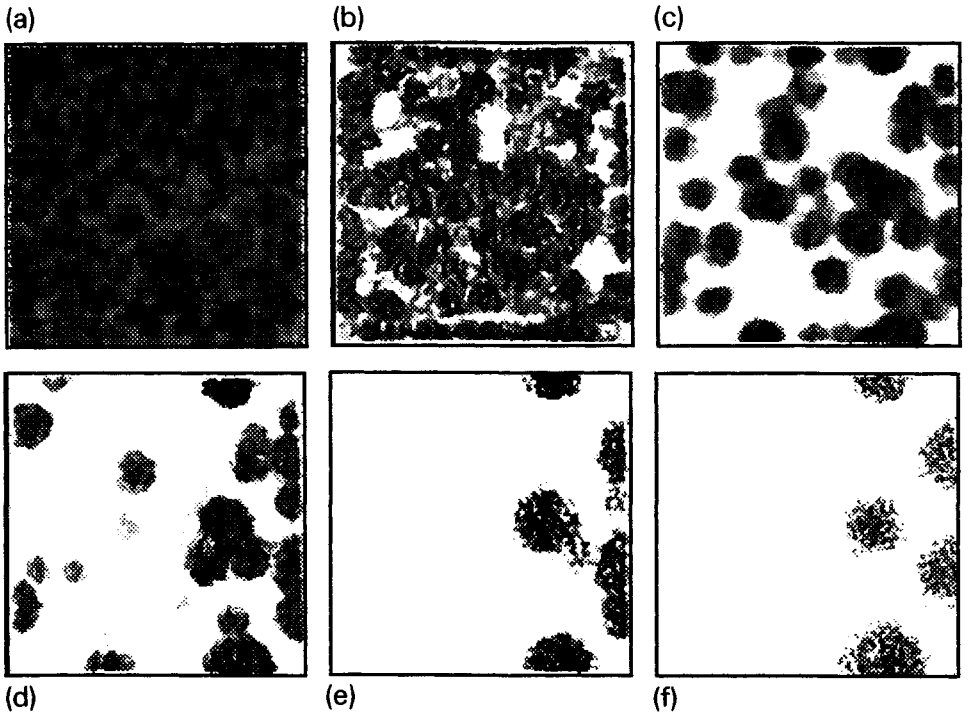

Figure 6.22b: Fingering in soil column consisting of top less permeable layer above more permeable layer.

Parameters of fingers, as d_F - finger diameter, q_F - average flux in the finger are dependent upon K_S, sorptivity S, and θ_S, θ_i, saturated and initial soil water content.

Theory of fingering is related to the geometry of porous media. With fractal characterization of fingering two type of models were created: Diffusion limited aggregation and Invasion percolation model, for quotation see Onody et al. (1995) and see Fig. 6.22a, too.

3. Irregularities in hydrophility

Dry soil of high organic content and peats are known to inhibit water infiltration, ultimately forcing water to flow via preferential paths through unsaturated vadose zone. Important is the value of critical soil water content θ_{CR}. If actual $\theta < \theta_{CR}$, the soil behaves as water repellent, i.e. hydrophobic with high value of the wetting angle above 90°. With water-entry value of the boundary wetting branch beneath the air entry value of the main drainage branch, perturbations occur leading to formation of fingers, Fig. 6.22c. (Ritsema and Dekker,1994, Ritsema, 1998). The observed fingering was up to now restricted to sandy soils with high organic matter content.

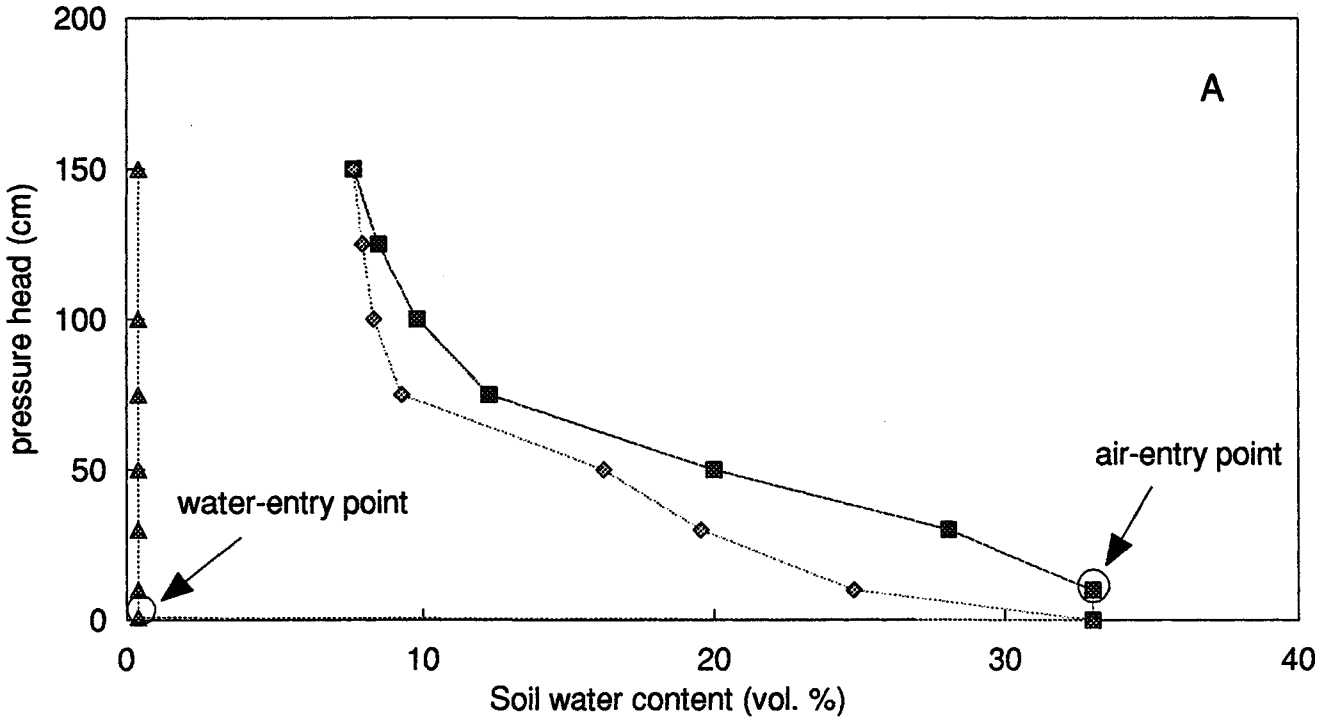

Figure 6.22c. Hysteretic water retention curve of the water repellent soil

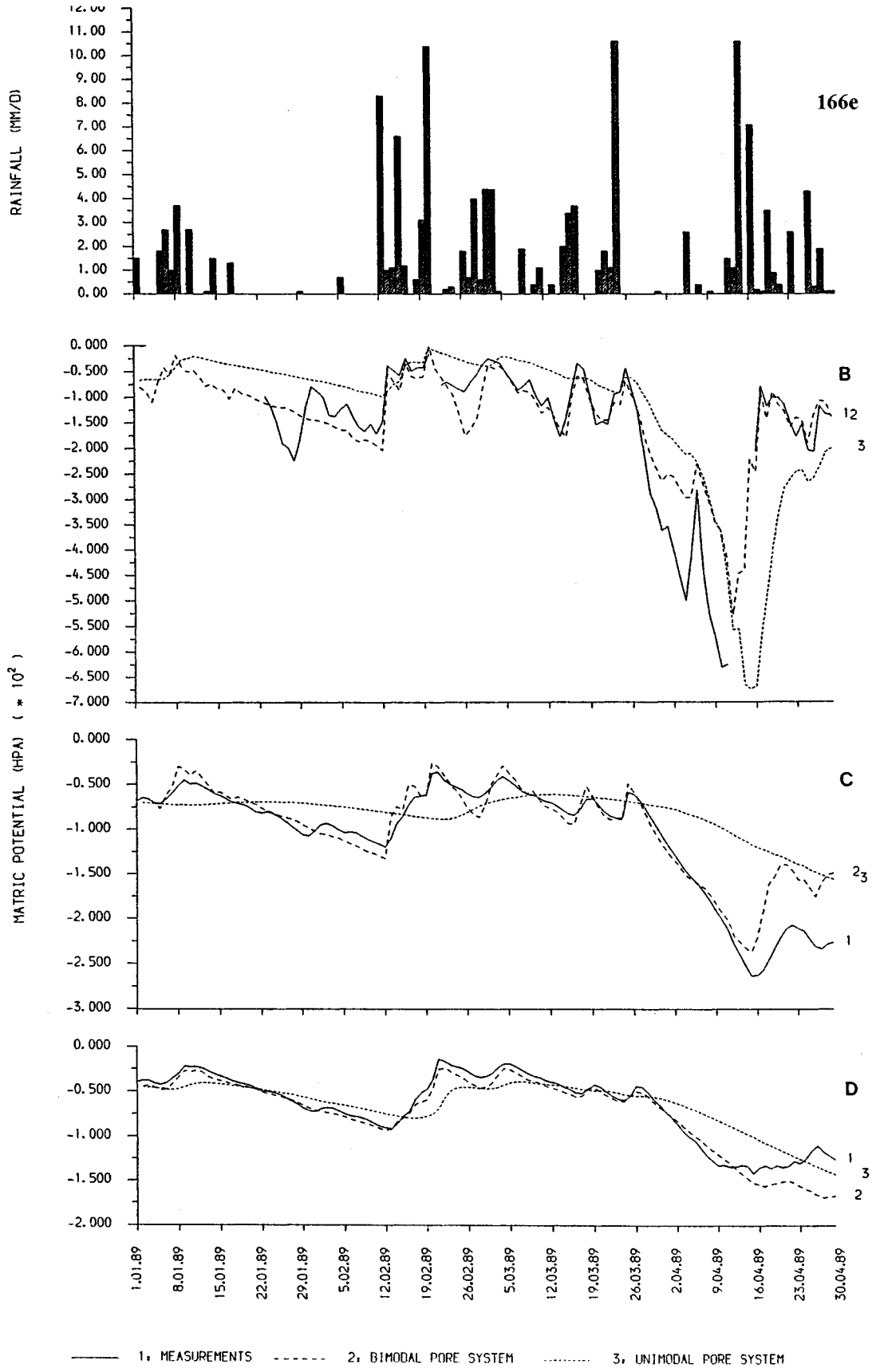

Figure 6.22d. Differences in h(t) seazonal development: 1. Denotes measured data, 2. Computed data with bi-modal model, 3. Computed data with monomodal model (Othmer et al., 1991)

valent cations is larger than that for mono-valent cations, but nevertheless orders of magnitude less than that of the original soil. The value of K_S of the seal and its thickness are both time dependent. The formation and quality of this seal are major factors responsible for the difference in infiltration rates between structured and structure-less soils, see Fig. 6.23. Surface sealing is not a rare phenomenon - indeed, it occurs with virtually all arable soils during ponded infiltration.

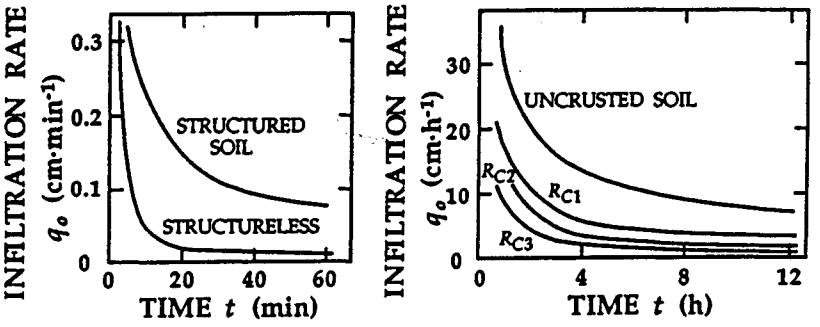

Figure 6.23. Infiltration rate $q_o(t)$ for DBC into a structured and structureless luvisol on loess (left) and $q_o(t)$ for a soil with different resistances (R_{C1} = 1, R_{C2} = 9.1 and R_{C3} = 17 d) on the surface (right) for a loess soil (Hillel and Gardner, 1970).

During *rainfall infiltration*, the slaking of aggregates is enhanced by the kinetic energy of the raindrops. The impact of raindrops upon the soil surface can be compared to a micro-bombardment. The drop after hitting the soil forms a micro-crater with some of the segregated fine soil particles relocating to clog pores and the remainder washed deeper into the soil with the infiltrating water. Inasmuch as the ponding time differs from one point to another, suspended clay particles are transported to small puddles and unevenly deposited across the soil surface. During the subsequent dry period after the rain, the newly formed seal consolidates and forms a crust. With repetitive rainfalls the process of sealing and crusting eventually forms a crust-topped soil. For such a soil crust, McIntyre (1958a and 1958b) defined two layers - a compacted thin layer called a skin and a less dense "washing-in layer". For an originally undisturbed soil having a value of K_S = 36 mm·h^{-1}, he reported a 0.1 mm thick skin having a K_S = 0.018 mm·h^{-1} and a 1.5 to 2.5 mm "washing-in layer" having a value of K_S = 0.115 mm·h^{-1}.

Mualem et al. (1990) defined two types of crusts. *Depositional crusts* are formed by fine particles settling from a suspension reaching a depositional site. The scale of this type of crust is related to the scale of observation. *Structural crusts* are caused by the destruction of soil aggregates exposed to the direct impact of raindrops as we discussed in the paragraph above.

Soil surface seals have relatively large values of bulk density ρ_T. The rate of increase of ρ_T depends upon the kinetic energy of the rain, nature of the soil and its aggregates and initial values of bulk density ρ_{Ti}. The smaller is ρ_{Ti}, the larger is the rate of change of $d\rho_T/dt$. Similar relations hold for K_S and other hydraulic functions of the seal.

Seal formation is more dependent upon rainfall energy than upon cumulative rainfall. Rainfall energy is closely correlated with rain intensity. The kinetic energy of rain which induces seals and crusts ranges from about 0.1 $J \cdot s^{-1} \cdot m^{-2}$ for a rain intensity q_r of about 0.3 $mm \cdot min^{-1}$ to 1.2 $J \cdot s^{-1} \cdot m^{-2}$ for $q_r \approx 2.5$ $mm \cdot min^{-1}$.

Once a seal is developed by a rain event, the physical properties of the seal are usually sustained. Repeated high intensity rainfall or sprinkler irrigation forms deleterious, undesirable crusts in the majority of agricultural soils. For example, below a 5 mm thick surface crust, Passerat de Silans et al. (1989) measured values of $\rho_T = 1.32$ $g \cdot cm^{-3}$ and $K_S = 1.3 \cdot 10^{-4}$ $m \cdot s^{-1}$. Within the crust $\rho_T = 1.45$ $g \cdot cm^{-3}$ and $K_S = 2.8 \cdot 10^{-6}$ $m \cdot s^{-1}$. Similar examples are reported in the literature, e.g. Callebaut et al. (1985). With the nature and extent of soil crusts being highly variable, their behavior falls between the one extreme of manifesting an earlier developed, constant hydraulic resistance and the other extreme of a gradually increasing hydraulic resistance as a seal develops during rainfall on an originally crust-free soil.

6.2.4.2 Infiltration into Crust- and Seal-Topped Soils

The first solution of infiltration into a soil profile having a surface seal of constant hydraulic resistance $R_1 = L_1/K_{S1}$ was proposed by Doležal and Císler (1969) assuming the Green and Ampt approximation, see (6.53). Analogous to (6.63) we obtain

$$\frac{dL_f}{dt}\Delta\theta = \frac{K_{S2}\left(h_o - h_f\right) + K_{S2}L_f}{K_{S2}R_1 + L_f} \tag{6.103}$$

where index 1 is for the seal, index 2 for the homogeneous soil below the seal and L_1 is the thickness of the seal provided that $L_1 \ll L_f$. After integrating between the limits $(0, t)$ and $(0, L_f)$, and using dimensionless terms (6.65) with dimensionless resistance χ^* where

$$\chi^* = \frac{R_1 K_{S2}}{h_o - h_f} \tag{6.104}$$

we obtain analogous to (6.66)

$$t^* = I^* + \left(\chi^* - 1\right)\ln\left(1 + I^*\right) \tag{6.105}$$

which is graphically demonstrated in Fig. 6.24. The primary disadvantage of this and similar approaches is the error introduced by the simplified conditions $L_1 \ll L_f$ and $\theta_2 = \theta_{S2}$ at the interface. When the wetting front is in the vicinity of the interface between the seal and soil, the soil water content θ_2 immediately below the interface is time dependent, see also Fig. 6.25. A similar approach was later published by Hillel and Gardner (1970).

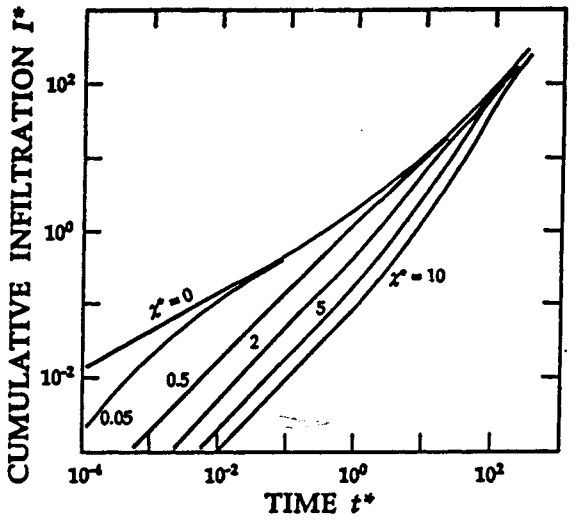

Figure 6.24. Dependence of dimensionless cumulative infiltration I^* upon dimensionless time t^* for DBC when the dimensionless resistance χ^* in (6.104) is defined on the soil surface (Doležal and Císler, 1969).

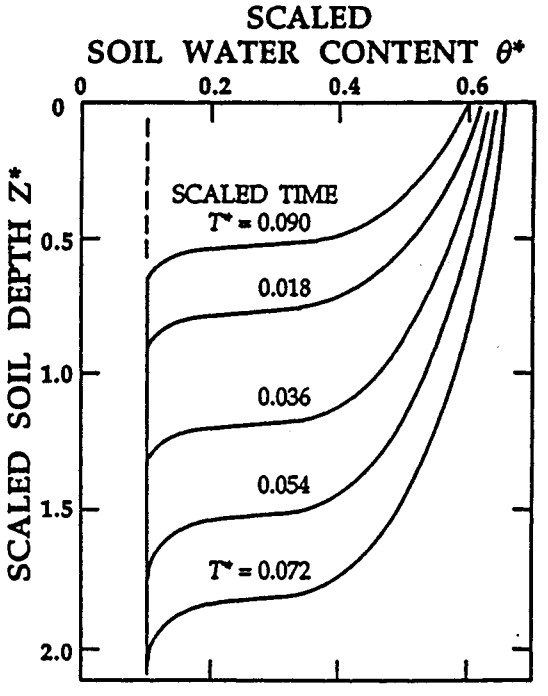

Figure 6.25. Infiltration into a silty clay loam with a seal for DBC. Soil water content profiles below the seal $\theta^*(Z^*, T^*)$ with scaled variables (Kutílek et al., 1991).

When the water capacity in the seal is neglected, the boundary condition at the seal-soil interface can be formulated as a Neuman boundary condition. Neglecting the seal thickness L_1 we write

$$q_o(t) = K(\theta) - D(\theta)\frac{\partial\theta}{\partial z} \qquad z = 0 \qquad t \geq 0 \qquad (6.106)$$

or

$$q_o(t) = -\frac{h(\theta) - h_o}{R} \qquad z = 0 \qquad t \geq 0 \qquad (6.107)$$

Here, the resistance transforms the original DBC to a NBC. The example in Fig. 6.25 (Kutflek et al., 1991) shows infiltration into a soil with a surface seal of resistance R. Water stored in the seal is neglected. The soil water profiles $\theta^*(Z^*,T^*)$ are typical for NBC, compare them with those in Fig. 6.20 or 6.22. We explain more about these scaled variables θ^*, Z^* and T^* in section 8.3.

For rain infiltration (i.e. for a Neuman boundary condition above the seal) a similar procedure leads to $\theta(z, t)$ analogous to that presented in Fig. 6.25. When the rain intensity $q_r > K_{S1}$, where K_{S1} is the saturated hydraulic conductivity of the crust, we obtain the reduced ponding time. The decrease of ponding time t_p with an increase of crust resistance R has a nearly exponential form. When R rises by one order of magnitude, the value of t_p may be reduced by nearly two orders of magnitude (Aboujaoude, 1991).

Up to now, we have considered approximate solutions of infiltration based upon the surface seal resistance being constant in time. However, rain-induced seals as well as their hydraulic functions are time dependent. Edwards and Larson (1969) observing an exponential decrease of K_{S1} (seal) with time during a high intensity rainfall proposed the following formulation of the saturated hydraulic conductivity of the seal

$$K_{S1}(t) = K_{SF} + (K_{So} - K_{SF})\exp(-\alpha E t) \qquad (6.108)$$

where K_{SF} is the final value of the saturated hydraulic conductivity of the seal (usually at the ponding time), K_{So} its initial value at the beginning of the rain (usually taken as K_{S2} of the underlying soil), E the energy of the rain and α a parameter which characterizes the susceptibility of the soil to seal formation including the eventual impact of water quality upon the slaking of the soil. Owing to the large, abrupt decrease in pressure head across the seal, microscopic bubbles of air released immediately below the saturated, compacted seal block the pores of the lower portion of the seal and contribute to a decrease in hydraulic conductivity of the seal. The effect of these bubbles is empirically included in the value of α. Inasmuch as the energy of the rain E is generally not measured, the term E is sometimes replaced by rain intensity q_r (and hence, $\alpha E = \alpha_1 q_r$) or the cumulative value of rainfall appears in the exponent. Inasmuch as the seal is almost instantaneously saturated with water at the beginning of the rainfall, other hydraulic functions of the seal are not needed for the infiltration solution.

Because the time dependency of $K_{S1}(t)$ of the seal shifts the ponding time t_p by only 10 to 20% compared with that for a soil manifesting a seal of constant hydraulic conductivity, the time dependency of a seal's hydraulic conductivity can often be neglected. Measurements and data collection should be aimed

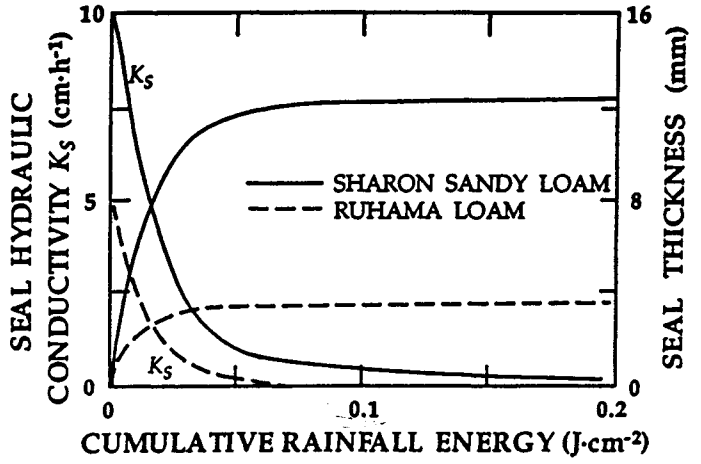

Figure 6.26. Hydraulic conductivity and seal thickness as functions of cumulative rainfall energy (Mualem et al., 1990).

primarily at the determination of K_{SF} in relation to the energy of the rain, see Fig. 6.26.

We denote the time dependency of the hydraulic conductivity of the seal described above as a short-time dependence. This short-time dependence of hydraulic functions of a soil wetted during infiltration remains more intuitive rather than being based upon exact evidence. In addition to a short-time dependence, a well-known large-time dependence of hydraulic functions exists mainly in the topsoil. The time scale of these changes embraces several months, an annual season or years. This large time infiltration variation is heavily dependent upon the plant canopy and the frequency and type of cultivation. Although the effects of cultivation appear to damp out after several months, the effect of root channels is more persistent (Gish and Starr, 1983).

6.2.4.3 Infiltration into Layered Soils

Infiltration is primarily dependent upon the relation of K in each of the layers to gradients of the respective pressure heads h. Let us consider infiltration under a NBC into a simplified profile consisting of only 2 layers: layer 1 on top is texturally finer than that of layer 2, e.g. loam over sand with $K_{S1} \ll K_{S2}$, where the indices 1 and 2 denote each of the layers. Because infiltration into a layered soil profile is dependent upon the relation $K(h)$, see earlier Fig. 5.9, the sandy sub layer, even if more permeable at saturation, behaves like a less permeable layer at $h < h_c$. As the wetting front approaches, the hydraulic gradient should increase at the interface of the two layers. The increase is realized through an increase of h at the bottom of layer 1 which is reflected by an increase of θ above the value θ_0 at the bottom part of layer 1, see Fig. 6.27. Although $h(z)$ is

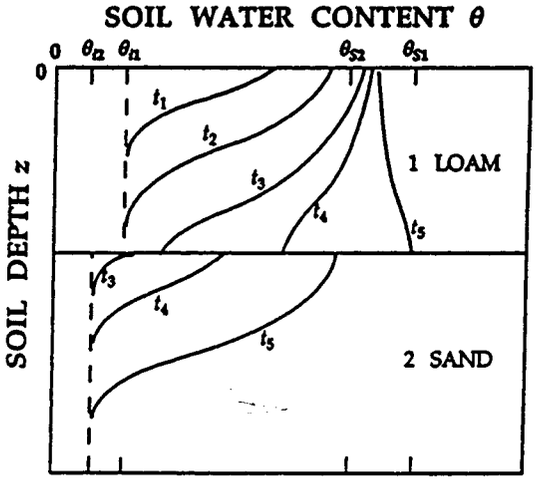

Figure 6.27. Soil water content profiles θ(z, t) for NBC-infiltration into a layered soil. At the interface between the layers, θ may reach θ_S in loam over sandy soil without saturation occurring at the soil surface.

continuous, θ(z) is discontinuous at the boundary of the layers. If indeed, there were a gravel layer instead of sand below the fine-textured topsoil, the water flux in these macropores and cavities would occur only if $h > 0$ above the interface.

This layering of a loam over a sand can also cause an instability of the wetting front visualized as finger-like wedges below a continuous wetting front during infiltration. The term fingering used by Hill and Parlange (1972) is commonly explained either by hydrodynamic instabilities (Diment et al., 1982) or by descriptive empirical approaches (Hillel and Baker, 1988). When the wetting front arrives at a textural or structural interface, h is too small in the upper layer to allow the entry of water into the coarse pores of the sub layer. As θ increases in the soil above the interface, h increases until it is large enough to allow water to enter clusters of fine pores of the sub layer, thus forming the nucleus of fingers. As the wetting front progresses, the average $\overline{h} > h_c$ with K_2 of the sub layer larger than K_{S1} of the topsoil. Because the topsoil supplies a limited amount of water $q_o = K_{S1}$, the sub layer conducts this water only through those originally preferential domains or clusters, and as a result, the fingers conduct the water and increase vertically in size. From the description of this fingering we immediately recognize an imperfection in our quantitative modeling of the soil porous system.

On the other hand, when the topsoil is a layer of loam or sandy soil over a clay sub layer, a zone of $h > 0$ is formed during infiltration governed by a NBC with $q_o < K_{S1}$ (topsoil). The height of this saturated zone in the bottom part of the top layer depends upon q_o and the ratio K_{S1}/K_{S2}. After a large infiltration time the $h(z)$ profile resembles that in the top part of the profile shown in Fig. 6.5. When infiltration starts with a DBC into an unsaturated topsoil underlain

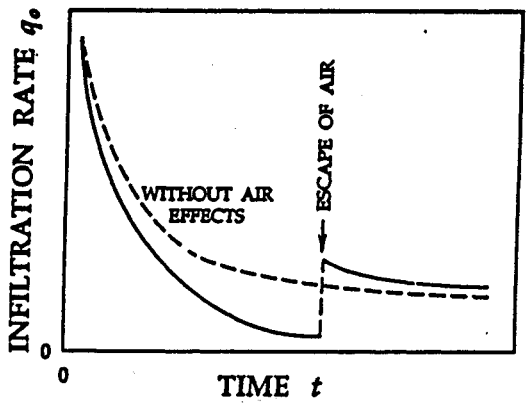

Figure 6.28. The influence of air compression ahead of the wetting front upon the infiltration rate $q_o(t)$.

by a clay subsoil which is either saturated or nearly saturated with water, the approaching wetting front displaces air giving rise to a pore air pressure ahead of the front that increases above atmospheric air pressure. At this time, the continuity of air-filled pores below the front with the atmosphere is interrupted. Hence, the air ahead of the wetting front cannot escape until eventually the increased pressure exceeds the air-entry value h_A of the soil. At that time, the monotonic decrease of q_o with t is interrupted giving rise to a sudden increase of q_o, see Fig. 6.28. On the other hand, if the increased air pressure does not lead to a bubbling of air through the wetted topsoil, the infiltration rate remains substantially decreased. The two-phase formulation of infiltration accounting for the effects of air and the behavior of the air pressure ahead of the wetting front for different values of θ_i has been presented by Morel-Seytoux (1976 and 1983).

6.2.4.4 Further Rainfall Infiltration Effects

Although the area of a rain-simulation plot is usually greater than the REV, local inhomogeneities together with a variable micro-relief oftentimes lead to some phenomena not yet satisfactorily described in theory. As an example, because the ponding time t_p is not well defined experimentally, Rubin and Steinhard (1964) defined three stages:

1. Stage A (absorption and retardation) occurs when the first perceptible retardation of raindrop absorption can be observed.
2. Stage P (puddle formation) occurs when about one-third of the soil surface is covered by puddles of rain water.
3. Stage C (completion of a water mantle) occurs at that instant when the last soil area not yet covered by a layer of free water disappears.

Irregularities of hydraulic properties at the soil surface also lead to the

horizontal redistribution of free water on the soil surface which contributes further to a non-uniform soil wetting depth within the infiltrated domain (Clothier and Heiler, 1983). When the surface runoff of water from a small plot is observed, point heterogeneities lead to a suppression of the ponding time indicative of observable runoff. This suppression of t_p by local heterogeneities was confirmed by models of elementary runoff (Vauclin and Vachaud, 1990). A further factor influencing rainfall infiltration and runoff is the existence of preferential flow paths. Their existence renders the quasi-constant infiltration rate q_c dependent upon the rain intensity q_r with the ponding time depressed and practically independent upon q_r, see Fig. 6.29. In such cases observations of infiltration $q_o(t)$ are different than the theoretical function shown in Fig. 6.19 because the micro-catchment area of each of the preferential flow paths is q_r dependent and film flow exists in the majority of the preferential flow paths (Peschke and Kutílek, 1976).

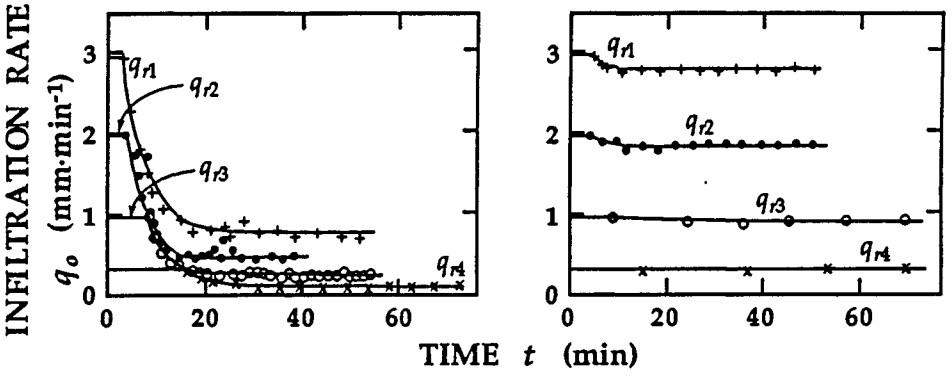

Figure 6.29. Rainfall infiltration measured with a rainfall simulator on a plot without (left) and with (right) macropores which cause the existence of preferential paths (Peschke and Kutílek, 1976).

6.2.5 Infiltration into Seasonally Frozen Soils

Within the season of frost additional factors exist which influence infiltration either directly from snow melt, or from rain combined with snow melt. We have shown in section 5.6.3 that frozen and unfrozen water co-exists at temperatures $T < 0°$ C. Under such a condition the value of the hydraulic conductivity is influenced by the ratio of those two phases of water and by the microscopic and macroscopic characteristic features of ice lenses in the soil, see Fig. 5.22. Generally, the hydraulic conductivity decreases strongly with a decrease in temperature. However, near 0° C the ratio of solid to liquid water is highly variable and under natural dynamic conditions, snow melt infiltration frequently occurs.

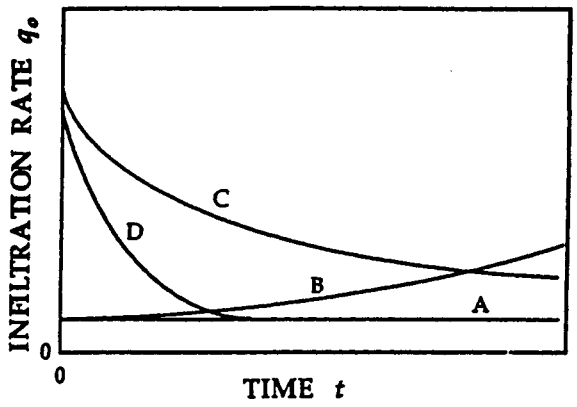

Figure 6.30. Four types of infiltration rates $q_o(t)$ into frozen soils (Gray and Male, 1981).

Because the flux of water is accompanied by a phase change, the simultaneous transfer of both heat and water must be considered. Additionally, the liquid and vapor phases of the water flux have to be treated separately. Water and heat transport processes have to be studied quantitatively in the period before infiltration starts inasmuch as they influence the initial water/ice content in the profile and the eventual occurrence of an impeding ice layer deeper in the profile.

Fig. 6.30 demonstrates the four basic types of infiltration curves $q_o(t)$ according to Gray and Male (1981):

Curve A is for a soil which is frozen when initially water saturated, or when an impervious ice layer develops on the soil surface during a melt period. The infiltration rate, practically constant with time, is very small and approximately equal to the hydraulic conductivity of the soil frozen at the given temperature.

Curve B is for a frozen soil having a large water content but distinctly below saturation. Some of the melt water penetrating deeper into the soil profile transfers heat and causes ice within soil pores to melt. Progressively, as the soil warms and the ice in the pores melt, the infiltration rate continually increases to values sometimes one-half an order of magnitude greater than that of the initial value of q_o. Eventually, the infiltration rate decreases because the topsoil approaches water saturation and the deeper layers of the frozen profile remain nearly impermeable.

Curve C is for a frozen soil having a small water content and at a temperature near or above freezing. With only the small pores filled with ice which thaws rapidly with a downward movement of infiltrating water, infiltration proceeds in a manner similar to that for a soil in an unfrozen condition.

Curve D is for a frozen soil having a small water content and at a temperature well below freezing when snow at its surface is melting Water initially infiltrates as in an unfrozen soil but after entering the extremely cold soil, it is frozen everywhere within the soil pores with its movement drastically inhibited Here, the infiltration rate being very small is described by Curve A

The curves given in Fig 6 30 provide only schematical information that must be tempered further by variations which occur that are dependent upon local heat-water-transfer conditions It should also be recognized that infiltration from snow melt is moderated or controlled by the flux of water through the snow cover The boundary condition at the soil surface is therefore not easily defined as can be recognized from the model of melt-water infiltration in subfreezing snow (Illangasekare et al , 1990) Although the modeling of melt-water infiltration is feasible and useful for a detailed study and interpretation of observed phenomena, the predictive use of such models remains questionable

6.3 SOIL WATER REDISTRIBUTION AND DRAINAGE AFTER INFILTRATION

After infiltration ceases, we can detect a gradual decrease of the soil water content even when the soil surface protected by a cover allows no evaporation The decrease of θ within the originally wetted topsoil is caused by a downward flow of soil water We distinguish two cases First, the drier soil below the wetting front is at a great distance from the ground water level, or more generally, we assume that free ground water is absent In this case, when water draining from the wetted topsoil wets the originally drier subsoil, we speak of *soil water redistribution* The second case exists when the wetting front is close to the ground water level or reaches the ground water level with water flow at or near steady state conditions, see Fig 6 1 When infiltration stops, transient conditions allow the excess water from the topsoil to pass directly to the ground water This process is denoted as *drainage to the ground water level*

6.3.1 Soil Water Redistribution after Infiltration

When infiltration ceases, a relatively large soil water potential frequently near $h = 0$ exists within the topsoil down to the depth of the wetting front z_f Below the wetting front, the value of h is very small, and hence, the soil water profile is in a dynamic state rather than one of equilibrium When we discuss this non-equilibrium process caused by infiltration, we denote the time of cessation of infiltration $t_o = 0$ The non-equilibrium produces a downward water flux within the soil profile without a contribution to the flux from the surface, i e at $z = 0$, $q_o = 0$ With the soil between $z = 0$ and $z = z_f$ being drained, water flows below z_f forming a new redistribution wetting front at z_r, see Fig 6 31 The soil water content profile $\theta(z)$ at t_o is the profile at the end of infiltration Subsequently, at

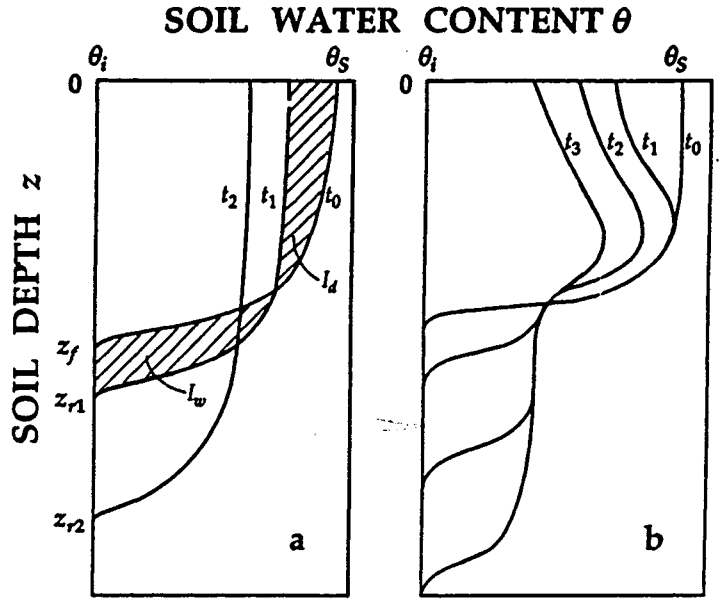

Figure 6.31. Soil water content profiles θ(z, t) during redistribution after infiltration.

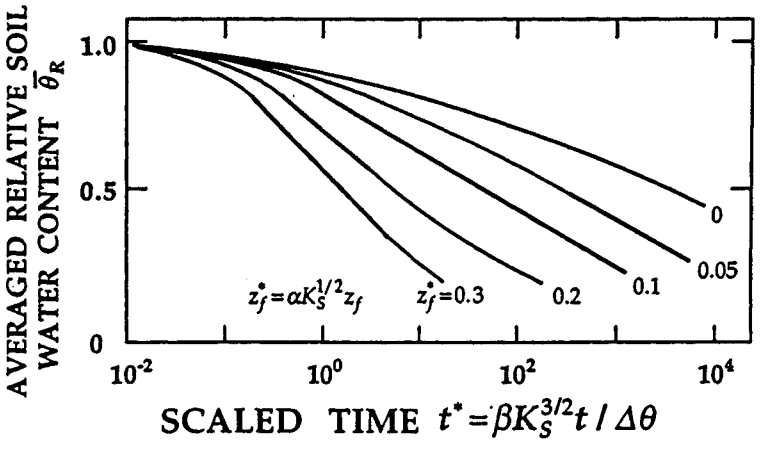

Figure 6.32. Averaged relative soil water content θ_R as dependent upon the depth of the wetting front after infiltration z_f^* and upon time t^* plotted in scaled quantities (Youngs, 1983).

times $t_1, t_2, t_3, \cdots$, redistribution profiles are observed. The cumulative drainage I_d and the cumulative wetting I_w below z_f are equal for the time interval $(0, t_1)$, see the hatched areas in Fig. 6.31a. As the redistribution front moves downward, the mean relative water content $\bar{\theta}_R$ [$= (\theta - \theta_i)/(\theta_S - \theta_i)$] between $z = 0$ and $z = z_f$

$$\bar{\theta}_R = \frac{1}{z_f}\int_0^{z_f} dz \qquad (6.109)$$

decreases with time, see Fig. 6.32. The rate of decrease depends upon the hydraulic conductivity and the depth of the original wetting front from the infiltration. The values of both are included in the scaled variables together with scaling factors α and β in the figure. The decrease of θ_R for the clay is much slower than that for sandy soils. If θ_i is relatively large, the force of gravity has a large influence. We note in Fig. 6.32 that the larger the value of $\Delta\theta$ ($= \theta - \theta_i$), the faster is the redistribution process. The flux density across the redistribution front decreases in time owing to two factors. First, the potential in the wetted topsoil decreases with a simultaneous decrease of the gradient of the total potential dH/dz. Second, the value of the hydraulic conductivity decreases strongly with only slight decreases of θ.

Inasmuch as water redistribution within a soil profile is composed of both drainage and wetting, the entire process is strongly influenced by hysteresis. Hysteresis not only slows down the redistribution process but prevents the soil from subsequently draining to a value of $\theta \leq \theta_i$ inasmuch as for a given h, $\theta_d > \theta_w$ (where the indices d and w again denote drainage and wetting, respectively). Inasmuch as $\theta_d(h_j) > \theta_w(h_j)$, redistribution profile $\theta(z)_{red} > \theta_i(z)$ even at equilibrium. Although a rigorous analytical treatment of redistribution is not feasible owing to hysteresis, approximate solutions of Gardner et al. (1970) confirm most of the above statements. Because analytical procedures are inadequate to predict redistribution in real soils, numerical methods are advisable (Rubin, 1967).

When soil water content profiles $\theta(z)$ are observed for particular time intervals $t_1, t_2, \cdots$, two different kinds of profiles are evident, see Fig. 6.31. Youngs (1983), reviewing his earlier studies of the problem, offered an explanation for the two kinds of profiles based upon the scaling of experimental data and hence, confirmed earlier proposals of Biswas et al. (1968, 6).

In Fig. 6.31a, the soil water profiles during redistribution maintain approximately the same shape of the initial infiltration profile, but progressively become "slimmer" as the soil water content of the topsoil gradually decreases. The soil water content above the sharp wetting front is nearly uniform. This situation develops when the cumulative infiltration is small or when the saturated hydraulic conductivity K_S of the topsoil is relatively small, i.e. that of a fine-textured soil. On the other hand, in Fig. 6.31b, the redistribution profile $\theta(z)$ shows a relative maximum of θ at some depth above the original infiltration wetting front z_f. Below this wetting front persisting during the redistribution at z_f a step-like profile manifesting a small increase in soil water content $\Delta\theta$ advances into the deeper, drier soil. With depth, we note that the value of $\Delta\theta$ ($= \theta_r - \theta_i$) remains relatively constant as redistribution continues. The soil surface desaturated to a greater extent than that portion of the profile near z_f is assumed to be typical for large volumes of cumulative infiltration into a coarse-textured soils.

Although some authors assume for case (a) in Fig. 6.31 that computed values of $\theta(z)$ are obtained when hysteresis is neglected, this type of profile is obtained even with hysteresis when gravity is neglected. In both cases during

redistribution , although θ decreases monotonically with time for $z < z_f$, the rate is however different. Below the position of the infiltration front the soil water content at $z > z_f$ first increases in case (a) to a certain maximum and then decreases slightly. In case (b), the soil water content increases monotonically to a constant value.

When a soil profile is layered, the redistribution soil water profiles are similar to NBC infiltration profiles of layered soils with $q_o < K_S$. Except when θ is close to θ_S, a sandy layer may either slow down or even stop redistribution. However, if θ_i was close to θ_S before infiltration and remains large just below the wetting front, a sandy layer in the subsoil may accelerate redistribution. During redistribution, large cavities and macropores will not be filled with water until $h > 0$. When a clay or loam layer is below a sandy soil, it may serve as an impeding layer and cause waterlogging above it.

The practical importance of redistribution is seldom fully appreciated. With the duration of redistribution being much longer than that of infiltration, redistribution plays an important role regarding soil water storage and its availability to plants. It contributes together with evaporation and transpiration to the initial boundary condition for the next infiltration and it contributes directly to the redistribution of solutes within the profile as well as their eventual transport to ground waters.

In addition to the redistribution which occurs after infiltration, redistribution can also occur during rainfall infiltration if the rainfall intensity $q_r(t)$ is strongly time dependent. We distinquish the occurrence of two cases. (i) After ponding time t_p has been reached, redistribution occurs during decreasing portions of $q_r(t)$ at times when q_r drops below K_S, provided that surface runoff is not inhibited. (ii) If $q_r(t)$ is sufficiently small that ponding never occurs, redistribution starts the moment q_r decreases and persists as long as $q_r(t)$ continues to decrease.

If surface sealing develops during rain infiltration, the hydraulic resistance of the soil surface increases. The time-dependent increase of the soil water content θ_o at the seal-soil interface is less pronounced than that of θ_o for a soil without a seal. Eventually, θ_o may even slightly decrease after reaching its maximum during infiltration. In such a case, infiltration is accompanied simultaneously with redistribution and hysteresis.

Detailed solutions of redistribution and its accompanying processes are available only from numerical methods.

6.3.2 Field Capacity

The practical importance of redistribution and its consequences for water stored in the soil profile was recognized early by soil physicists in the last century (Heinrich, 1886). The terms "field capacity", "specific retention" and "retention capacity" were coined to describe the amount of water held in the topsoil after a thorough wetting followed by excessive water draining (now we should say redistribution) to the drier subsoil. The downward movement of water is assumed to stop, or nearly so, within 2 to 3 days. This assumed state of

equilibrium (or quasi-equilibrium) is verified in the field by measuring the soil water content as a function of time to ascertain the value of θ when $d\theta/dt = 0$. This field capacity value θ_{FC} was supposed to be a real, universal characteristic constant of a soil. However, when the theory of soil water flow is applied, it can be simply demonstrated that the assumption of universality and constant character of θ_{FC} is not a reality and that the value of θ_{FC} is a rough approximation to be used as a "rule of thumb". The value of θ_{FC} measured in the field for a given soil depends upon θ_i before thoroughly wetting the topsoil and upon the depth to which the soil was wetted before the commencement of redistribution. Because the rate at which $d\theta/dt \rightarrow 0$ is not unique even for a given soil, a rigorous quantification of θ_{FC} is not possible. For a detailed discussion and criticism of the field capacity concept, see Hillel (1971), Baver et al. (1972) and Cassel and Nielsen (1986).

In spite of our theoretical reservations the concept of field capacity is useful in the design of field management schemes for approximating soil water storage. Field capacity θ_{FC} is taken as an upper threshold value of θ within each soil layer such that any water in excess of θ_{FC} quickly drains to the next deeper soil layer. With this concept, the soil profile is considered a vertical sequence of reservoirs with the overflow level for each reservoir representing the value of θ_{FC} for each corresponding layer. During irrigation or rainfall the top reservoir is first filled up to the overflow and if more water flows in, the excess water flows over to fill the next lower reservoir etc. With a judicious selection of the depth of each soil layer, this simple analog of the soil profile is easily modeled and computed.

Inasmuch as field measurements are laborious and time consuming, the value of θ_{FC} is frequently estimated in the laboratory using soil core samples. The traditional European procedure calls for the sample to be first thoroughly saturated and then allowed to drain for a designated time, e.g. for 2 hours on a many layered mat of filter papers or on a layer of dry soil. Terms such as capillary or retention capacity are used to describe the characteristic value of θ derived from specified laboratory procedures (Kopecký, 1914 and Rode, 1952). The American school generally estimates θ_{FC} as the value of θ on the SWRC at 1/3 bar or less. Sometimes, especially for sandy soils, the value of θ corresponding to 0.1 bar defines field capacity. To avoid misunderstanding, the characteristic is called simply the 1/3 bar soil water content with its value recognized as an approximation of field capacity. In general, the European procedure provides a better correlation to field capacity than the 1/3 bar soil water content. However, in both cases, we must keep in mind that these laboratory-determined characteristics are two steps removed from reality. We first assumed that redistribution stops at field capacity. The second step substituted a laboratory procedure for a field test. Therefore, we should be fully aware of the possibility of the laboratory approximation not being a reliable estimate of θ_{FC} or the retention of water in a field soil profile.

6.3.3 Drainage to the Ground Water Table

Here, we differentiate between two conditions. For the first condition, we consider drainage from the soil profile after steady infiltration has ceased. With the ground water table kept at constant depth Z, the profiles $h(z)$ and $\theta(z)$ at $t = 0$ correspond to those in Fig. 6.1 except that now $z = 0$ is at the soil surface and the ordinate z is oriented down positive. Because $\theta(z)$ is greater than the SWRC [$\theta(z) > \theta(h)$] and $dH/dz < 0$, water flows downward to the ground water table. We recognize that the flux density q is time dependent based upon the following discussion. In the topsoil ($0 \le z \le z_c$) where $dh/dz = 0$ and $dH/dz = -1$, $q = K$. If we assume an exponential model (5.39) describes $K(h)$, we obtain

$$\ln q = A + ch \tag{6.110}$$

and for $K(\theta_R)$, (5.34) becomes

$$\ln q = A + n \ln \theta_R \tag{6.111}$$

where $A = \ln K_S$. Values of θ_R decrease rapidly at the beginning of drainage and eventually approach an equilibrium distribution within the profile $\theta_R(z) = \theta_R(h)$, the drainage branch of the SWRC. The position of z_c moves upwards with time. Neglecting the change in θ_R along the curved part of $h(z)$, we obtain

$$\frac{dz_c}{dt} \approx K_S \, \theta_R^{n-1}. \tag{6.112}$$

The rate of change of the flux $q(t)$ leads for the water storage $W = \theta z_c$ to the second derivative of θ with t. The total height of water drained is

$$W_D = \int_0^Z \theta \, dz - \int_{h=-Z}^{0} \theta(h) dh \tag{6.113}$$

where $\theta(h)$ is the SWRC.

The second condition of drainage to the ground water table is when water flows from a totally saturated soil profile. Swartzendruber (1969) modified the procedure of Gardner (1962) by linearizing Richards' equation

$$\frac{\partial \theta}{\partial t} = \frac{\partial}{\partial z}\left[K(\theta)\left(\frac{\partial z}{\partial \theta} - \frac{\partial h}{\partial \theta}\right)\frac{\partial \theta}{\partial z}\right] \tag{6.114}$$

using

$$N = -K(\theta)\left(\frac{\partial z}{\partial \theta} - \frac{\partial h}{\partial \theta}\right)\frac{\partial \theta}{\partial z} \tag{6.115}$$

for conditions

$$\theta = \theta_S \qquad 0 \le z \le Z \qquad t = 0 \tag{6.116}$$

$$\theta = \theta_S \qquad z = Z \qquad t > 0 \tag{6.117}$$

$$\frac{\partial \theta}{\partial z} = \frac{\partial \theta}{\partial h} \qquad z = 0 \qquad t \ge 0 \tag{6.118}$$

With the SWRC being simplified to

$$\theta = \theta_S + bh, \tag{6.119}$$

boundary condition (6.118) becomes

$$\frac{\partial \theta}{\partial z} = b \qquad z = 0 \qquad t \ge 0 \tag{6.120}$$

Equation (6.114) now transformed to

$$\frac{\partial \theta}{\partial t} = N \frac{\partial^2 \theta}{\partial z^2} \tag{6.121}$$

is solved using separation of variables. Neglecting all except the first term of the infinite series solution, we obtain

$$\frac{W(t)}{W_c} = 1 - \frac{32}{\pi^3}\exp\left[-\left(\frac{\pi}{2Z}\right)^2 Nt\right]. \tag{6.122}$$

With a weighted diffusivity $\overline{D}$ (Gardner, 1962) the above equation becomes

$$\frac{W(t)}{W_c} = 1 - \frac{8}{\pi^2}\exp\left(-\frac{\pi^2\overline{D}t}{4Z^2}\right) \tag{6.123}$$

where

$$W_c = Z\theta_S - \int_{h=-Z}^{0}\theta(h)dh \tag{6.124}$$

or with (6.119)

$$W_c = Z(2\theta_S - bZ)/2. \tag{6.125}$$

By following procedures of Broadbridge and White (1988), Warrick et al. (1990) extended this solution to more realistic soils of a non-linear character with SWRC characterized by parameter C, see Fig. 6.22. However, the general features of the solution embracing the non-linear character of D do not differ from those of (6.122) or (6.123). In other words, the volume of water draining from the profile decreases exponentially with time and the deeper the ground water table, the slower is the drainage.

Collis-George and Yates (1990), reviewing earlier publications on the role of encapsulated air in drainage, found for $t > 0$ during the first stage of drainage that water leaves the soil without any pores being drained. During this period, drainage occurs as a consequence of the encapsulated air expanding with the value of h decreasing below 0. They designate this early behavior as the first stage of drainage from ponded soils. As we noted earlier, they state that both analytical and numerical solutions of the influence of encapsulated air are virtually impossible with only qualitative descriptions being feasible.

6.4 EVAPORATION FROM A BARE SOIL

Evaporation of water from bare soil is one of the simple processes of water loss from land to the atmosphere. It is not just an academic exercise of theoreticians trying to simplify the more complicated processes of water loss from land surfaces. Such a simple process occurs from plowed soils, from fallow land, from soil between tree and row crops and frequently from agricultural lands during non-vegetative periods. Evaporation involves three events: (i) the transport of water to an evaporating surface located either within the soil profile or on the geographic soil surface, (ii) a phase change from liquid water to vapor water and (iii) the transfer of water vapor from the soil surface to higher elevations within the atmosphere. And, in general, the process also includes the simultaneous transport of matter and heat according to conservative concepts of mass and energy.

In this section, we assume that an energy balance is implicitly included as evaporation occurs from a free water surface, and that the evaporation from a free water surface is identical to that from a saturated soil when both are

subjected to equal atmospheric conditions. Theoretically, these two evaporation rates cannot be equal for the same atmospheric conditions because the properties of the two evaporating surfaces are different. The albedo, surface roughness, area of air-water interface, heat capacity and heat conductance each differ and lead to different surface temperatures of the free water and saturated soil. Hence, our assumption regarding the equality of evaporation from a free water surface and from a water saturated soil is merely an approximation which appears acceptable within the limitations of our experimental observations.

We denote the upward water flux density q_o across the soil surface as the evaporation E [LT^{-1}] and conventionally take E as a rate. Similar to the description of infiltration, we distinguish between steady and unsteady evaporation. The intensity of steady or unsteady evaporation is dominated by the evaporativity or potential evaporation E_p. It is quantified here as the evaporation rate from a free water surface. In this section we ignore temperature fields.

6.4.1 Steady Evaporation

Owing to the condition of steady flow ($\partial q / \partial z = 0$), we are solving the transport equation in its simplest form, i.e. the Darcy-Buckingham equation (5.31) for the boundary condition $z = 0$, $h = 0$ and for z positive upward from the ground water table similar to that described in section 6.2.1.1.

6.4.1.1 Homogeneous Soil Profile

For the exponential form of $K(h)$ [see (5.39)], we obtain an equation identical to (6.5) except that $q > 0$ and the sign in the denominator of (6.4) is changed. The solution is (Gardner, 1958)

$$\frac{z}{h} = \frac{1}{ch}\ln\left[\frac{K_S E^{-1} + 1}{K_S E^{-1} + \exp(ch)}\right] + 1 \qquad (6.126)$$

where $q_o = E$. We obtain values of $z(h)$ for a given evaporation rate E, or we can compute E if h is known at any elevation z. The maximum possible evaporation rate E_{max} for a ground water table at depth Z is found with the assumption of the most extreme condition of dryness at the soil surface. We integrate (6.4) for $h \to -\infty$ at $z = Z$ and obtain

$$\frac{K_S}{E_{max}} = \exp(cZ) - 1. \qquad (6.127)$$

If E_{max} in this solution is greater than the potential evaporation E_p, $h > -\infty$, and hence, we obtain $E = E_p$ from (6.126) using the appropriate value of h at $z = Z$.

When $K(h)$ is expressed in the hyperbolic form of (5.38), the solution for E_{max} for the boundary conditions above is (Císler, 1969)

$$Z = \frac{\pi b^{1/m}}{m \sin(\pi/m)}\left(\frac{a}{bE_{max}}\right)\left[\frac{a}{bE_{max}} + 1\right]^{(1-m)/m} \qquad (6.128)$$

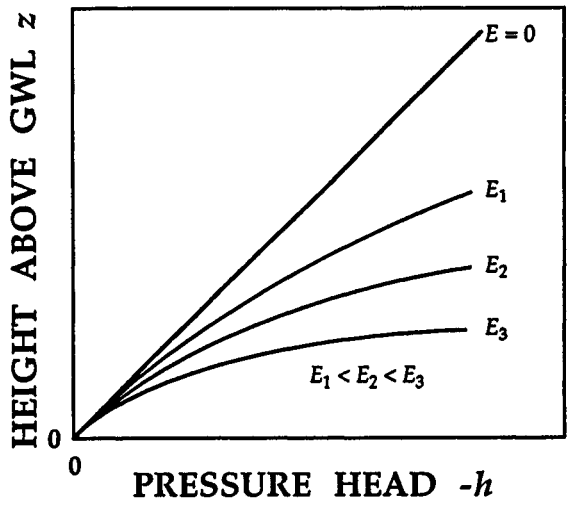

Figure 6.33. Steady evaporation from a soil with ground water level depth z. The distribution of pressure head h with z depends upon the rate of evaporation E.

Numerous solutions available in the literature have been reviewed by Raats and Gardner (1974) and Warrick (1988).

The distribution $h(z)$ within the soil profile during steady evaporation is illustrated in Fig. 6.33. If no evaporation is occurring ($E = 0$), $dh/dz = -1$ and $h = -z$. If $E > 0$, $dh/dz < -1$, and an increase in the evaporation rate is accompanied by a decreased hydraulic gradient dh/dz. Accordingly, $d\theta/dz$ also increases with an increase of E especially near the soil surface, where θ may approach the hygroscopic soil water content θ_H. If the top soil layer manifests a value of $\theta \leq \theta_H$, water also moves as a vapor. In this top layer water transport occurs predominately by diffusion which is a much slower process than liquid flow even for the same hydraulic gradient. Thus, this top layer functions as a strong hydraulic resistance that causes the actual evaporation E_A « the potential evaporation E_p.

The real situation is far from the simplifications considered to obtain the solution above. Atmospheric conditions are never constant in time, evaporation rates from a free water surface usually follow a periodicity of 24 hours and the soil-atmosphere system is not isothermic. Nevertheless, steady evaporation solutions provide practical guidelines for some field situations. For example, they can be used to estimate the depth of the ground water table necessary to substantially reduce evaporation, to estimate the contribution from a given water table depth to supply water to plant roots or to estimate the critical depth of the water table to minimize soil salinization. Such guidelines for field soils can be improved by considering some more approximate solutions of steady evaporation from layered soil profiles.

6.4.1.2 Layered Soil Profiles

Steady evaporation from a layered soil profile is formulated similarly to that from a homogeneous profile where the vertical axis is oriented positively upward, i.e. in the direction of flow. The bottom layer (soil 1) is in contact with the ground water table where $z = 0$ and $h = 0$. At the soil surface the soil is assumed to be completely dry ($h \rightarrow -\infty$). The simplest case is that of two layers. At the interlayer boundary z_1 (see Fig. 6.34) it is assumed that h is continuous.

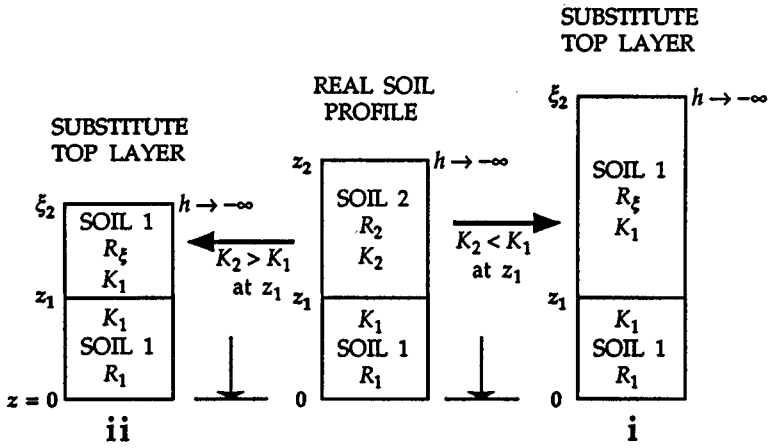

Figure 6.34. Steady evaporation from a layered profile is equal to that from a homogeneous profile of a substitute length ξ offering the same hydraulic resistance.

In the solution, two strategies exist. In the first one we search for the value of h_1 at the interlayer boundary z_1. Evaporation from the top layer is computed for boundaries z_1 and z_2 and for pressure heads h_1 and $-\infty$, respectively. By plotting separate graphs of flux density versus pressure head for the thickness of each layer, Willis (1960) matched the graphs to obtain the evaporation rate and the value of h_1 at z_1. From his graphical iterative procedure he concluded that the evaporation rate from a system of fine-textured soil overlying a coarse soil is only slightly greater than that from a homogeneous, fine-textured soil profile. On the other hand, a large effect on the evaporation rate was observed when the order of the layers was reversed. Willis' conclusions, valid for the conditions he studied, demonstrate the great variation of evaporation rate expected in relation to the hydraulic characteristics, length and relative position of the soil layers. Hadas and Hillel (1972) using the same strategy solved the problem by numerically integrating

$$\int_0^{z_1} dz + \int_{z_1}^{z_2} dz = \int_0^{h(z_1)} \frac{dh}{1+E/K(h)} + \int_{h(z_1)}^{h(z_2)} \frac{dh}{1+E/K(h)}. \qquad (6.129)$$

For the second strategy, we consider the resistance of each of the individual layers in a manner similar to that for saturated flow in layered systems, see Fig. 5.2 and (5.9). For a 2-layer profile, indices 1 and 2 represent the bottom and top layers, respectively. Hence, the total resistance $R = (R_1 + R_2)$. Determining the resistance of each layer follows from the dependence $K(z, E)$ which, in turn, follows from $K(h)$ and $h(z, E)$. We distinguish two cases illustrated in Fig. 6.34. (i) This case illustrates a soil with a mulch on its surface or a freshly tilled soil having an increased porosity and an increase in the number of large pores that increase K_S. However, because K/K_S decreases rapidly with decreasing values of h, usually $K_1 > K_2$ at the interface where $h = h_1$. Evaporation from this two-layer profile (case i) will be the same as that from a homogeneous profile consisting only of soil 1 but of a length greater than z_2. Let us denote the elevation of this fictitious substitute surface of the homogeneous profile as ξ. Then $R_\xi = R_2$. Here for case (i), $\xi_2 > z_2$. When ξ_2 is found, the maximum evaporation is simply obtained from (6.127). (ii) This case illustrates a soil with a compacted top layer where K decreases with decreasing h much more slowly than in the subsoil. With the exception of some soil profiles that are water saturated up to nearly the soil surface, usually $K_1(h_1) < K_2(h_1)$. Evaporation from this two-layer profile equals that from a homogeneous profile of soil 1 having a length smaller than z_2. Here, $\xi_2 < z_2$. inasmuch as $R_\xi = R_2$.

For an approximate solution for both cases, we make three assumptions. First, we assume that soils 1 and 2 have an identical functional relationship for $K(h)$ with unique values of parameters that describe each soil. Later we assume that function is (5.39) with K_{S1}, c_1 for soil 1 and K_{S2}, c_2 for soil 2. Second, we assume the inequality of $K_1(h_1)$ and $K_2(h_1)$ properly characterizes the top soil layer as being either less or more permeable in the region $h_1 > h > -\infty$. Third, we assume that h_1 is very low and K changes nearly linearly between h_1 and h_{z2} with $K(h_{z2}) \rightarrow 0$.

With the resistance R_2 of layer 2 being first approximated, the substitute resistance R_ξ is found for substitute layer of soil 1. From $R_2 = R_\xi$, we obtain with further approximations (Kutflek and Mls, 1975)

$$\frac{\xi_2 - z_1}{z_2 - z_1} = \frac{K_{S1}}{K_{S2}} \left[\frac{exp(c_1 \xi_2) - exp(c_1 z_1)}{exp(c_1 z_1)[exp(c_1 \xi_2) - 1]} \right]^{\frac{c_1 - c_2}{c_1}} . \qquad (6.130)$$

From the value of ξ_2 we can obtain the maximum evaporation rate E_{max} using (6.127) where K_S and c are data of soil 1.

If a soil consists of more than two layers, numerical procedures for the solution are appropriate. In general, when we wish to relate the depth of the water table to evaporation, we should consider the primary role played by the layer having the greatest resistance within the profile. The resistance is that obtained from the unsaturated hydraulic conductivity corresponding to the measured pressure head profile $h(z)$. Resistances estimated from ratios of saturated hydraulic conductivity values K_S for different layers only are obviously not correct. For example, a loamy sand layer in the middle of a loamy profile usually reduces evaporation provided that the layer is considerably above the water table. Or, a sandy layer above a water table and overlain by a

loam layer reduces evaporation compared with that of a homogeneous loam profile, provided again that the boundary between the layers is well above the water table.

6.4.2 Unsteady Evaporation

Evaporation from a soil in the absence of a water table is a transient process even for the following most simplified initial and boundary conditions:

$z = 0$	$t = 0$	$\theta = \theta_S$	(6.131)
$z = 0$	$t > 0$	$q_0 = -E$	(6.132)
$z = L$	$t = 0$	$\theta = \theta_S$	(6.133)
$z = L$	$t > 0$	$q = 0$	(6.134)

Here, a soil column of length L initially saturated by water has its soil surface open to evaporation at $t > 0$ and its bottom at $z = L$ closed with no flux across it. Both experiment and theory have shown that three distinct evaporative stages of drying of a soil column exist, see Fig. 6.35 (Kossovitch, 1904, Lemon, 1956, Gardner, 1959, Gardner and Hillel, 1962).

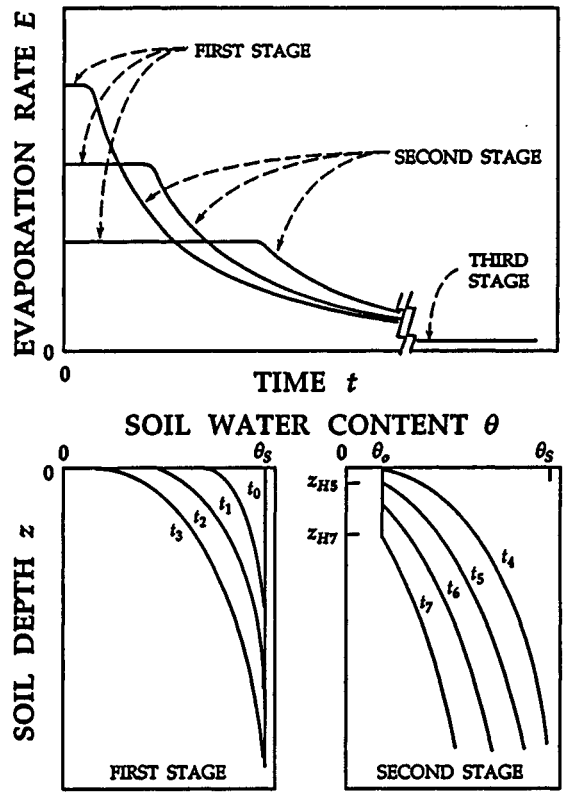

Figure 6.35. Three stages of evaporation from a soil during constant atmospheric conditions. Top: Evaporation rate E as a function of time t for three values of potential evaporation E_p. Bottom: Profiles of $\theta(z)$ for increasing times from t_0 to t_3 in the first stage and from t_4 to t_7 in the second stage of evaporation.

In the initial, first stage evaporation is governed exclusively by external atmospheric conditions and we denote it as potential evaporation E_p. This value of E_p is sustained as the soil water content decreases with time in the topsoil owing to the hydraulic gradient increasing sufficiently to compensate for the concomitant decreasing value of K. Eventually, as still more water is lost from the topsoil, the hydraulic gradient can no longer increase especially when the soil water pressure head approaches a value equivalent to the partial water vapor pressure p/p_o of the adherent atmosphere and $\theta = \theta_o$. At this time when the decrease of K is not compensated by an increase of the hydraulic gradient, the first stage of evaporation ends.

Gardner (1959) derived an approximate description of evaporation during the first stage by neglecting the gravitational force. Assuming water loss by evaporation from a soil profile of depth L is

$$E = -L\frac{\partial \theta}{\partial t} \tag{6.135}$$

and that the diffusivity equation (5.73) with the soil water diffusivity D expressed by (5.74), he obtained after still further approximations, the expression

$$W^* = ln\left(1+\frac{1}{D^*}\right) \tag{6.136}$$

where

$$W^* = \frac{\beta W}{L} \tag{6.137}$$

and

$$D^* = \frac{2D_o}{E_p \beta L} \tag{6.138}$$

with $D_o = D(\theta_o)$ and W the water storage in the entire soil profile at the end of the first stage $t = t_1$ being

$$W = \int_0^L \theta(z,t_1)dz. \tag{6.139}$$

Instead of (6.136), Kutílek (1978) provided the exact solution

$$W^* = (D^*+1)^{1/2} ln\left[\frac{(D^*+1)^{1/2}+1}{(D^*+1)^{1/2}-1}\right] - 2. \tag{6.140}$$

The difference between the two solutions can approach 30%, see Fig. 6.36. For a steep $D(\theta)$ relation characterized by a large value of β, the amount of water storage W at the end of the first stage is large. On the other hand for a $D(\theta)$ relation typical of a linear soil, W is substantially reduced.

The duration of the first stage depends upon both atmospheric and soil conditions. If the atmospheric conditions and therefore E_p are the same, the period of the first stage is greater for a clay soil than for a sandy soil, and greater for a structureless soil than for a structured soil. Therefore, the quality of the soil surface influences the length of the maximum evaporation E_p period and the cumulative evaporation. Mulching the soil shortens this first stage of evaporation and increases the amount of water stored in the soil profile. Depending upon the atmospheric conditions, the smaller the value of E_p, the longer is the period of the first stage. And, if the value of E_p is very small, the

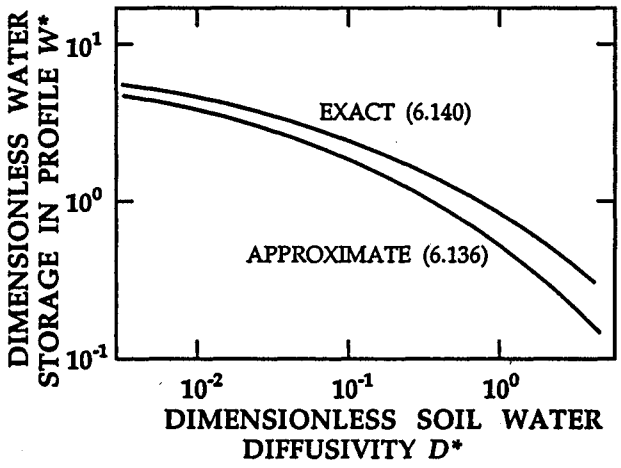

Figure 6.36. The approximate (Gardner, 1959) and the exact (Kutílek, 1977) solution of the first stage of evaporation with $D = D_o exp[\beta(\theta - \theta_o)]$ plotted in dimensionless terms.

soil profile is dried more uniformly with depth owing to the small hydraulic gradient required to provide water conduction through the profile.

The second stage of evaporation is characterized by a gradual decrease of the evaporation rate with time with actual evaporation E being less than potential evaporation E_p and the difference between both increasing with time. In addition to atmospheric conditions, evaporation depends upon the rate of transport of water from deeper parts of the profile to the soil surface. Soil water content continues to decrease with time as well as the value of the hydraulic conductivity. Because the increase of the hydraulic gradient is small and often negligible, it approaches a constant value in time, and hence, the rate of water movement to the soil surface layer as well as E decreases. With the soil water content near the soil surface being extremely small and near the value of the hygroscopic θ, the thickness of this dried surface layer increases with time. The progress of this dry front with soil depth is dependent upon $t^{1/2}$ with the water flux through the dry soil surface layer realized as water vapor transport achieved through molecular diffusion. Here, the dry layer acts as a hydraulic resistance and as its thickness increases with time, its resistance also increases.

For an analytical solution of this second stage of evaporation, Gardner (1959) applied solutions for diffusion published by Crank (1957). The description of the boundary conditions was simplified by assuming that the first stage of evaporation did not exist. Hence, it was assumed that $E_p \rightarrow \infty$ when the second stage starts at $t = 0$. Subsequently, Gardner uses (5.73) assuming that the influence of gravity is negligible and that $dD/dz = 0$. When D is expressed as a mean weighted diffusivity $\overline{D}$ in (5.80) for boundary conditions

$$\theta = \theta_i \qquad 0 \leq z \leq L \qquad t = 0 \tag{6.141}$$

$$\theta = \theta_o \qquad z = 0 \qquad t > 0 \tag{6.142}$$

the evaporation rate after additional approximations is

$$E = (\theta_i - \theta_o)\left(\frac{\overline{D}}{\pi t}\right)^{1/2}. \tag{6.143}$$

And, the cumulative evaporation is

$$E_c = 2(\theta_i - \theta_o)\left(\frac{\overline{D}\, t}{\pi}\right)^{1/2}. \tag{6.144}$$

The dependence of $E(t)$, demonstrated graphically in Fig. 6.35, is only approximately valid for very long soil columns. When the condition of uniform θ with z is not fulfilled, we can assume in accordance with a similar analysis of heat flow (Carslaw and Jaeger, 1958), that soon after the start of evaporation the terms expressing the influence of a non uniform θ(z) disappear.

In some later attempts to achieve an analytical solution, the term desorptivity [$LT^{-1/2}$] was introduced analogous to sorptivity. However, if $E_p \rightarrow \infty$ is not assumed, the solution for both the first and second stage of evaporation must be treated as a continuous process and without simplifying approximations such as neglecting gravity. Inasmuch as no appropriate analytical solution exists, our discussion here is based upon numerical procedures. Boundary condition (6.142) is replaced by

$$0 < t \leq t_I \qquad z = 0 \qquad q_o = E_p \tag{6.145}$$

$$t > t_I \qquad z = 0 \qquad \theta = \theta_o \tag{6.146}$$

where t_I is the time dividing the first two stages of evaporation, and a zero flux at $z = L$ is still maintained. Numerical solutions as well as experimental data show that E during the second stage depends upon E_p. Evaporation E_c accumulated from the soil during small values of E_p can exceed that during larger values of E_p. Such relations depend primarily upon the hydraulic functions and θ_i of the soil (Jalota and Prihar, 1990). The extent to which evaporation is reduced by mulching not only depends upon the soil hydraulic functions but upon the value of E_p. On relatively fine-textured soils when the value of E_p is small, shallow tillage or mulching greatly reduces evaporation for long periods of time. On the other hand, tillage or mulches do not alter cumulative evaporation from coarse-textured soils for large values of E_p. Between these two extremes a wide range of situations exist (Jalota and Prihar, 1990).

The simplifying assumption that a zero flux condition is maintained at depth L necessitates additional interpretation. When this condition is released, evaporation is accompanied simultaneously by redistribution, and hence, evaporation rates as well as the duration of the first stage are reduced. The redistribution rates are reduced substantially in the presence of evaporation compared with those in the absence of evaporation – the case of zero flux at $z = 0$ considered in section 6.3.

Solutions for evaporation considering isothermal conditions differ markedly from those accounting for non-isothermal conditions (e.g. Hadas, 1975). Errors approaching 20% or more, especially in layered soils are commonly made if temperature fluctuations are ignored.

Jackson et al. (1973) showed that the concept of three stages of evaporation does not strictly hold in field conditions. Diurnal temperature fluctuations and

other atmospheric processes induce diurnal fluctuations of evaporativity in the field. During night-time when the air temperature is low, heat flow upward within the topsoil is accompanied by water flow. Additionally, inasmuch as dew causes the value of θ to increase at the soil surface, $E \approx E_p$ at sunrise for a brief time interval followed by a period later on when $E < E_p$. Moreover, cyclic periods of downward heat flow induces coupled downward water flow, especially water vapor to reduce actual evaporation. The overall impact of the temperature induced field effects causes the second (falling) stage of evaporation to begin even before the soil water content has reached hygroscopic values (Jackson et al., 1976).

Soil cracking and other inhomogeneities of field soils can influence evaporation up to 50% in a mild climate. In such cases, quantitative solutions are strongly influenced by thermal fields. For example, within cracks of relatively small depth, water vapor flows downward owing to thermal gradients (Hatano et al., 1988).

The time at which the third stage of evaporation begins is not well defined by the condition $E \rightarrow E_{min}$ or when $dE/dt \rightarrow 0$. A quantitative measure of the time at which these negligibly small evaporation rates occur within a meaningful fiducial limit is presently not feasible.

In field studies, the depth within the soil profile at which the water flux density is zero is of major importance and relatively easy to measure. It is commonly called the "zero flux plane" z_o. Above that depth, the soil water content decreases owing to evaporation. Below z_o any change of θ is attributed to redistribution. The position of z_o is identical to that depth where $dH/dz = 0$. Here, $H = (h + z)$ with h simply measured using tensiometers, see Fig. 6.37.

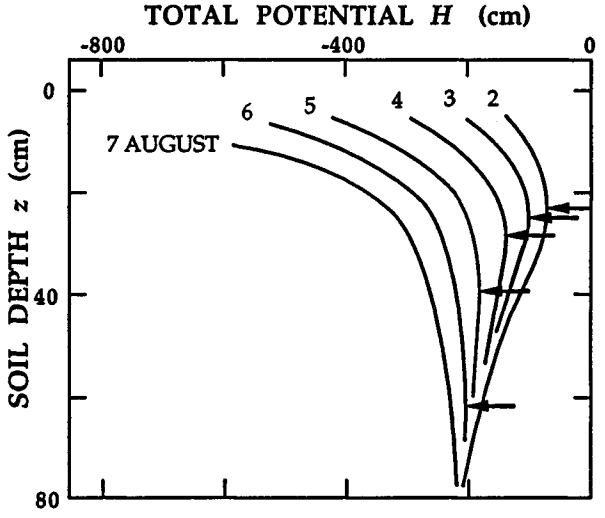

Figure 6.37. Total potential head H(z, t) measured in 1-day intervals during August with a mean evaporation rate E = 3.5 mm·day^{-1} from a soil profile having a silty loam overlying a fine sand. Positions of the zero-flux plane z_o are denoted by arrows (Thony et al., 1979).

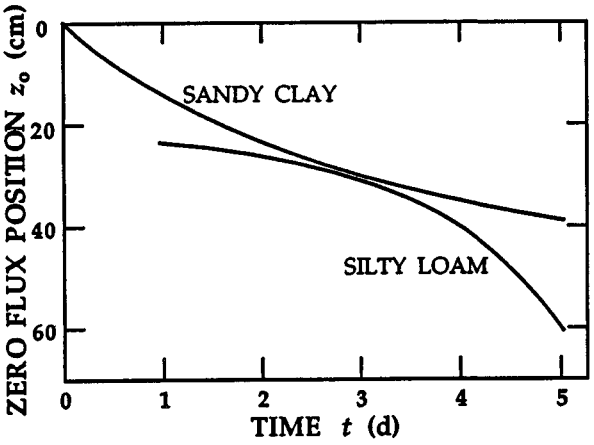

Figure 6.38. The progress of the zero-flux plane position with time in a sandy clay ferrallitic soil (Kalms et al., 1979) and in a silty loam fluvisol (Thony et al., 1979).

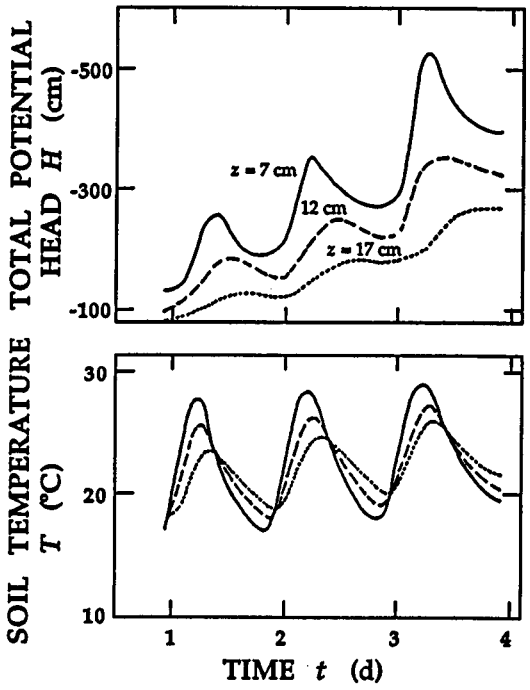

Figure 6.39. Diurnal fluctuation of the total potential head H owing to variations of evaporation as a consequence of temperature variations (Thony et al., 1979).

Although the zero flux plane gradually moves downward, a general relationship for $z_o(t)$ is not unique. Its functional shape depends upon the soil water content distribution before evaporation starts, the soil hydraulic characteristics and the evaporation rate. The position of z_o as a function of time for two soils, a sandy clay and a silt loam, is given in Fig. 6.38. The data were collected for comparable evaporation rates by the same researchers using the same kind of equipment. Diurnal variations of evaporation dominantly influence the diurnal fluctuations of θ, see Fig. 6.39. The daily fluctuations of H as well as those of soil temperature are clearly evident as the average value of both increase during a 3-day period (Thony et al., 1979).

A better knowledge of the role of non-isothermal conditions is obtained when solutions of an isothermal process are compared with those of non-isothermal evaporation. For the latter case, coupled fluxes and the basic equations were shown in section 5.6.2. Milly (1984) made such a comparison using two types of boundary conditions at the soil surface: (i) a step-like change of θ and T and (ii) a sinusoidal variation of T. He first neglected the thermal water vapor flux component, and next the thermal liquid flux component. The thermal liquid flux is negligibly small in wet soils. When soils having water contents somewhat less than saturation are subjected to the step-like boundary condition, the thermal liquid flux does not have a dominant role near the soil surface. And, it is acceptable to ignore the thermal liquid flux in the prediction of the evaporation. The thermal and isothermal vapor fluxes for diurnal variation of temperature are approximately equal and of opposite direction in wet soil (Jackson et al., 1974). As the soil dries out, the net contribution of vapor transport increases. Errors induced by neglecting the thermal vapor flux are of the same order of magnitude as those for the total flux for short time periods. If the soil surface layer is dry ($h < -10^5$ cm), the thermal vapor flux is responsible for increasing evaporation during the night. On the other hand, neglecting thermal effects for a month introduces an error of only about 1% of the average evaporation rate. Hence, isothermal theory is adequate for estimating cumulative values of evaporation for long time periods. Detailed, non-isothermal models offer estimates for short time predictions but are plagued with uncertainties in the determination of the transport and the coupled coefficients. Recent formulations of coupled heat and mass flow by Passerot de Silans et al. (1989) are sets of equations describing the fluxes, transport coefficients, storage coefficients, aerodynamic resistances and terms for forced and free convection in full complexity. In addition to the classically described fluxes in soil, atmospheric fluxes of water vapor are considered at the same level of physical accuracy. The physics of evaporation into the atmosphere is concisely described by Brutsaert (1982).

6.5 EVAPOTRANSPIRATION

When a plant is rooted in a soil, evaporation E from the soil surface is accompanied by evaporation from the plant, which is commonly denoted as transpiration T_R. Water for transpiration is extracted from the soil by the root

system. Macroscopically, we do not describe the influx of water into individual roots, but consider the flux averaged over a representative volume of roots as we did with the flux of water in soil without roots. Although detailed, microscopic studies of a single root-soil interface are highly informative, we keep the description of transpiration here on the same scale as that of evaporation, and hence, the root action is considered macroscopically. Influx into a root hair has its counter part in the description of water flow in an individual soil pore by Navier-Stokes equations. Here we use the macroscopic description of soil water extraction by the root system as a partner in the Darcian formulation of soil water flow. Therefore, the continuity equation (5.62) in its one dimensional form (6.2) is complemented by the extraction term S (Whisler et al., 1968)

$$\frac{\partial \theta}{\partial t} = -\frac{\partial q}{\partial z} - S(z,t). \tag{6.147}$$

The change of soil water content θ in time t is now caused by the change of flux q as well as the extraction of water by roots on a scale of the REV. The dimension of S is $[L^3L^{-3}T^{-1}]$ or, simply $[T^{-1}]$. Transpiration T_R is given by

$$T_R = \int_0^Z \int_0^t S(z,t)\,dt\,dz \tag{6.148}$$

where Z is the depth of the root zone. When (6.147) is combined with the Darcy-Buckingham equation, we obtain

$$\frac{\partial \theta}{\partial t} = \frac{\partial}{\partial z}\left[K(\theta)\frac{\partial H}{\partial z}\right] - S(z,t) \tag{6.149}$$

or some other expression equivalent to (5.64), (5.66) or (5.68).

Because the combination of the two processes (evaporation E and transpiration T_R) is not simply separable, we consider their sum unique and use the term evapotranspiration E_T

$$E_T = E + T_R. \tag{6.150}$$

In section 6.5.2.2 we shall learn that neither $E_T > T_R$ nor $E_T > E$ is a generally applicable condition, even if $E_T > T_R$ and $E_T > E$ occur very frequently.

Evapotranspiration has its deterministic elements in the evaporative demand of the atmosphere and in the transport processes of heat and water vapor from soils and plants through the sublayers which are next to the evaporative surfaces and through plant canopies to the outer atmosphere. The transport processes of heat and water vapor are treated in evapotranspiration principally in two groups of theories. In the first group, the entire plant canopy is considered a single, homogeneous layer characterized by bulk resistances which reflect all molecular transfers through boundary layers as well as turbulent transport. This consideration yields Penman-Monteith equations or their equivalent.

In the second group, the micro climate of the canopy is studied with turbulence within and above the canopy described using multi-layered models. This second approach, not fully covered here owing to its complexity and extensiveness, is considered more as a research topic while the first approach is commonly and extensively used in practice. Quantitative descriptions of individual phenomena and an objective explanation of the dynamics of evapotranspiration can be achieved with the second approach. An appreciation

for the second approach is available in review papers (e.g. Thom, 1975, and Raupach, 1988).

We first limit our discussion to transpiration only in order to explain some of its special features, and subsequently in the following section, treat the more complex topic of evapotranspiration.

6.5.1 Transpiration

6.5.1.1 Transport of Water in Plants

Water extracted from soil by the plant root system is partitioned by the plant into that metabolized into plant tissue and that transpired into the atmosphere. The ratio of the mass of water extracted from the soil to that of the dry organic matter of the plant is denoted as the transpiration coefficient (or ratio). The transpiration coefficient for cultivated plants ranges from 300 to 900, and that for trees of the temperate zone from 150 to 700 (Penka, 1985). Water is the main constituent of plant tissues. Although the percentage of water in hydrophytes is about 80 to 85% and that in cultivated plants about 70 to 80%, the water content of individual cells or particular plant parts deviates greatly. The metabolically most active plant parts and young tissues contain about 90% water in relation to dry organic matter, leaves of cultivated plants 70 to 90%, wood of trees about 50 to 60% and seeds as little as 5 to 10% (Penka, 1985, and Slatyer, 1967). The water content in individual parts of the cell usually follows the sequence, cell wall < protoplasm < vacuole. Detailed studies of plant composition and transpiration [e.g. Slatyer (1967 and 1973) and Penka (1985)] lead to the conclusion that about 95% or even more of the water extracted from soil is transpired and flows through the soil-root-stem-leaves-atmosphere system. Water transpired through the tissues of the stem is relatively small. The concept, Soil-Plant-Atmosphere-Continuum (SPAC), describes the water flux through the above system.

According to SPAC, the driving force of the water transport is the gradient of the water potential. Resistances at the soil-root and leaf-atmosphere interfaces and those inside the plant, soil and atmosphere influence the actual fluxes, see Fig. 6.40. The analogy between water flux in the SPAC and current in an electrical resistance network illustrated in the figure was first suggested by Gradmann in 1928 and further elaborated by van den Honert in 1948 according to Molz (1981).

The water potential in plant tissues is defined analogously to that in soils. The total plant water potential is usually partitioned into two components: (i) turgor or turgor pressure p_T identified with a pressure potential and osmotic pressure p_O. Hence, as illustrated in Fig. 6.41,

$$\psi = p_T + p_O. \tag{6.151}$$

Inasmuch as the cell volume is not constant, its reference value is taken as that volume at zero turgor ($p_T = 0$). An increase of turgor is accompanied by an increase of cell volume and a decrease of p_O to $\psi = 0$ at full turgor. A decrease of turgor owing to dehydration causes the cells to shrink and at a certain threshold

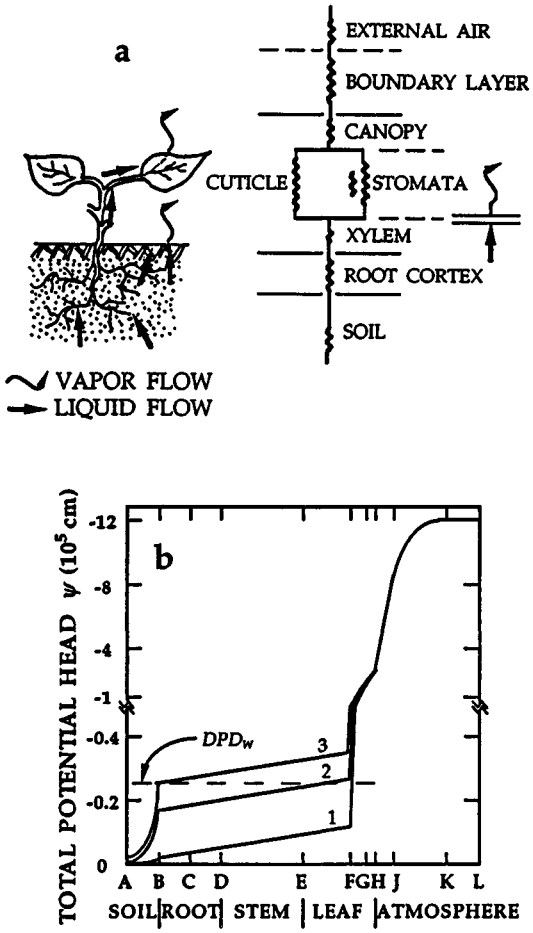

Figure 6.40. a. Schematic demonstration of the concept of soil-plant-atmosphere-continuum (SPAC) with the most important of the hydraulic resistances in the individual parts of SPAC. b. Profiles of the total potential head ψ in the SPAC according to Philip (1957e): 1. normal transpiration, 2. temporary wilting and 3. permanent wilting. Points along the transpiration path are A. a definite distance in the soil away from plant roots, B. surfaces of root hairs and of absorbing epidermal cells, C. the cortex, D. the endodermis, DE. vessels and tracheids in xylem, E. leaf veins, F. mesophyll cells, FG. intercellular space and stomatal cavity, GH. stomatal pore, HJ. laminar sublayer, if present, JK. turbulent boundary layer and KL. the free atmosphere. DPD_W denotes the value of at incipient plasmolysis of root cells.

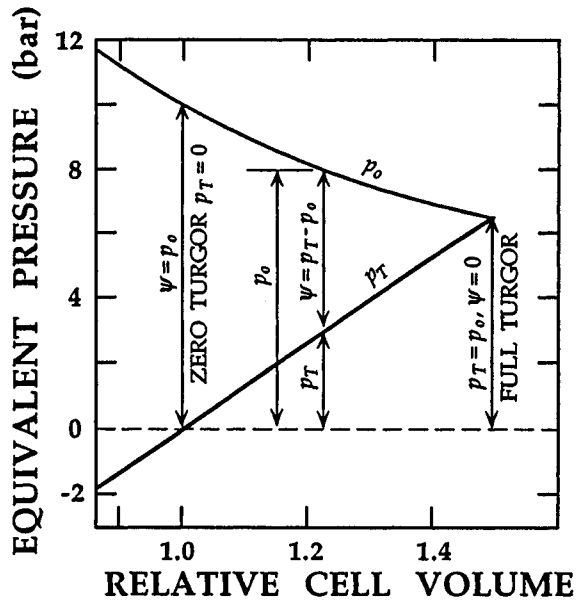

Figure 6.41. Relationship between turgor pressure p_T, osmotic pressure p_O and water potential ψ in an idealized osmotic cell (Höfler 1920, after Slatyer, 1967).

value is macroscopically observable as the wilting of leaves. Complete wilting occurs at $p_T \approx 0$ with p_O occurring in a broad range from 0.5 to 20 MPa (Slatyer, 1967). The total potential ψ at permanent wilting can manifest a broad range of values that depend upon the species and stage of development of the plant, the actual water stress resistance of the plant and the local environmental conditions. This extreme decrease of p_T is accompanied by irreversible morphological changes inside of the cells. Some plant physiologists still denote the absolute value of the water potential of plants as the diffusion pressure deficit $DPD = -\psi$ or $[= (p_O - p_T)]$.

Although the above description of SPAC may appear mechanistically restrictive, regarding processes within and between cells of living organisms, it does not exclude detailed descriptions of metabolic systems which regulate resistances, permeabilities of cell membranes, etc. Resistances, especially those in roots and leaves which vary with transpiration rate, can also be included. A full description of these mechanisms not presented here can be found in the literature on physiology of water regimes in plants.

As a first approximation to a simplified but realistic cross-section of a cell (Fig. 6.42a, b), we show mechanistic models of water transport in series of cells, see Fig. 6.42c, d and e. The first model in the series of cells considers the simple transport from vacuole to vacuole (Fig. 6.42c) as was originally proposed in a quantitative study by Philip (1958a). Although this series is realistic for water

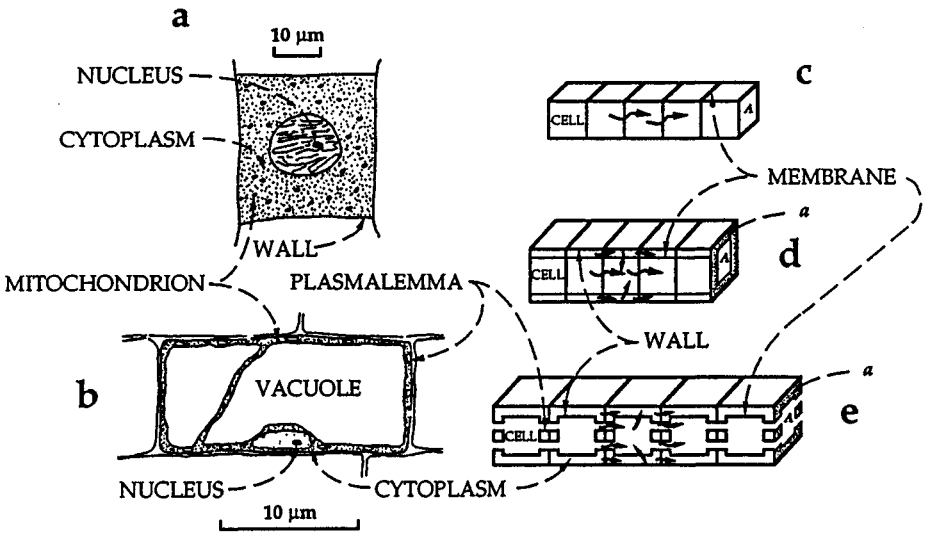

Figure 6.42. Left: Sketches of a. young and b. adult cells from higher plants (Briggs et al., 1961, after Slatyer, 1967). Right: Models of water transport in cells, c. from vacuole to vacuole, d. with contribution of cell walls and e. with contribution of cytoplasm of the cell walls (Molz, 1981).

flow in young cells, it includes a contradiction for adult cells. That is, inasmuch as the cell walls parallel to the direction of flow do not contribute to the total flux, only the perpendicular walls are permeable. Transport in cells is included in the next model given in Fig. 6.42d. In the most complex model, Fig. 6.42e, water transport in cytoplasm realized through plasmodesmata in the walls (cytoplasm pathway) is accompanied by parallel transport in the walls (apoplasm pathway). The main fluxes do not exclude the coexistence of water exchange between the cell wall and the vacuole. Molz (1981) conducted quantitative studies primarily focused on water transport in roots. In spite of the above simplifications, these models provide quantitative insights into the water regime of plants, especially when further developments included the effects of diffusible solutes.

Water enters the plant primarily through the most active part of young roots and root hairs. Hence, if L is the length of the roots, dL/dt is primary information on the proportion of active roots. The cross section of a young root given in Fig. 6.43 allows visualization of the pathway of water entering a root. Water enters the root through root hair cells and through the epidermis of young roots. Its path through the cortex is the location of greatest hydraulic resistance. With this resistance regulated by the plant itself, Molz (1981) concluded from his models that it takes about a half hour for the root cortex to respond fully to a boundary condition change at the endodermis. Thereafter, with quasi-steady fluxes being apparent, water potential gradients in the cortex were greater than those in the neighboring soil. Hence, we should correct the

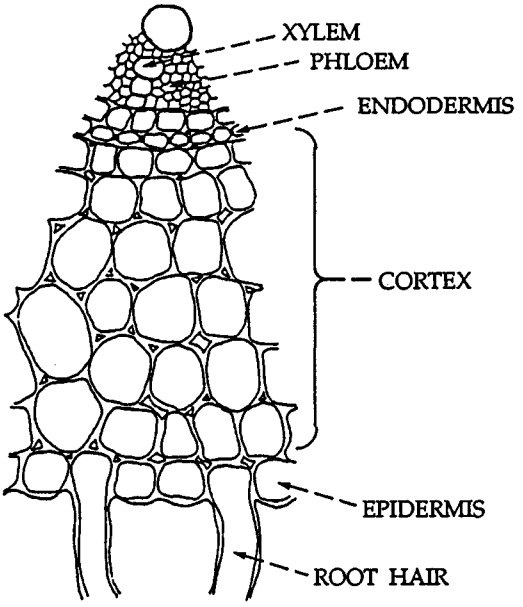

Figure 6.43. Cross section of a young root (Kramer 1959, after Slatyer, 1967).

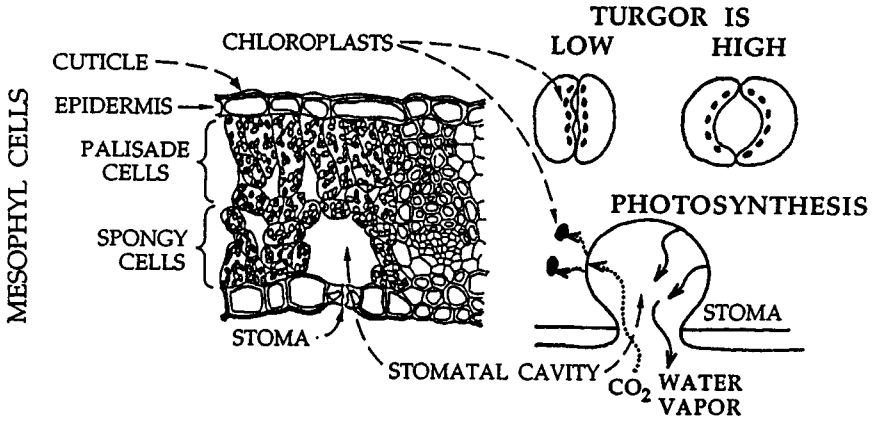

Figure 6.44. Left: Cross section of a leaf (Meyer and Anderson, 1952, after Slatyer, 1967). Right: Closed and opened aperture of stoma and gas exchanges in the open stoma.

original graph of Philip in Fig. 6.40b. Water, after passing the cortex and endodermis, enters the xylem of the root which has a very small hydraulic resistance. Aging of a root is accompanied by cutinization and suberization with cork eventually completely replacing cortex in the roots of woody species. The hydraulic resistance of those aging tissues drastically increases.

From the root xylem water enters the stem xylem where it easily and continuously flows at a very small resistance. Xylem can be considered the main "river bed" of water transport in plants.

The dominant locality of transpiration is the leaf. A schematic cross section is in Fig. 6.44. The surface of a leaf is constituted by an epidermis having its outer cell walls thickened and lined with cutin and further covered by a "crusty" often waxy cuticle. This epidermal outer surface has a large hydraulic resistance. In the epidermis, micro holes or pores called stomata exist at a density of 50 to 500 mm^{-2} (Slatyer, 1967). Stomata occur on both surfaces of the leaf of cultivated plants, but they may occur more commonly on the lower surfaces of tree leaves. The shape, opening and closure of each stoma is regulated by its two kidney-shaped guard cells. With the turgor in the leaf cells transferred to the guard cells, a decrease of turgor deforms the guard cells to initiate closure of the stoma. An increase of turgor functions an opposite way to open the stoma. The aperture of each stoma forms a pathway for diffusive transfer of water vapor. However, the function of the guard cells including stomatal opening and closure is not a simple process that reacts only to cell turgor and simply to plant water stress, see Zeiger (1983). Sensors below each stoma react to concentration of CO_2 in the air, radiation, temperature etc. For example, the presence of toxic gases in the air causes stomatal closure. Potassium ion concentration and proton transport across the membrane of guard cells play a dominant role regarding the dynamics of opening and closing of stomatal apertures (Raschke,1975). The proton transport is accompanied further by biochemical reactions.

The actual transformation of water from the liquid to the vapor phase takes place within two domains of the leaf, see Fig. 6.40a. The first domain is that of the outer epidermal wall through which water vapor flows through its cuticle with great difficulty owing to its resistance r_c being constant and of very large value. The upper part of the mesophyll cells is the second domain where water vapor flows through the air-filled space below and through stomata to the atmosphere. Inasmuch as the resistance r_S is determined by the area of the stomatal aperture, its value is not constant. Water vapor moves readily through stomata regardless of them being fully open or nearly completely closed. Even when they are closed, the flux through them is roughly equal to the flux through the cuticle. The total resistance to vapor transport by the leaf r_L is

$$\frac{1}{r_L} = \frac{1}{r_S} + \frac{1}{r_c} \tag{6.152}$$

where r_S is the stomatal resistance and r_c the cuticle resistance which does not change substantially. The primary self-regulating mechanism of transpiration by a plant is realized through r_S. With a gradual closing of the stomata, r_S increases and transpiration decreases. Transpiration does not stop however, even if the stomata close completely. And, if the transpiration flux exceeds the influx into the roots, the plant tissues loose water and turgor. If the loss of turgor continues beyond a critical threshold value, wilting occurs. Wilting can occur even if the soil is fully moist when the evaporative demand of the atmosphere is large and the influx to the roots is lower than the transpiration loss. Often during a hot summer midday, plants having large leaf areas (e.g., the sugar beet) temporarily

wilt. Subsequently, in the evening hours when the extreme air conditions cease and the transpiration rate decreases, turgor in the leaf tissues returns. When extreme air conditions prevail or when the soil remains relatively dry for several days, the loss of turgor in cells accompanied by irreversible changes in the plant finally causes permanent wilting. Stomata apertures also provide pathways into the plant for CO_2 needed for photosynthesis and the growth of plant tissues. Hence, a correlation between transpiration and crop yields exist and is frequently documented. Some authors claim that the priority for receiving CO_2 necessary for photosynthesis indeed regulates stomatal aperture.

6.5.1.2 Potential and Actual Transpiration

Analogous to potential evaporation E_P, potential transpiration T_{RP} is defined as the loss of water from plant tissues to the atmosphere according to the evaporative demands of the atmosphere with the stomata fully opened. Additionally, it is understood that water movement from the soil to the plant roots does not limit the process. With atmospheric conditions including the energy source and radiation controlling the phase change of water, energy regulates the process for a given stomatal density. The term unstressed transpiration is also used for T_{RP}.

Let us now assume that the soil water content θ suddenly decreases. Concomitantly, values of both h and unsaturated hydraulic conductivity K drastically decrease. In such a case, the evaporative flux is maintained by the gradient of the water potential ψ increasing – the cell water potential continually decreases and is accompanied by a loss of cell turgor. Inasmuch as the regulating mechanism of stomatal dynamics is not uniquely controlled by the water potential, we can not precisely define the critical value of guard cell turgor at which the stomata start to close. This critical value also depends upon plant type, its variety, its susceptibility to water stress and upon the local environmental conditions – quality and intensity of light, CO_2 concentration and surface temperature of leaves. We must also remember that transpiration has an important cooling effect on the plant. If we hold all conditions constant except the evaporative demand of the atmosphere, the critical value of turgor pressure h_D when stomata start to close depends upon the value of the potential transpiration T_{RP}, see Fig. 6.45. After this critical value is reached, the decreasing cross sectional area of the stomata causes a rise of the stomatal resistance r_S and hence, a rise of the leaf resistance. With the transpiration rate being reduced, the actual transpiration $T_{RA} < T_{RP}$. With further extraction of soil water, the unsaturated hydraulic conductivity decreases substantially and the compensating increased soil water potential gradient causes a drastic decrease of plant water potential and a sufficient decrease of turgor to initiate complete closure of stomatal apertures. The greatly reduced transpiration rate allows the cell turgor in the leaf to decrease to such an extent that wilting is clearly evident, see the range of wilting in Fig. 6.45. The whole process depends upon the value of T_{RP}, see Fig. 6.45. Close to saturation ($\theta/\theta_S \rightarrow 1$), when redox conditions in the soil reduce the root activity of cultivated plants, $T_{RA} < T_{RP}$ in the range RO. For

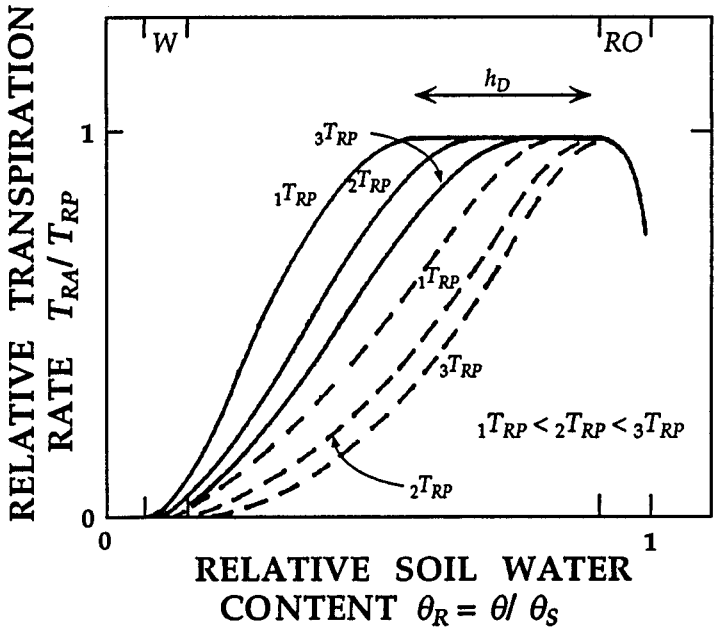

Figure 6.45. The dependence of actual transpiration rate T_{RA} upon relative soil water content θ/θ_S and upon the rate of potential transpiration T_{RP}. The full curves are for dense rooting while the broken curves are for half density of roots.

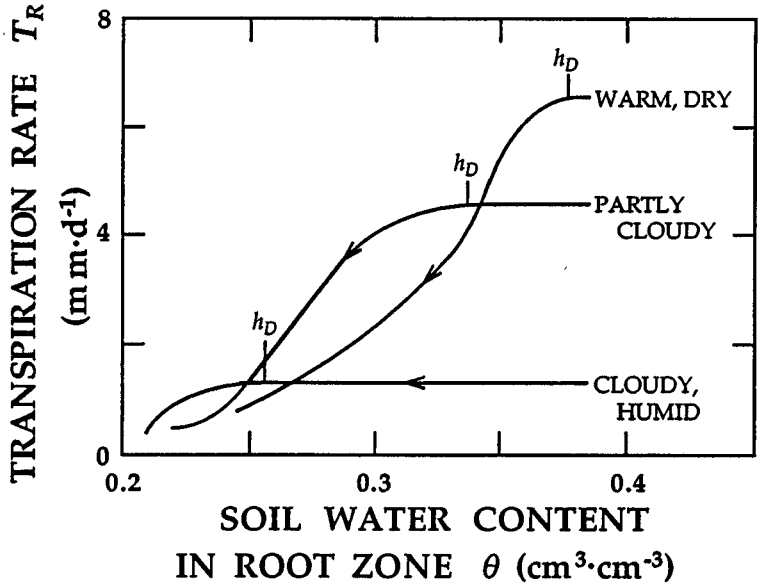

Figure 6.46. The decrease of actual transpiration rate T_{RA} with a decrease of soil water content q under different meteorological conditions (Denmead and Shaw, 1962, after Hillel, 1980).

a range of θ/θ_S very often between field capacity and θ corresponding to h_D in the range of -500 to about -3000 hPa, $T_{RA} = T_{RP}$. If the earlier-mentioned factors are kept constant, the value of h_D associated with decreased availability of soil water depends upon the evaporative demand of the atmosphere characterized by T_{RP} in Fig. 6.45. From model studies of Federer (1982) whose results appear in Fig. 6.45, we recognize that the density of the root system is not negligible. The shift of h_D and the dependence of T_{RA} upon meteorological conditions demonstrated by Denmead and Shaw (1962) are illustrated in Fig. 6.46.

Up to now we have dealt only with average values of transpiration. However, as was already mentioned earlier in the section on evaporation, the evaporative conditions of the atmosphere manifest large diurnal amplitudes. A detailed analysis of factors which contribute to diurnal fluctuations can be found in Brutsaert (1982). Such atmosphere characteristics occurring during the day and night cause fluctuations of leaf water potential, see Fig. 6.47. In the root, the amplitude of the water potential is smaller than that in the leaf and occurs later manifesting a lag or shift of phase. In the root zone, diurnal amplitudes of soil water potential driven by atmospheric demand are negligible, except perhaps at shallow soil depths where large daily temperature fluctuations occur.

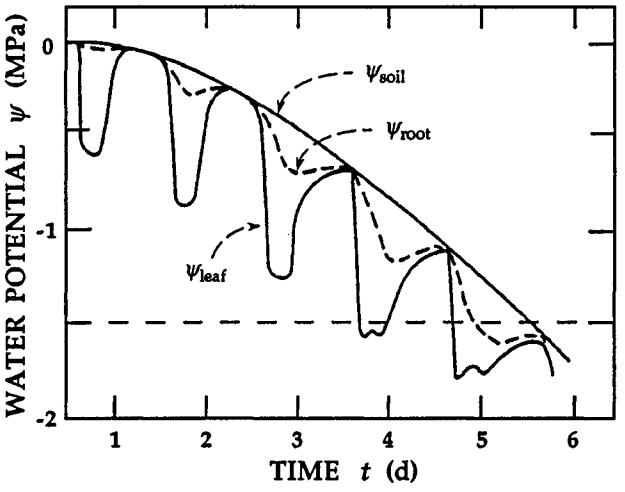

Figure 6.47. Scheme of diurnal changes in leaf and root water potential ψ together with soil water potential in a sequence of days without precipitation (Slatyer, 1967).

Having now used the microscopic approach to describe water flow within the plant and its path within the SPAC, we now return to (6.148) to macroscopic formulations frequently used to model transpiration in soil hydrology or plant production. Two different kinds of extraction terms S can be grouped together. In the first group, the value of potential transpiration is related to the maximum value of soil water extraction S_{max} by roots extending within the

profile to a root zone depth z_r by $T_{RP}/z_r = S_{max}$. This relation is subsequently reduced schematically in a fashion similar to that in Fig. 6.45, or by some deterministic function of root length or related plant parameter. Using a formulation belonging to this first group, Feddes et al. (1978) suggested:

$$S = 0 \qquad 0 \geq h > h_1 \qquad (6.153a)$$

$$S = S_{max} \qquad h_1 \geq h > h_D \qquad (6.153b)$$

$$S = S_{max}\left(\frac{h - h_W}{h_D - h_W}\right) \qquad h_D \geq h > h_W \qquad (6.153c)$$

$$S = 0 \qquad h_W \geq h \qquad (6.153d)$$

Here, inasmuch as S_{max} is assumed constant, any change of S is caused by a decrease of θ beyond the limits of h shown above. The threshold value h_1 is related to the gas diffusion coefficient of the soil to avoid anaerobiosis. The corresponding θ/θ_S varies roughly between 0.85 and 0.95 and depends upon both soil texture and soil structure. The broad range of possible values of h_D was shown in Fig. 6.45. Pressure head of wilting h_W will be discussed in the next section. Later on, instead of S_{max} being constant with depth, S_{max} was assumed to decrease linearly with depth (Prassad, 1988) or exponentially with depth (Novák, 1987). Inasmuch as S_{max} depends upon the development of the root system, we suggest that it is entirely appropriate to describe $S_{max}(z, t)$.

In the second group, the resistance to water flow is considered at the soil-root interface or within the roots. The water flux in the plant is computed and related to T_{RP} by an iterative procedure. Inasmuch as direct measurement of resistances of plant water flow and xylem water potentials is difficult, plant hydraulic characteristics are frequently obtained from values of plant parameters adjusted to match directly measured or computed T_{RP}.

Combining both of the above approaches, Novák (1987) derived and experimentally confirmed $S_{max}(z)$ as being

$$S_{max}(z) = T_{RP}\left[\frac{\alpha exp(-\alpha z/z_r)}{1 - exp(-\alpha)}\right] \qquad (6.154)$$

where α is an empirical constant usually of order 10^0 for well-developed root systems and leaf canopies. The above relation, nearly identical to the distribution patterns of active roots in the soil profile, is valid for $h > h_D$ when transpiration reaches its potential value. When $h < h_D$, formulations (6.153) apply. Instead of the linear relation between S and h within the range $h_D \leq h \leq h_W$, a smooth curve is sometimes introduced even though it does not necessarily lead to greater accuracy. Generally, when $h < h_D$, $S(z)$ reflects roughly $h(z)$. Consequently, the soil depth manifesting h_{max} is the position of the greatest value of $S(z)$.

In the above discussion we have shown that transpiration as well as $S(z, t)$ are strongly influenced by stomatal resistance. If formulated as functionally dependent upon leaf water potential and solar flux, stomatal resistance can be modeled to an external control of transpiration. A review of this type of modeling is given by Lynn and Carlson (1990).

6.5.1.3 Wilting Point

We have already shown that if the rate of soil water extraction by plant roots is insufficient to meet a reduced transpiration rate, the plant is wilting. If the plant does not regenerate its turgor and biological activity after a rewetting of the soil, we define such θ as the soil water content of wilting. Resuming the discussion of flow of water within plants, we recognize that the soil water content of wilting is not the same for different plants. Even if we restrict our consideration to a particular cultivar, the soil water content of wilting depends upon the developmental stage of the plant, its water stress susceptibility and the evaporative conditions of the atmosphere. Moreover, the composition and concentration of the soil solution plays a role. An increased soil solution concentration increases the soil water content of wilting through a decrease of the total soil water potential. The increased value of K and D owing to an increased soil solution concentration may also influence the value of the soil water content of wilting provided that there are no other solution effects linked to soil structure and transport across cell membranes.

Because the soil water content of wilting separates soil water into two categories (one useful and available to plants and one that is not) practitioners introduced the concept of the wilting point θ_W especially for the production of cultivated crops. The "point" is indeed nothing more than an average of soil water content of wilting values which are closely correlated with the permanent wilting percentage.

Wilting point is now defined in soil science as the soil water content at a soil water potential of -1.5 MPa (or equivalently as the logarithm of the pressure head expressed in cm, pF = 4.18). Inasmuch as this value is usually reached as the soil becomes progressively drier, the wilting point is that θ which is related to the pressure head on the drainage branch of the soil water retention curve. The pressure plate method is commonly used to measure θ_W at -1.5 MPa. Because soil structure does not significantly influence the value of θ_W, soil samples need not have to be the volume of a REV. Desiccator methods were previously employed to estimate θ_W using a relative partial pressure of water vapor either above a saturated solution of K_2SO_4 or above 3% H_2SO_4 at a temperature of 20°C.

With the concept of continuous water flow in SPAC accepted, it would appear more appropriate to relate the soil water content of wilting to the dynamic characteristics of soil water quantified by values of the unsaturated hydraulic conductivity K or soil water diffusivity D. However, measuring soil water potentials in the vicinity of the root system is much easier than measuring K and D to ascertain critical flux conditions. Assessing critical flux conditions offers a real challenge to our understanding of SPAC. For example, if we assume that $D = 10^{-3}$ cm^2·min^{-1} is a critical minimal value for avoiding wilting of plants, this value is never attained in the whole range of soil water contents in confined vertisols having small values of EC with ESP > 15% (Kutílek, 1973).

The definition of wilting point based upon biological experiments requires a standardized observation of the permanent wilting of an indicator plant (e.g. barley).

Soil texture can be used as an indicator of the wilting point. In 1924, Solnař suggested that θ_W = (silt + clay)/2.4, where (silt + clay) is the percentage of particles < 0.01 mm (Kutílek, 1978).

6.5.2 Potential Evapotranspiration

Just as we defined potential evaporation and potential transpiration, we assume an unlimited supply of evaporating surfaces with water in the definition of potential evapotranspiration. However, before proceeding, we must first clear up some specific terminology.

The reference value denoted as the potential evapotranspiration E_{TP} is often taken to be the evaporation from a plant stand of densely covered short cut grass freely supplied with water. Penman (1963) and his colleagues (see e.g. Monteith, 1981) have used the term potential transpiration inasmuch as evaporation from the soil is truly negligible for a densely populated grass. We note that Penman's (1948) original derivation described evaporation from a free water surface or any surface freely covered by water (e.g. a plant canopy immediately following rainfall). On the other hand, Thornthwaite (1948) coined the term potential evapotranspiration. The terminology is further confused by some authors who prefer to speak of evaporation from vegetation. Inasmuch as the soil surface is frequently not completely shadowed by a plant canopy, we prefer the term potential evapotranspiration. An unambiguous definition of E_{TP} in practice is only achieved by reporting the method of its computation or the procedure by which it was measured.

6.5.2.1 Computational Methods for Estimating E_{TP}

Provided that steady state fluxes and conditions are maintained, evaporation from any surface can be obtained from three basic equations using the so-called turbulent diffusion theory. From latent heat transport from the surface with roughness for water vapor z_o to the atmospheric surface layer position z_a, the evaporation rate E [kg·m^{-2}·s^{-1}] is

$$E = \rho_A D_t (e_o - e_a), \tag{6.155}$$

the turbulent flux of heat Q_A [W·m^{-2}] is

$$Q_A = \rho_A c_p D_t (T_o - T_a) \tag{6.156}$$

and the partitioning of the net radiation R [W·m^{-2}] at the evaporative surface is

$$R = Q_S + Q_A + \chi E.. \tag{6.157}$$

These equations express the similarity between turbulent heat and water vapor transport where D_t is the turbulent transfer coefficient [m·s^{-1}] which is assumed to be identical for latent and sensible heat transfer, χ the latent heat of vaporization [J·kg^{-1}], Q_S the flux of heat into the soil [W·m^{-2}], T_o [°C] the temperature of the surface at the scalar roughness for sensible heat z_{oh}, T_a [°C] the temperature of the atmospheric surface layer at z_a, c_p the specific heat of air

at constant pressure [J·kg^{-1}·K^{-1}], ρ_A the density of air [kg·m^{-3}] and e_o and e_a [kg·kg^{-1}] the specific humidity at z_0 and z_a, respectively.

Values of T_o and e_o are not routinely measured at standard micro meteorological stations owing to the difficulty of their observation. For the purpose of estimating E_{TP}, their measurement is eliminated by the following procedure. The functional dependence of the saturated vapor pressures at the surface $e^*_{So}(T)$ and $e^*_{Sa}(T)$ are known. Using a Taylor series expansion leads to the major approximation of Penman (1948)

$$e^*_{So} = e^*_{Sa} + (T_o - T_a)\phi_a \tag{6.158}$$

where e^*_{So} is the air saturated vapor pressure at the temperature of the surface at z_o, e^*_{Sa} the air saturated vapor pressure at the temperature of the surface z_a and ϕ_a is the derivative $d\, e^*_S / dT$ at T_a. The specific humidity e is related to the vapor pressure e^* by $e = 0.622\, e^*/(R_d T_a \rho_A)$ where R_d is the Universal gas constant for air (R_d = 287.04 J·kg^{-1}·K^{-1}). Substitution of (6.157) into (6.155) and combining the result with (6.156) and (6.157) yields an equation for the potential evapotranspiration (Novák and Hurtalová, 1987)

$$E_{TP} = \frac{\phi_a (R - Q_S) + \rho_A c_p D_t (e^*_{Sa} - e^*_a)}{c_p + \chi \phi_a}. \tag{6.159}$$

Note that $(e^*_{Sa} - e^*_a)$ is equivalent to the saturation deficit at elevation z_a. Equation (6.159) is comparable to Penman's (1948) equation which is traditionally written as

$$\chi E_{TP} = \frac{\phi_a}{\phi_a + \gamma} H_Q + \frac{\gamma}{\phi_a + \gamma} \chi E_A \tag{6.160}$$

where E_A is the "drying power of the air" (i.e. a function of wind velocity and saturation deficit of the air) and γ the psychometric constant [Pa·K^{-1}] in (6.160) defined by

$$\gamma = \frac{c_p p_A M_A}{\chi M_V} \tag{6.161}$$

where p_A is the air pressure [Pa] and M_V and M_A are values of the molecular mass of water vapor and air, respectively. $H_Q = (R - Q_S)$ comprises the radiative flux minus the soil heat flux as well as heat storage in the vegetation and photo synthetically used energy according to Penman which are often neglected.

The net radiation R is either measured or computed according to standard methods (FAO, 1977). Although the integral of E_{TP} usually yields a negligible value of the heat flux into the soil Q_S for a day, its diurnal values should be estimated for periods shorter than a day. A major problem is estimating the turbulent transfer coefficient D_t. And, the difficulty is not normally overcome by using Penman's empirical definition of $E_A = f(\mu)d$ where $f(\mu)$ is a wind velocity function and d the saturation deficit ($e^*_{Sa} - e^*_a$) [Pa].

In Penman's original equation and in subsequent modifications, the use of a wind velocity function is probably appropriate in order to obtain E_{TP} for integral values of a day or even somewhat longer periods. On the other hand, for diurnal (say hourly) computations the variation of atmospheric stability

plays an important role. Expressions of D_t which account for atmospheric stability to solve the problem are discussed in detail by Brutsaert (1982). When atmospheric stability plays a role, we have

$$\chi E_p = w(R - Q_s) + \chi(1-w)E_A \tag{6.162}$$

where $w = \phi_a/(\phi_a + \gamma)$ on a diurnal basis and the drying power function E_A may be written in terms of atmospheric Monin-Obukhov (1954) similarity theory,

$$E_A = k u_* \rho (e_{Sa} - e_a)\left[\ln\left(\frac{z_a - d_{ov}}{z_{ov}}\right) - \psi_v\left(\frac{z - d_{ov}}{L}\right)\right]^{-1} \tag{6.163}$$

where von Karman's constant $k = 0.4$, $u_* = (\tau_o/\rho)^{1/2}$ is the frictional velocity, τ_o the surface shear stress, d_{ov} the displacement height for water vapor and e_a and e_{Sa} are the specific humidity of the air and the saturation specific humidity at the air temperature, respectively (Brutsaert, 1982, and Katul and Parlange, 1992). The stability correction function ψ_v depends upon $(z - d_{ov})/L$ with L being the Obukhov length defined by

$$L = \frac{-u_*^3}{kg\left[H_v/(\rho c_p T_a)\right]} \tag{6.164}$$

where $H_v = (Q_A + 0.61\, T_a c_p E_p)$ is the specific flux of the virtual sensible heat at the surface. The value of u_* is obtained from the mean horizontal wind speed v defined by the surface layer model of Monin-Obukhov as

$$v = \frac{u_*}{k}\left[\ln\left(\frac{z - d_o}{z_o}\right) - \psi_m\left(\frac{z - d_o}{L}\right)\right] \tag{6.165}$$

where d_o is the momentum displacement height, z_o the surface roughness and ψ_m the momentum stability correction function. For unstable conditions ($L < 0$),

$$\psi_m = \ln\left[\frac{(1+x)^2(1+x^2)}{(1+x_o)^2(1+x_o^2)}\right] - 2\tan^{-1}x + 2\tan^{-1}x_o \tag{6.166}$$

and

$$\psi_v = 2\ln\left(\frac{1+x^2}{2}\right) \tag{6.167}$$

where $x = (1 - 16y)^{1/4}$, $y = (z - d_o)/L$ and $x_o = (1 - 16z_o/L)^{1/4}$. For stable conditions ($L > 0$),

$$\psi_v = \psi_m = -5\ln\left(\frac{z - d_o}{z_o}\right). \tag{6.168}$$

The scalar roughness z_{ov} can be substantially smaller than z_o. Some suggestions are given by Brutsaert (1982) for possible parameterizations of z_{ov}. An iterative scheme is required to actually solve for E_{TP}. With values of ψ_v and ψ_m set equal to zero for the first iteration, (6.165) is solved for a first estimate of u_* and (6.163) for E_A. Next a first estimate of L in (6.164) is made using E_p from (6.162) and the surface energy balance to obtain Q_A. Next, the stability correction functions are included in (6.165) and (6.163). This system of calculations are repeated until the value of E_p converges. Usually convergence is achieved in only a few iterations. Katul and Parlange (1992) and Parlange and Katul (1992) tested this formulation of Penman's equation for a wet bare soil and found it to be remarkably accurate

during the day even under conditions with strong, dry winds passing over a wet land surface such that $Q_A < 0$ (i.e. $L > 0$) and $\chi E_p > (R_M - Q_S)$. In these extreme conditions, sometimes called an oasis problem or effect as found in arid regions (e.g. western United States or Australia), it is crucial to account for atmospheric stability to ultimately ascertain the total daily evapotranspiration.

At least two other approaches should be mentioned here regarding evapotranspiration equations. Thornthwaite (1948) proposed an empirical equation based upon air temperatures and an air temperature dependent empirical heat index. The equation provides integral monthly values of E_{TP} and its use is restricted to mild climatic zones. Efforts to obtain daily data from the equation appear to be useless. A second approach is that of Priestley and Taylor (1972). They proposed a simplified version of the Penman equation to calculate potential evapotranspiration

$$E_{TP} = \alpha\left[\frac{\phi_a(R-Q_S)}{\gamma+\phi_a}\right] \tag{6.169}$$

for extended wet surface conditions with symbols used in (6.159) and (6.160) such that $Q_A > 0$. The empirical coefficient α falls between 1 and $(\phi_a + \gamma)/\phi_a$ and is best estimated according to Priestley and Taylor with a value of 1.26. Inasmuch as this model will break down when there is strong local advection as described above, prudence should be exercised.

6.5.2.2 Structure of Evapotranspiration

The ratio of the two components of evapotranspiration, transpiration T_R and evaporation from soil E is called the structure of evapotranspiration (Budagovskij, 1969). This ratio has a diurnal rhythm – during the day the plant canopy is intensively transpiring, and during the night transpiration practically ceases while evaporation from the soil plays a more important role. During the season, the structure of E_{TP} depends upon the leaf area index ω which is the ratio of the total area of leaves and other green parts of plants related to the reference area of the soil. Methods for measuring ω are described in the literature on photosynthesis. The value of ω is also seasonally dependent and usually has a range $0 \leq \omega < 10$. An example of the seasonal evolution of $\omega(t)$ of wheat is given in Fig. 6.48. We should note that ω of wheat reaches very high values compared to those of other cultivated plants, especially row crops. Quantifying the canopy density with a value of ω is important in order to convert the evapotranspiration from a densely populated crop with complete canopy cover to that from a frequently observed incomplete canopy cover. Ritchie (1972) found that the ratio of radiation R_a above a canopy to that at the soil surface R_S below the canopy has the exponential form

$$\frac{R_a}{R_S} = \exp(-\alpha\omega) \tag{6.170}$$

with $\alpha = 0.398$. Novák (1981) applying the procedures of Budagovskij (1969) based upon a set of equations describing the transport of water vapor and heat in the canopy obtained similar relationships and distinguished the contributions

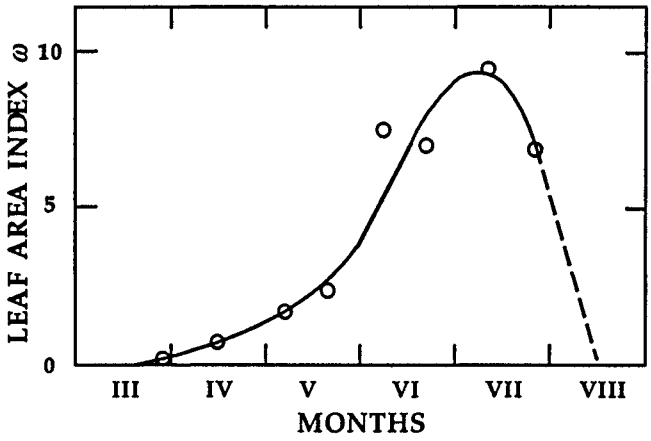

Figure 6.48. The seasonal dependence of leaf area index ω measured for wheat in Slovakia (Novák, 1981).

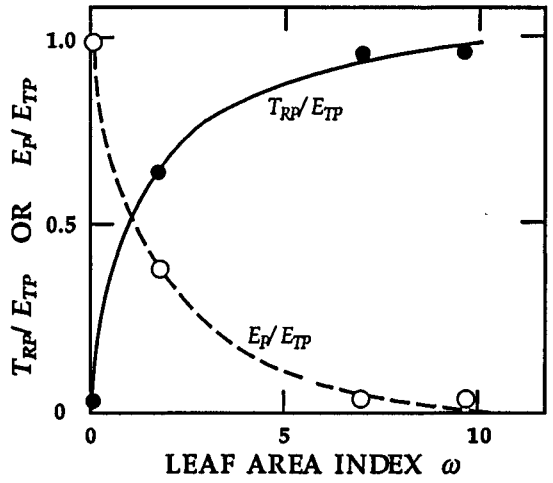

Figure 6.49. The ratio T_{RP}/E_{TP} and E_P/E_{TP} as related to leaf area index ω in Fig. 6.48. T_{RP} is potential transpiration, E_{TP} potential evapotranspiration and E_P potential evaporation from the soil only (Novák, 1981).

of transpiration T_{RP} and evaporation from soil E_P (see Fig. 6.49) as

$$T_{RP} = E_{TP}\exp(-\alpha\omega) \tag{6.171}$$

and

$$E_P = E_{TP}\left[1-\exp(-\alpha\omega)\right]. \tag{6.172}$$

We note in Fig. 6.50 that the ratio T_{RP}/E_{TP} is closely related to ω for various plants. Moreover, the constant value of the coefficient α is probably not

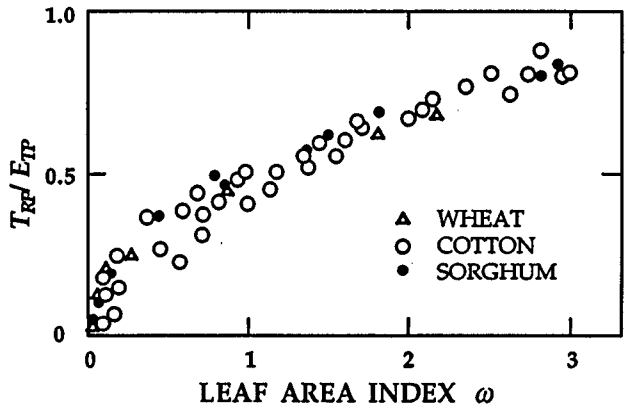

Figure 6.50. The dependence of T_{RP}/E_{TP} upon leaf area index of various plants. Data collected from the literature by (Novák, 1981). T_{RP} is potential transpiration and E_{TP} potential evapotranspiration.

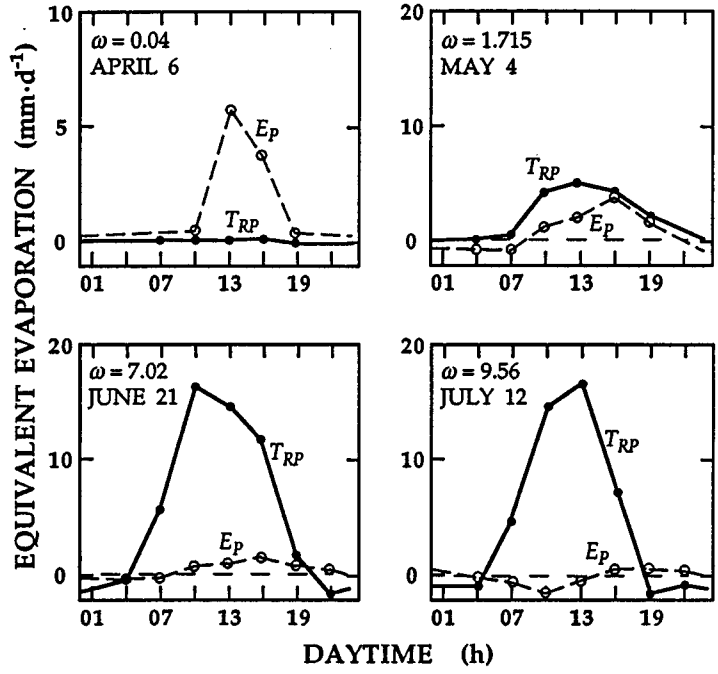

Figure 6.51. The diurnal variation of separated potential terms – E_P is soil evaporation and T_{RP} is transpiration (Novák, 1981).

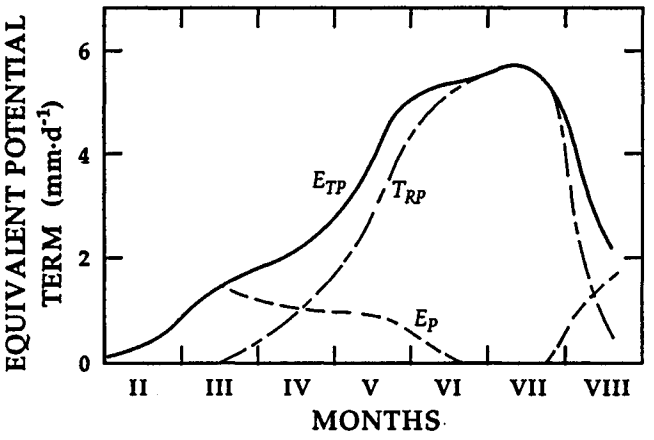

Figure 6.52. The seasonal behavior of separated potential terms for a chernozem on loess in Slavakia. E_P is soil evaporation and T_{RP} is transpiration separated from evapotranspiration E_{TP} for wheat (Novák, 1981). All terms represent potential values.

universally applicable. Daily values of E, T_R and E_T strongly depend upon the plant's ontogenesis stage. With an increase of ω the daily sum of E_P decreases and the maximum peak shifts to the afternoon hours [phase shift of the quasi-sinusoidal curve $E_P(t)$]. At about $\omega \geq 1$ condensation of water vapor occurs at the soil surface and the length of this occurrence is extended as ω increases. This increase is manifested when $E_P < 0$ (see Fig. 6.51) and even when $E_{TP} < T_{RP}$ during a summer midday. An illustration of the seasonal separation of evaporation and transpiration for wheat in Slovakia is given in Fig. 6.52. In this case of wheat, integral values for the entire vegetative period manifest values of $T_{RP}/E_{TP} = 0.78$ and $E_P/E_{TP} = 0.22$.

6.5.3 Actual Evapotranspiration E_{TA}

Let us first recall that potential evapotranspiration occurs only when the surfaces are wet, and when they are not wet, we indeed have actual evapotranspiration, because there is a limited quantity of water reaching the evaporating soil and plant surfaces. The term actual evapotranspiration E_{TA} is introduced, $E_{TA} \leq E_{TP}$.

The general procedure for transforming the potential evapotranspiration E_{TP} to the actual evapotranspiration E_{TA} follows several steps to theoretically compute the real E_{TA} at a particular location.

1. E_{TP} is computed for the reference short green grass with wet surfaces and adequate water supply without advection.
2. This reference E_{TP} is transformed using specific site related values influenced by slope, land use and albedo.

3. The site related E_{TP} is adjusted to the particular type of vegetation including its stage of development.
4. The value of E_{TA} is obtained by reducing the value of the site related E_{TP} to account for the limited supply of water derived from the soil profile. This reduction is achieved empirically by applying relations like (6.152) or by introducing actual resistances which reduce the flux through the SPAC system.

When steps 2 and 3 are omitted, we have the development presented by Monteith with the final result often being named the Penman-Monteith equation. Here, with the stomatal resistance r_S being introduced, the Penman-Monteith equation for E_{TA} is

$$E_{TA} = \frac{\frac{\phi_a}{\gamma}\left(\frac{H_Q}{\chi}\right) + \frac{\rho_A c_p d}{\chi \gamma r_A}}{\phi_a + \gamma\left(1 + \frac{r_S}{r_A}\right)} \tag{6.173}$$

where r_A [s·m^{-1}] is the aerodynamic resistance against the turbulent transfer of water vapor from the evaporating surface to the atmosphere. Its values are in the range $10 \leq r_A \leq 300$. This equation describes the actual evapotranspiration of a particular reference plot owing to an extension of Penman's equation by Monteith (1981). It represents the entire canopy as a "big leaf" (Lynn and Carlson, 1990) and is still in agreement with the integral single layer concept of Penman.

Deterministic models of stomatal resistance (see Lynn and Carlson, 1990) can also be applied for estimating E_{TA}. Alternatively, soil water models which empirically describe water absorption by plant roots expressed by (6.153) allow calculations of E_{TA} or E_{TA}/E_{TP}.

The bulk stomatal (or surface) resistance r_S in (6.173) is generally considered a "fitting" parameter in land surface simulation models or a diagnostic water stress index of plant canopies (e.g. Brutsaert, 1982). Recently, many complicated models of r_S have been proposed for drying land surfaces, especially in the context of atmospheric modeling, but for practitioners in the field, r_S is generally unknown. Because it is so difficult in practice to obtain a field scale measure of r_S to assess the aridity of a region, we mention here models based upon ideas of Bouchet (1963) concerning potential evaporation and the drying of the land surface. In these approaches (e.g. Brutsaert and Stricker, 1979, and Morton, 1983) the aridity of the region is assessed from atmospheric measurements. Bouchet basically suggested that as an initially wet surface dries, the decrease in actual evaporation corresponds to an equivalent increase in potential evaporation. When the land surface is wet

$$E(actual) = E_p(potential) = E_{p_*}(surface\ is\ wet). \tag{6.174}$$

As the water supply to the surface becomes limiting ($E < E_{p_*}$) for the same amount of energy available for evaporation,

$$E - E_{p_*} = q_1 \tag{6.175}$$

such that q_1 becomes available and increases E_P. Bouchet proposed that

$$E_p = q_1 + E_{p_*} \tag{6.176}$$

in order that the complementary relationship

$$E + E_P = 2E_{P_e} \tag{6.177}$$

assures that q_1 does not alter the available energy and that no external energy suddenly enters the region.

Brutsaert and Stricker (1979), adopting the Penman equation for potential evaporation E_P and the Priestley-Taylor equation for E_{P_e}, solved (6.177) for E. The primary restriction of this model is that the Priestley-Taylor model is only valid when there is no local advection. Parlange and Katul (1992a and b) showed that in order to conserve energy whenever $Q_{A_r} < 0$ ($Q_{A_r} = R - Q_S - \chi E_P$) the Priestley-Taylor formulation of E_{P_e} must be adjusted by taking $\chi E_{P_e} = [\chi E_{P_e}$ (Priestley-Taylor) + $|Q_{A_r}|]$. Parlange and Katul tested this model using 20-minute time step measurements and found it to be extremely accurate, though more work is needed before it becomes more widely accepted and verified. The advantage, of course, is that r_S does not have to be specified.

Inasmuch as all models or estimates have to be first verified against directly measured data, we shall briefly discuss the measuring techniques of evapotranspiration in the field. The methods can be grouped into three classes: (i) soil water balance, (ii) plant measurement and (iii) micro meteorological methods.

6.5.3.1 Soil Water Balance

The basic water balance of an elementary area where horizontal fluxes are negligible is

$$E_{TA} = I + Q_V + \Delta W \tag{6.178}$$

where I is the cumulative infiltration from irrigation and rain equal to precipitation if surface runoff is eliminated, Q_V the vertical flux at the base of the soil profile (when the groundwater table is very deep, $Q_V < 0$ and usually represents the vertical drainage component) and ΔW the difference in water storage for a given period of time Δt ($t_2 - t_1$) from which E_{TA} is evaluated. Measuring the water content distribution within the soil profile $\theta(z, t)$ at times t_1 and t_2 allows the magnitude of ΔW to be ascertained using

$$\Delta W = \int_0^Z \theta(z,t_1)dz - \int_0^Z \theta(z,t_2)dz \tag{6.179}$$

where Z is the depth of the bottom of the soil profile where Q_V is evaluated. The principle of the zero flux plane Z_z is used if $Z_z > z_r$ where z_r is the rooting depth. The determination of the zero flux plane (where $Q_V = 0$) was previously explained and illustrated in Fig. 6.37. If tensiometers are installed and the soil hydraulic functions known, the flux across the plane at Z can be computed.

In spite of the relative simplicity of the soil water balance method, soil heterogeneity, described in Chapter 8, plays an important role in the strategy of selecting observation sites (Vachaud et al., 1983) and defining field scale hydraulic properties based upon evaporation measurements (Parlange et al., 1992 and 1993).

In order to integrate the diverse distribution of vertical and potentially horizontal fluxes occurring at the microscale, lysimeters are frequently used to measure Q_V at the bottom of the soil profile. The term indicates that the measurement of soil leaching was the original aim of lysimeters. Nowadays, the term identifies a container filled with soil covered with natural or cultivated vegetation. The water percolating through the soil is collected either gravimetrically or through a suction plate which is maintains a negative soil water pressure head h identical to that in the field next to the lysimeter. Because gravitational drainage from a lysimeter of finite length differs from that in the field and disturbs the natural development of $h(z)$, the depth of the lysimeter should be as great as possible. To achieve the same internal structure of the porous system as in the natural soil, it is desirable to place a monolithic block of field soil into the container. Lysimeters containing soil whose natural structure has been disturbed have limited applicability.

Lysimeters are either weighable or non weighable. Weighable lysimeters provide information about the change of water storage W for any time period even in the absence of percolating water, while non weighable lysimeters yield only the water percolating from the soil column. Instead of directly measuring the weight of a lysimeter, weight changes are sometimes determined from fluid displacements in a larger surrounding container in which the lysimeter is "floating". These floating lysimeters can be instrumented to observe the force required to keep them centered within the larger container within which they float. These observations provide additional information regarding the shear stress of the wind as it passes through and over the vegetative canopy.

6.5.3.2 Plant Surface Measurements

These measurements neglect the soil water evaporation component of evapotranspiration. In forests, the sap flow in the tree trunk is measured. The time required for either a heat pulse or a radioactive tracer pulse to travel along the trunk is measured by an appropriate technique. A similar approach is also applied to trace the flux of water within the xylem of cultivated plants.

The porometer method is more fully developed. With the flux of water measured on individual leaves, the stomatal resistance r_S is obtained from an appropriate calibration. The canopy resistance r_c ($r_c = r_S/\omega$) is calculated from r_S and the leaf area index ω. Models of evapotranspiration include values of r_c as directly measured information.

Integral values of evapotranspiration are also estimated from remote sensing. Values of E_{TA} are obtained from a surface energy model which has inputs of measured surface temperatures based upon infrared (IR) images. The sensible heat flux Q_A can be calculated from Monin-Obukhov similarity using

$$T_S - T_a = \frac{Q_A}{k u_* \rho c_p}\left\{\ln\left[\frac{z-d_{oh}}{z_{oh}}\right] - \psi_h\left[\frac{z-d_{oh}}{L}\right]\right\} \qquad (6.180)$$

where T_S is obtained from IR remote sensing of surface temperature, T_a is taken in the surface layer of the atmosphere, z_{oh} is the heat roughness length, d_{oh} the sensible heat displacement height (often taken equal to d_o) and ψ_h the sensible

heat stability correction function taken equal to the value of ψ_v defined earlier. Actual evapotranspiration is solved once more from the energy balance ($\chi E = R - Q_S - Q_A$) in an iterative scheme where once again ψ_m and ψ_h are initially set equal to zero, E is estimated from the energy balance and a first estimate of L can then be obtained. The system is repeated with the iterative values of ψ_m and ψ_v until the value of E converges.

Alternatively, temperatures of a reference plot (where E_{TP} exists) with an optimal water supply are monitored and used for evaluating E_{TA} of a vegetative cover under natural conditions for which temperatures are monitored.

6.5.3.3 Micrometeorological Methods

These methods are used to estimate the value of E_{TA} from directly measured atmospheric data above the land surface.

In eddy covariance methods, the use of fast response sensors permits measured vertical wind speed fluctuations w' to be correlated with measured temperature and humidity fluctuations T' and q', respectively. Hence, average values of the flux of water vapor during short time intervals (e.g. one hour or less) are obtained where $E = \rho \overline{w'q'}$ and $Q_A = \rho c_p \overline{w'T'}$. The fluctuations for the measurement time period (e.g. T') are defined by $T' = T - \overline{T}$, where $\overline{T}$ is the mean value over the time period of interest and the condition $\overline{T'} = 0$ holds. For further study of eddy covariance methods, see Stull (1988) or Qarratt (1992).

The Bowen ratio β ($= Q_A/\chi E$) is applied in order to partition the energy budget and from it, E_{TA} is estimated. Note the Bowen ratio is the ratio of the sensible and latent heat fluxes. It is obtained by measuring temperature and the partial vapor pressure at two heights together with the atmospheric pressure assuming the transport of heat and water vapor are identical.

Aerodynamic methods are based upon Monin and Obukhov (1954) similarity theory which provides a good description of the mean boundary layer surface layer flow (in the turbulence sense). The main theory is given here for completeness. The flux of momentum, sensible heat and water vapor can be given by

$$v = \frac{u_*}{k}\left[\ln\left(\frac{z-d_o}{z_o}\right) - \psi_m\left(\frac{z-d_o}{L}\right)\right] \tag{6.181}$$

$$T_r - T = \frac{Q_A}{k u_* \rho c_p}\left\{\ln\left[\frac{z-d_o}{z_r-d_o}\right] - \psi_h\left[\frac{z-d_{oh}}{L}\right] + \psi_h\left[\frac{z_r-d_{oh}}{L}\right]\right\} \tag{6.182}$$

and

$$q_r - q = \frac{E}{k u_* \rho}\left\{\ln\left[\frac{z-d_o}{z_r-d_o}\right] - \psi_v\left[\frac{z-d_{ov}}{L}\right] + \psi_r\left[\frac{z_r-d_{ov}}{L}\right]\right\} \tag{6.183}$$

where the subscript r refers to a reference height near the surface and d_{oh} is the displacement height for heat. These three equations can be iteratively solved simultaneously when atmospheric surface layer measurements of wind speed, temperature and humidity are available.

As it follows from this brief presentation, the majority of difficulties in the estimation of E_{TA} is in fact the direct measurement of water vapor fluxes into the atmosphere is not simple in practice and that reliable flux meters have not yet been developed. However, this is not only the case for atmospheric fluxes but for the direct measurement of soil water fluxes as well as we discuss in the next chapter.

PROBLEMS

1. Derive the solution $z(h)$ of steady infiltration into a homogeneous soil profile if $K(h)$ is described by (5.38) for $m = 1$ and for $m = 2$. Follow a procedure analogous to that in the derivation of (6.5). Hint: Insert $A = b - a/q$ into the denominator of the integral.
2. Derive the implicit equation for h_l in a crust-topped profile (Fig. 6.4) if $K(h)$ is described by (5.39) and the crust (layer 2) is fully saturated.
3. What is the least value of L_1 in Fig. 6.4 when the value of $dh/dz = 0$ just below the crust. L_1 is the thickness of subsoil 1 between the crust and the ground water level GWL. Is the solution also valid for a homogeneous soil without a crust with L_1 the depth of the GWL and $q_o < K_{S1}$?
4. Modify (6.12) for soil 1 with air-entry value h_{A1} when you solve steady infiltration into a crust-topped profile.
5. Assuming steady infiltration, what is the elevation of the water level in each of the two piezometers – one inserted in the soil profile at the top and the other at the bottom of the zone of saturation in Fig. 6.5?
6. Determine the soil water content $\theta(x)$ at 2-cm intervals along a soil column during horizontal infiltration at time $t_2 = 100$ min. based upon the following measurements of $\theta(x)$ at time $t_1 = 25$ min.:

x (cm)	0	2	4	6	8	10	12	14
θ ($cm^3 \cdot cm^{-3}$)	0.507	0.505	0.497	0.470	0.408	0.312	0.185	0.082

   Values of θ_S and the initial soil water content θ_i are 0.507 and 0.082, respectively.
7. Using the Green and Ampt approximation, derive the value of m in the relation $A = mK_S$ where A is the parameter in (6.67).
8. For Green and Ampt's approximate solution of vertical infiltration, derive the validity of
$$\lim_{t \to \infty} q_o(t) = K_S.$$
9. For a constant rainfall rate, derive the value of the ponding time t_p for infiltration when infiltration for DBC is described by Green and Ampt's approximation. Proceed analogously to the derivation of (6.93).
10. Derive the value of h_f in Green and Ampt's approximation (6.53) when you use: a. (5.38) or b. (5.39) for $K(h)$.
11. Is $(\theta_{FC})_1 <$ or $> (\theta_{FC})_2$ if field capacity is measured on the same soil once at θ_{i1}, second time at θ_{i2} and $\theta_{i1} > \theta_{i2}$?
12. Sketch the change of soil water content θ versus time for the two redistribution processes (a. and b. demonstrated in Fig. 6.31) when θ is measured at $z_{r1} > z_f$.

13. With the GWL being 180 cm below the soil surface of two different soil columns, find the difference in maximum evaporation rate E_{max} from the two columns. Column A is a homogeneous profile of a loamy soil characterized by (5.39) with $c = 0.02$ cm^{-1} and $K_S = 20$ cm·d^{-1}. Column B is a profile of the same loamy soil having an interlayer of sand [characterized by (5.39) with $c = 0.08$ cm^{-1} and $K_S = 200$ cm·d^{-1}] extending from 80 to 110 cm below the soil surface.
14. Estimate the actual evapotranspiration rate at $\theta/\theta_S = 0.5$ if potential evapotranspiration is 5 mm·d^{-1} for which the critical pressure head of decreased availability h_D (Fig. 6.45) is related to $\theta/\theta_S = 0.7$ and the wilting point is at $\theta/\theta_S = 0.35$. Assume linear relationships.